# 行政院國家科學委員會專題研究計畫　成果報告

## 類神經網路結構安全監測系統之發展(3/3)

計畫類別：個別型計畫
計畫編號：NSC92-2211-E-009-040-
執行期間：92 年 08 月 01 日至 93 年 07 月 31 日
執行單位：國立交通大學土木工程學系(所)


計畫主持人：洪士林
共同主持人：黃炯憲


報告類型：完整報告

處理方式：本計畫可公開查詢

中　華　民　國 93 年 12 月 13 日

# 類神經網路結構安全監測系統之發展（3/3）

## 摘 要

本計畫之目的是利用類神經網路來架構用於監測結構行為之整體監測網路。這些監測網路除可用於結構系統識別之外，尚可透過觀察監測網路之輸出誤差來偵測破壞之發生或是其位置。在第二項研究主題上，本文提出兩階段的結構破壞診斷方式。第一階段之工作在於偵測破壞產生之位置。研究中證明基於結構模態參數而得之破壞特徵（DLF）僅與破壞位置相關，而與破壞程度無關。於是，DLF 便可作為辨識破壞位置之參考指標。另外，由觀測訊息進而推求結構可能之破壞狀態為一逆運算問題，其處理程序可視為樣本識別（pattern recognition），因此結構破壞偵測之問題相當適合以非監督式模糊神經網路來處理。利用合適的數值模型，吾人可事先建立不同破壞狀態下之解析破壞特徵。當真實之破壞情況發生時，依據系統識別模式所獲得的結構模態參數，便可用於計算實際之量測破壞特徵。接著利用非監督式模糊神經網路，藉由比對量測破壞特徵以及解析破壞特徵，便可診斷出破壞產生之位置。待破壞發生之可能位置決定後，第二階段便可透過本文所述之演算法來評估破壞的程度。藉由數值或實驗室案例，於分析研究中所發展之模式或方法得以驗證，驗證之結果顯示其於應用上之可行性。

計畫中，吾人設計了一棟四層樓鋼構架作為試體，以便進行勁度損失模擬之震動臺實驗。實驗中以樓層層間勁度之降低來模擬結構之退化(deterioration)。於該試體上共裝置了三種不同的感測器，如加速度計、光纖光柵感測器（FBG sensor）、以及傳統電子式應變計（RSG），以量測試體於實驗中之結構加速度以及應變反應。根據分析研究以及實驗研究之成果，提出一整合型的結構監測以及破壞診斷系統架構。該系統將具有即時系統識別、結構監測、破壞診斷、以及提供正確警示之功能。

# Development of Artificial Neural Network Based Structure Health Monitoring System (3/3)


## ABSTRACT

The objective of the research is to develop a novel ANN-based system identification (ANNSI) model for identifying the modal parameters of a structure from its vibratory responses to monitor the health condition of the structure. The modal parameters can be directly estimated from the weighting matrices of a trained ANN, and further be used for diagnosing a structure. Following, a damage detection approach, which is based on the damage localization feature (DLF) and an unsupervised fuzzy neural network (UFN), is proposed. It is shown that DLF is correlated with damage location but independent of damage extent. As a result, it is used as indicator to identify the damage location. Detection of structural damage is an inverse problem, and the solving procedure for this problem is a kind of pattern recognition which is very suited to be implemented by unsupervised fuzzy neural networks. Through the use of the UFN, the damage site is located by matching two sets of the damage feature, the analytical DLF which is generated from an analytical model and the measured DLF which is computed according to the identified modal data. Subsequently, estimation of the damage extent is implemented by the proposed algorithms after the damage location is identified. The developed model or approaches in the analytical study are examined by either numerical or laboratory examples. The simulation results reveal the capability and practicability of the proposed methods.

Moreover, a scaled-down four-story steel frame structure was designed to conduct the health monitoring study on the shaking table. The structural deterioration is simulated by reduction of the story stiffness. Three types of sensors, such as accelerometers, fiber Bragg grating (FBG) sensors, and resistant strain gages (RSGs) were installed on the specimen to measure the structural acceleration and strain responses during the shaking table tests. Based on the results from analytical and experimental study, an integrated health monitoring system is proposed in this dissertation. The system is designed to be capable of on-line system identification, monitoring, diagnosis, and warning.

# CONTENTS

# List Of Tables

# LIST OF FIGURES

# Chapter 1 Introduction

## 1.1 Background and Motivation

The civil infrastructure ages and deteriorates with time due to aging of materials, excessive use, overloading, climatic conditions, etc. All these factors contribute to the discard of constructed systems. As a result, health monitoring system which is capable of health monitoring (including damage diagnosis), issuing warning message, and providing maintenance guidance, become necessary to ensure the safety of the infrastructure and public. Health monitoring refers to the use of in-situ, nondestructive sensing, and analysis of system characteristics, including structural response, for the purpose of detecting system changes, which may indicate damage or degradation. Health monitoring techniques may be categorized into two groups, global and local health monitoring. Global approaches attempt to simultaneously assess the condition of the structure whereas local approaches employ non-destructive evaluation (NDE) tools on specific structural components.

Currently available NDE methods are mostly non-model methods, i.e., either visual or localized experimental methods, such as acoustic or ultrasonic methods, magnetic field methods, radiographs, eddy-current methods and thermal field methods. Shortcomings of currently available NDE methods indicate a requirement of damage inspection techniques that can give global information on the structure and they do not require direct human accessibility of the structure. Furthermore, among with the continuous competing requirements of improving the weight, interdisciplinary performance, and reliability of structures, the development of effective, reliable, and real-time non-destructive health monitoring techniques based on the dynamic characteristics of the structures is receiving growing attention. Among them, the techniques of detect damage by monitoring changes in the dynamic characteristics or in the dynamic responses of the structure seem to be attractive and promising.

Consequently, for the security and reliability during the service life, smart structures should have the potential to achieve the ultimate objective in damage detection, i.e., predicting the remaining useful life of the structure. The goals of developing smart structures in health monitoring is that the structure could, through the system identification process using vibratory observations, be able to detect damage as it is incurred by the structure, determine the location and extent of the damage, predict if and when disastrous failure of the structure will occur, and alert the operator as to how the performance of the structure is affected as that appropriate steps can be taken to remedy the situation. Therefore, system identification and damage assessment techniques are the foundations of developing the health monitoring system of smart structures. Figure 1.1 illustrates the relationship between system identification and damage assessment techniques.

## 1.2 Literature review

Numerous investigations in the damage detection or health monitoring of structures have been vigorously carried out in the past decades. Since the health monitoring approaches in this work are based on the modal parameters obtained from the structural vibrations, most reviews are focused on the modal-based (i.e. based on structural modal parameters) methods. Moreover, by the efforts of some researchers during these years, artificial neural network-based methods have become a major branch of studying structural health monitoring. Therefore, the health monitoring and damage detection related studies which were based on neural networks will also be reviewed herein.

The modal-based methods utilize the information from modal parameters to detection and assess structural damage. The majority of this group of methods uses the lower modal frequencies and can best describe the global behavior of the structure. Therefore, they hold promise for global non-destructive inspection of a variety of structures, because surface measurements of a vibrating structure can provide information about the health of the internal members without costly dismantling of the structure. Also, because of their global nature, these techniques allow the customization of measurement points. Another major advantage is that the modal information is easy to extract from the measurements obtained through free, ambient, and forced vibration tests. A number of damage assessment techniques based on changes in structural modal parameters have been proposed. The concept underlying such an approach is that damage to a structure reduces its natural frequencies, increases the modal damping, and changes the modal shapes.

In early research, structural damage detection methods use natural frequencies as damage indicator. Salawu [1] made a comprehensive review on the detection of structural damage trough changes in frequency. However, from dynamic tests on bridges, Alampalli and Fu [2] and Salawu and Williams [3] concluded that the change in natural frequencies is not spatially specific and not sufficiently sensitive to detect local damage in the structure so that its application is limited. The results of their work indicate that the modal assurance criterion (MAC) and the coordinate modal assurance criterion (CMAC), which are based on mode shape data, are useful in detecting local structural change. Since mode shapes can provide much more information than natural frequencies, many studies have concentrated their efforts on damage detection with mode shapes information [4-6].

For the damage localization problem, Cawley and Adams [7] proposed the first model by employing the changes in the natural frequencies, together with a finite element model (FEM), to locate the damage site of a given structure. Following their works, some researches [8, 9] have found this method susceptible to measurement errors, and ways of improving the localization have been introduced. Hearn and Testa [10] have illustrated that the ratio of the elemental strain energy to the total kinetic energy of the whole system is a fraction of the eigenvalue, and the ratio of this fraction for two different modes is dependent only on the location of the damage. Shi *et al.* [11, 12] presented a method based on modal strain energy for locating damage in a structure. Their method makes use of the change of modal strain energy in each structural element before and after the occurrence of damage. Some properties of the modal strain energy change are given to illustrate its sensitivity in locating damage.

By employing control-based eigenstructure assignment techniques, a subspace rotation algorithm was proposed by Zimmerman and Kaouk [13], in which the damage vector and relative rotation angle are used to identify the DOFs affected by damage. Lim and Kashangaki [14] put forward a similar method in concept using best-achievable eigenvectors, however, to identify the damaged structural members directly.

Yao *et al.* [15] presented a structural diagnosis technique using vibratory signature analysis and the concept of strain mode shape. When a structure experiences a damage or change, a new state of force equilibrium is realized. Since force distribution is, in general, greatest near the damaged area, the location of damage is implicitly identified by the severity of the strain mode shape change. Due to its sensitivity to local damage, strain mode shape change seems to be a suitable damage indicator for locating structural damage.

Stubbs and Kim [16] presented a methodology to localize and estimate the severity of damage in structures for which only postdamage modal parameters are available for a few vibratory modes. First, a theory of damage localization and severity estimation that utilizes only changes in mode shapes of the structures is outlined. Next, a system identification method that combines the experimental modal data and the modal parameters of a finite element model of the structure is developed to yield estimates of the baseline modal parameters for the structure. This method is attractive when the baseline modal information for the structure is unavailable.

Topole and Stubbs [17] used natural frequencies with mode shapes and showed the importance of introducing mode shape orthogonality to identify the location and extent of damage on a structure. Messina *et al.* [18] developed an assurance criterion for detecting single damage site of structures. And this method was extended to identify the relative amount of damage at multiple sites [9, 19]. Recently, Shi *et al*. [20] proposed a sensitivity-and statistical-based method to localize structural damage by direct use of incomplete mode shapes. This method is an extension of the work by Messina *et al*.[19]. The damage detection strategy is to localize the damage sites first by using incomplete measured mode shapes, and then to detect the damage site and extent again by using the more accurate measured natural frequency information.

Another important and interesting category uses the characteristics of the flexibility matrix. Unlike the stiffness matrix, the flexibility matrix can be formed more accurately through the usage of first several order experimental modal data. Lin [21] used this flexibility matrix to multiply the pre-damaged FEM stiffness matrix to determine the damage locations. Pandey and Biswas [22] used the change in flexibility matrix before and after the occurrence of damage in the structure as damage index to identify the location and amount of damage. An important advantage in this category is that the usage of the analytical model can be avoided. Also, some researchers used some special information such as curvature modes [23-26] and strain data [27] to search for the damage locations.

For the estimation of damage extent, one important class of methods for correlating measured modal data with analytical finite element models is the minimization or elimination of modal force error. This error is that resulting from the substitution of the analytical FEM and the measured modal data into the structural eigenproblem. Various approaches have been presented to minimize some measure of the error in the eigenproblem by perturbing the baseline values in the analytical model, such as the components of the stiffness, damping, and mass matrices. One type of method, known as sensitivity-based model update, uses the sensitivities of the modal response parameters of the FEM to the structural design parameters (such as Young's modulus, density, etc.) to iteratively minimize the modal force error [28, 29]. Another type of method, known as eigenstructure assignment, designs a controller that minimizes the modal force error [13, 14]. Further, another type of method, known as optimal matrix update, solves a closed-form equation for the matrix perturbations that minimize the modal force error or constrain the solution to satisfy it [30, 31].

Using modal parameters, Koh *et al*. [32] proposed an improved-condensation method to estimate the stiffness matrix that corresponds to observed degrees of freedom. Then, these authors detected local structural changes by quantifying changes in stiffness. Based on their own previous work [12], Shi et al. [33] further proposed an improved structural damage quantification algorithm. The algorithm includes the analytical stiffness and mass matrices of the system in the damage quantification. It reduces significantly the modal truncation error ad the FE modeling error from higher analytical modes in the computation.

Over the last two decades, artificial neural networks have gradually been established as a powerful tool in the fields of prediction and estimation, pattern recognition, and optimization [34-38]. Due to the features of robustness, fault tolerance, and powerful computing ability, the model of artificial neural networks becomes a promising tool in solving civil engineering problems, such as linear/nonlinear system identification, structural control and health monitoring.

Recently, some researches have investigated the suitability and capabilities of ANNs for damage detection purposes. Ghaboussi *et al.* [39] and Wu *et al.* [40] discussed use of neural networks for detection of structural damage in a three-story frame with rigid floors. They trained neural networks to recognize the frequency response characteristics of undamaged and damaged structures. The varying damage levels were simulated by adjusting the properties of individual members. Elkordy *et al.* [41] question the reliability of the traditional methods for structural damage diagnosis and monitoring that rely primarily on the visual inspection and simple on-site tests. They proposed a structural damage monitoring system for identifying the damage associated with changes in structural signatures using neural networks. For training, they used an FEM to develop failure patterns that were used to train a neural network so that it can later diagnose damage in the reference structure. Szewezyk and Hajela [42] presented a neural network approach based on mapping the static equilibrium requirement for a structure in a finite element formulation with the assumption that structural damage is reflected in terms of stiffness reduction. The results showed that even with input noise and incomplete measured data, neural networks can still obtain satisfying diagnosis.

Pandey and Barai [43, 44] trained a multilayer perceptron and a time-delay neural network respectively for the detection of steel-truss bridge structures. Zhao *et al*. [45] used a counter-propagation neural network to locate structural damage for a beam, a frame, and support movements of a beam. The required data such as natural frequencies, mode shapes and their other derivatives are obtained through the use of FEM.

The studies presented by Masri *et al.* [46] used neural network-based approaches for the detection of changes in the characteristics of structure-unknown systems. Their approaches rely on the use of vibration measurements from a ‘healthy’ system to train a neural network for identification purposes. Subsequently, the trained network is fed comparable vibration measurements from the same structure under different episodes of response in order to monitor the health of the structure. Differ from other approaches, the attractive advantages of these approaches are that they do not require the analytical model for a real structure and only vibratory responses are used.

Zapico *et al.* [47] proposed a multi-layer-perceptron-based procedure for damage assessment in a two-storey steel frame and steel-concrete composite floors structure. A simplified finite element model is used to generate the training data. Sahin and Shenoi [48] presented a damage detection algorithm using a combination of global (changes in natural frequencies) and local (curvature mode shapes) vibration-based analysis data as input in ANNs for location and severity prediction of damage in beam-like structures. A FE model is used to introduce the damage scenarios to generate the training data. Other recent published works can be referred to the references [49-54].

## 1.3 Objectives

The object of this research is to assemble a framework of the health monitoring system in a smart structure via artificial neural network (ANN) approaches. In the health monitoring system, it is considered to involve three core parts which are the system monitoring, the system identification, and the damage assessment mechanisms. Figure 1.2 illustrates the relationship between these mechanisms.

To accomplish this goal, ANN-based system identification models have been developed to provide the information (such as the structural modal data) about the structure through the vibration measurements (such as the acceleration and strain responses) and can be used to continuously monitor the structure. Based on structural information provided by the identification models, the damage condition is assessed through the two-stage damage assessment approaches: an unsupervised fuzzy neural network for locating structural damage and estimating the damage extents of the structure. In addition to the theoretical developments in system identification and damage assessment techniques, experimental study is also conducted to complete this work.

# CHAPTER 2 ARTIFICIAL NEURAL NETWORKS

## 2.1 Introduction

An artificial neural network (ANN) model is a functional abstraction of the biological neural structures of the central nervous system. They are composed of many simple and highly interconnected computational elements, also called neurons, that operate in parallel and are arranged in patterns similar to biological neural nets. The neurons are connected by weighted links passing signals from one neuron to another. Each neuron receives a number of input signals through its connections. The output signal is transmitted through the neuron's outgoing connection. The outgoing connection, in turn, splits into a number of branches that transmit the same signal. The outgoing branches terminate at the incoming connections of other neurons in the network.

It is generally thought that a neural network is highly sophisticated nonlinear dynamic system. Although each neuron is primitive both in architecture and in function, a network comprising many neurons is intricate. In addition to its nonlinear nature, neural network is a signal processing system. The inherent dynamic process can be classified as a fast process and a slow process. The former is a numerical process to evolve to an equilibrium status with given inputs. The latter is a learning process where the values of the connective weights between neurons are adjusted according to the environment. After learning, environmental information is stored on the connective weights.

In 1943, McCulloch, a neurobiologist, and Pitts, a statistician, published a seminal paper [55] which inspired the development of the modern digital computer. At approximately the same time, Rosenblatt [56] was also motivated by this paper to investigate the computation of the eye, which eventually led to the first generation of artificial neural networks, known as the perceptron. Since then, the theory and design of ANNs have advanced significantly.

Over the last two decades, ANNs have found application in pattern recognition, signal process, intelligence control, system identification, optimization, etc. [57-59] because of their excellent learning capacity and their high tolerance to partially inaccurate data. They are suitable particularly for problems too complex to be modeled and solved by classical mathematics and traditional procedures. A good review article by Adeli [60] summarized the applications of the ANNs in civil engineering during the 20th century.

Artificial neural networks are typically characterized by their computational elements, their network topology, and the learning algorithm used. According to the learning approaches adopted, ANNs can be classified into two major groups: supervised and unsupervised. A supervised network is given both inputs and desired outputs pairs for training or learning. The network adjusts its weights until the errors between its outputs and the desired reach a predefined bound. An unsupervised network is commonly used for classification or clustering. Its weights are adjusted using predefined criteria until the network has performed a classification. In this work, an unsupervised neural network with fuzzy reasoning algorithm, termed as UFN, is employed to perform the damage detection of structures.

## 2.2 Unsupervised Fuzzy Neural Network Reasoning Model

The unsupervised fuzzy neural networks (UFN) reasoning model was proposed by Hung and Jan [61]. This model had been successful applied to the problems of preliminary design [62, 63] and control of building structures [64], and is further applied to the damage detection of structures [65]. The UFN reasoning model consists of an unsupervised neural network with a fuzzy computing process. The basic concept of the proposed model is that, the solution of a new instance can be solved by retrieved the similar instances from a collection of solved instances, named as ***instance base***, to a specified domain. The following is a brief review of the UFN reasoning model.

The UFN reasoning model is implemented in the following steps (Figure 2.1):

(1) measuring the similarities between new instance and existed instances;

(2) generating the fuzzy set of similar instances; and

(3) synthesizing the solution based on the fuzzy set of similar instances.

The first step involves searching for instances that similar to the new instance (**Y**) in the instance base (**U**$_j$) according to their inputs ($Y_i$ and $U_{j,i}$). It is performed through a single-layered laterally-connected network with an unsupervised competing algorithm. The similarity measurement is implemented by calculating the degree of difference between two instances. The function of degree of difference is defined as

$$d_{Yj} = diff(Y_{i,} U_{ji}) = \sum_{m=1}^{M} \alpha_m (x^m - u_j^m)^2 \tag{2.1}$$

where $d_{Yj}$ denotes the discrepancy between the inputs of the new instance **Y** and the *j*th instance **U**$_j$ in the instance base; $\alpha_m$ denotes predefined weight which is used to represent the degree of importance for the *m*th decision variable in the input.

After the values of $d_{Yj}$ for all instances are calculated, the degree of similarity of instances **Y** and **U**$_j$ can be derived by the following fuzzy membership function.

$$\mu_{Yj} = f(d_{Yj}, R_{\max}, R_{\min}) = \begin{cases} 0 & if \quad d_{Yj} \geq R_{\max} \\ \dfrac{R_{\max} R_{\min} - R_{\min} d_{Yj}}{(R_{\max} - R_{\min}) d_{Yj}} & if \quad R_{\min} < d_{Yj} < R_{\max} \\ 1 & if \quad d_{Yj} \leq R_{\min} \end{cases} \tag{2.2}$$

The terms $R_{\max}$ and $R_{\min}$ define the upper and lower bounds of the degree of difference. In case the degree of difference is less than the upper bound $R_{\max}$, any two instances are treated as similar in some measure. Obviously, Equations (2.1) and (2.2) show that the smaller the discrepancy $d_{Yj}$ is, the higher is the degree of similarity.

It is obvious that the upper bound $R_{\max}$ heavily influences the measurement of similarity. A large $R_{\max}$ implies a loose similar relationship between instances. Consequently, a large number of instances are considered as similar instances. Since the solution of the new instance is based on the similar instances been taken, a selection of large $R_{\max}$ could result in inferior solution. On the other hand, a small $R_{\max}$ indicates that a strict similar relationship is adopted. Accordingly, most of the instances in the instance base are sorted as dissimilar to the new instance, and the UFN reasoning model could generate no solution. Therefore, a linear correlation analysis is employed to systematically determine the appropriate value of $R_{\max}$.

The second step entails representing the fuzzy relationships among the new instance and its similar instances. The instances with the degree of difference smaller than $R_{\max}$ (the fuzzy membership value larger than zero, in other words) are extracted from the instance base as similar instances. Subsequently, the fuzzy set of "similar to **Y**" is then formed with the similar instances and their corresponding fuzzy membership values and is expressed by

$$S_{\sup,Y} = \{S_1(\mu_1), S_2(\mu_2), ..., S_p(\mu_p), ...\} \tag{2.3}$$

where $S_p$ is the $p$th similar instance to instance **Y;** and $\mu_p$ is the corresponding fuzzy membership value.

Finally, the solution for instance **Y** is generated by synthesizing the outputs of similar instances according to their associated fuzzy membership value through the center of gravity (COG) method. As a result, the output $Y_o$ of instance **Y** via the COG method is defined as follows:

$$Y_o = \frac{\sum_{k=1}^{p} \mu_k S_{k,o}}{\sum_{k=1}^{p} \mu_k} \tag{2.4}$$

# CHAPTER 3 DAMAGE DETECTION OF STRUCTURES VIA NEURAL NETWORKS

## 3.1 Introduction

The damage of a structure is conventionally assessed from observed dynamic responses by detecting changes in the modal parameters of the structure. The concept underlying such an approach is that damage to a structure reduces its natural frequencies, increases the modal damping, and changes the modal shapes. In early research, structural damage detection methods use natural frequencies as damage indicator. However, the frequencies are not spatially specific and are not very sensitive to damage so that its application is limited. Since mode shapes can provide much more information than natural frequencies, many studies have concentrated their efforts on damage detection with mode shapes information.

Recently, structural damage identification based on vibration monitoring techniques has paid much attention. Various damage identification algorithms have been developed for dealing with three key problems, i.e., detection of the presence of damages, detection of the structural damage locations, and estimation of the damage extents. For the problems stated above, most of the existing methods can be thought of as a two-stage algorithm in which damage locations are detected at first, and then damage extents are estimated. Generally, the first step may be more important, but probably more difficult.

Due to the features of robustness, fault tolerance, and powerful computing ability, the model of artificial neural networks becomes a promising tool in solving civil engineering problems. Masri *et al.* [66] has demonstrated in their study that neural networks are a powerful tool for the identification of systems typically encountered in the structural dynamics field. Some researches have investigated and proven the suitability and capabilities of ANNs for damage detection purposes. Consequently, the ANNs are also employed to develop the damage detection methods in this work.

By using the modal data extracted from the structural responses via the aforementioned ANNSI model, the damage locations and extents in the structure can be identified and evaluated. A two-stage damage assessment approach for building structures is used in this study. The first stage focuses on identifying the damage locations of the damaged structure by using ANNs and the second stage works on the estimation of the damage extents.

## 3.2 Damage Detection Using The UFN Model

Based on recent developments in measuring and data analyzing techniques, modal data (such as natural frequencies and mode shapes) of a structural system can easily be obtained through utilizing system identification procedure. Therefore, the damage detection approach has been developed on the basis of the available natural frequencies and mode shapes of the structures.

### 3.2.1 Index for Damage Localization

For an undamaged structure, the modal characteristics are described by the following eigenvalue equation:

$$[\mathbf{K} - \lambda_i \mathbf{M}]\phi_i = 0 \qquad \text{for } i = 1,\ldots, N \tag{3.1}$$

where $\lambda_i$ is the *i*th modal eigenvalue which presents the square of the natural frequency of the structure; $\phi_i$ is the *i*th eigenvector which presents the mode shape of the structure; $\mathbf{K}$ and $\mathbf{M}$ are symmetric system stiffness and mass matrices, respectively.

Generally, the damage of a structure is assumed to be the reduction of stiffness but not the loss of mass in structural elements, then the eigenvalue equation for such a damaged structure becomes

$$[(\mathbf{K} - \Delta\mathbf{K}) - (\lambda_i - \Delta\lambda_i)\mathbf{M}](\phi_i - \Delta\phi_i) = 0 \tag{3.2}$$

Assume the system stiffness matrix is the combination of individual member stiffness matrices. The change in stiffness matrix due to damage then be expressed as

$$\Delta \mathbf{K} = \sum_{e=1}^{N_d} \alpha_e \mathbf{k}_e \tag{3.3}$$

where $\mathbf{k}_e$ is the individual stiffness matrix for the *e*th element; $N_d$ is the total number of damaged elements in the structure; and $\alpha_e$, which is within the range between 0 and 1, is the coefficient defining a fractional change of the *e*th elemental stiffness matrix. Therefore, the index, $\alpha$, which is damage extent-dependent, makes estimation on the damage extent and the suffix, *e*, which is damage location-dependent, offers the information about the location of the damage. In the case of $\alpha_e = 0$, the *e*th structural element is not damaged. When $\alpha_e = 1$, in contrast, it means that the *e*th structural element is totally damaged. Accordingly, the problems of locating the damage site and evaluating the damage extent are focus on identifying the index *e* and computing the corresponding value of $\alpha_e$.

Expand equation (3.2) and neglect the higher order terms of $\Delta$ yields

$$-\Delta \mathbf{K}\phi_i + \Delta\lambda_i \mathbf{M}\phi_i - \mathbf{K}\Delta\phi_i + \lambda_i \mathbf{M}\Delta\phi_i = 0 \tag{3.4}$$

Pre-multiply equation (3.4) with $\phi_i^T$, the change in eigenvalue is then expressed by

$$\Delta\lambda_i = \frac{\phi_i^T \Delta \mathbf{K} \phi_i}{\phi_i^T \mathbf{M} \phi_i} \tag{3.5}$$

This equation expresses the relationship between the structural damage and the change in eigenvalue of the damaged structure. The eigenvalue change is direct proportion to the extent of damage. It is seen that the change in eigenvalue is damage location-dependent (the index, *e*) as well as damage extent-dependent (the index, $\alpha$).

Subsequently, the relationship between the structural damage and the change in eigenvector is derived. Pre-multiply equation (3.4) with the transpose of the *j*th eigenvector, $\phi_j^T$, and use the relationship, $\phi_j^T \mathbf{K} = \lambda_j \phi_j^T \mathbf{M}$, which leads to the following equation:

$$(\lambda_j - \lambda_i)\phi_j^T \mathbf{M}\Delta\phi_i = -\phi_j^T \Delta\mathbf{K}\phi_i \tag{3.6}$$

where $\Delta\phi_i$ is assumed to be a linear combination of the mode shapes [2], i.e.

$$\Delta\phi_i = \sum_{k=1}^{N} c_{ik}\phi_k \tag{3.7}$$

Substitute equation (3.7) into equation (3.6), and introduce the orthogonal property, equation (3.6) is rearranged as

$$c_{ij} = \frac{-\phi_j^{\ T}\Delta\mathbf{K}\phi_i}{(\lambda_j - \lambda_i)\phi_j^{\ T}\mathbf{M}\phi_j} \tag{3.8}$$

Impose equation (3.8) onto equation (3.6), the expression show the change in *i*th eigenvector of the system.

$$\Delta\phi_i = \sum_{j=1}^{N} \frac{-\phi_j^{\ T}\Delta\mathbf{K}\phi_i}{(\lambda_j - \lambda_i)\phi_j^{\ T}\mathbf{M}\phi_j}\phi_j \tag{3.9}$$

Again substituting $\Delta\mathbf{K}$ in the above equation with equation (3.3) yields

$$\Delta\phi_i = \sum_{j=1}^{N} \frac{-\phi_j^{\ T}\sum_{e=1}^{N_d}\alpha_e\mathbf{k}_e\phi_i}{(\lambda_j - \lambda_i)\phi_j^{\ T}\mathbf{M}\phi_j}\phi_j \tag{3.10}$$

This equation, as equation (3.6), also shows that the change in eigenvector is damage location-dependent as well as damage extent-dependent. It is clear that equations (3.6) and (3.10) show the expression of changes in modal values and vectors, respectively. The changes in modal values and vectors are direct proportion to the stiffness change.

Finally, suppose single damage or multiple damages with similar severity (i.e. all $\alpha_e$, $e$=1~$N_d$, are identical) exist in the structure. With this assumption, the expression for the change in the *i*th modal vector divided by the changes in the *j*th modal value (i.e. divide equation (3.10) by equation (3.6)), termed Damage Localization Feature (DLF) in this work, can be used as an indicator for identifying the location of structural damage.

The location of damage to a structure is dependent only on the ratio of change in modal vectors and modal values, and can be identified by matching the measured damage localization feature and the analytical damage localization feature. This kind of problem solving process may be categorized as the technique of pattern recognizing. And the unsupervised neural network model had been widely applied and approved an efficient tool for the problem of pattern recognition [67].

### 3.2.2 UFN for the Damage Detection of Structures

In the studies of damage detection that based on certain damage indices or features, two main approaches are usually adopted to deal with the detection or diagnosis process. One computed the discrepancy between the measured (or real) damage index and the FEM-based analytical damage index for all potential damage states to a structure. The case with the smallest discrepancy represents the current state for the structure [68, 69]. The other optimizes the specified objective function in which the measured information is included to search for the possible damage state [70]. Accordingly, no matter what approach is adopted, the key point of damage detection is how to rapidly and correctly identify the possible damage state according to the measured data. Therefore, one can establish the damage features for every possible damage state via the analytical FEM. When the measured damage feature is available from measurement, the damage state can then be identified through finding the same or most similar damage features. In most previous methods, the damage case with the smallest discrepancy between the measured and analytical damage features is selected to be the possible damage state on the structure. However, the identification of damage state basing on certain measured damage features is an inverse problem; two similar but different damage scenarios could possibly result in similar measured damage features. The relationship from the damage features to the damage state should be fuzzy but not crisp. Therefore, the damage cases with sufficient degree of ‘similarity’ between the measured and analytical damage features are selected as candidates to identify the damage state on the structure.

Note that, the Damage Localization Feature (DLF) was derived based on two assumptions: first, the higher order terms of $\Delta$ in equation (3.2) were neglected; second, the damage extents for multiple damages were identical when imposing equation (3.3) on equations (3.6). A consequence was made that the damage location is depended only on $\frac{\Delta\phi_i}{\Delta\lambda_j}$. That means, no matter what the damage extents are, $\frac{\Delta\phi_i}{\Delta\lambda_j}$ is invariant for the same damage class (i.e. different damage extent but same damage location). However, basing on the aforementioned two assumptions, the actual computed values, $\frac{\Delta\phi_i}{\Delta\lambda_j}$, will no longer be identical for a specific damage class. For example, the respectively computed values, $\frac{\Delta\phi_i}{\Delta\lambda_j}$, for the damage occurred at the 1st story with 10% and 20% damage extent will lead to a discrepancy between each other. The higher the difference in damage extent is, the more the discrepancy. Meanwhile, for the example of multiple damages, such as the damage occurred at the 1st and 2nd story with 10% and 20% damage extent, the computed $\frac{\Delta\phi_i}{\Delta\lambda_j}$ will also be different to that of the damage occurred at the same stories but with 20% and 10% damage extent. Even though, one can find out from the example that the DLF is still an effective feature for determining the damage location. Accordingly, the process of using DLF to find the damage location is more like pattern recognition than functional mapping. Consequently, instead of the most utilized supervised neural network (which is powerful for the functional mapping problems) in the related studies on damage detection or health motoring, this study employs an unsupervised-typed neural network model, the Unsupervised Fuzzy Neural Network (UFN) reasoning model, to implement the damage localization process.

Together with the theories of DLF and the UFN reasoning model introduced in section 2.3, this study makes use of the DLF as the input variables and the existence of the damage site as the output vector for the UFN. Basing on the analytical model, the Analytic Damage Localization Feature (ADLF) for various possible damage cases can be calculated in advance to construct an ADLF *instance base*. With proper deployment of sensors, the vibration signals of the structure can be easily measured through ambient, free, or forced vibration tests, and the modal parameters can also be generated through the ANNSI model. When the modal parameters of the structure are available, the damage location can then be located by matching the Measured Damage

Localization Feature (MDLF) with the ADLF through the UFN reasoning.

### 3.2.3 Input-Output Patterns for the Neural Network

For the UFN, the ADLF is treated as input variable of the neural network. Moreover, the output vector for the UFN represents the condition of the structural elements. Herein, binary value is adopted to represent the condition of the structural element. If the element is damaged, the value is set to be 1 to the associate element; otherwise, the value is set to be 0 to indicate an undamaged element. An example is presented in the next section to examine the feasibility of the proposed approach.

## 3.3 Estimation Of Damage Extent

After the possible damage locations were identified via damage localization procedure, the damage extent for each damage location can be assessed by the estimation algorithms. Almost all of the proposed estimation algorithms of damage extent in previous works, such as Kaouk and Zimmermann [30], Stubbs and Kim [16], Messina *et al.* [18, 19], Shi *et al.* [11, 12, 20], and Law *et al.* [71], rely on an analytical model for the real structural system to provide certain basic information, such as modal mass and elemental stiffness matrix. Based on the analytical model, the estimation algorithms can be employed to assess the structural damage extent. Herein, a simple approach for assessing the damage extent is introduced as follow.

The equation (4.2) cab be rewritten as

$$[(\mathbf{K}-\Delta\mathbf{K})-(\lambda_i-\Delta\lambda_i)\mathbf{M}](\phi_i-\Delta\phi_i)=0 \qquad (3.11)$$

Expand this equation and then pre-multiply with $\phi_i^T$ yields

$$-\phi_i^T\Delta\mathbf{K}\phi_i+\Delta\lambda_i\phi_i^T\mathbf{M}\phi_i-\phi_i^T\Delta\mathbf{K}\Delta\phi_i+\Delta\lambda_i\phi_i^T\mathbf{M}\Delta\phi_i=0 \qquad (3.12)$$

After imposed equation (3.3) on (3.12) and rearranged, equation (3.12) becomes

$$\Delta\lambda_i = \frac{\phi_i^T \sum_{e=1}^{N_d} \alpha_e \mathbf{k}_e (\phi_i - \Delta\phi_i)}{\phi_i^T \mathbf{M}(\phi_i - \Delta\phi_i)} = \frac{\phi_i^T \sum_{e=1}^{N_d} \alpha_e \mathbf{k}_e \phi_{di}}{\phi_i^T \mathbf{M} \phi_{di}} \tag{3.13}$$

where $\phi_{di} = \phi_i - \Delta\phi_i$ is the *i*th mode shape after the structure was damaged. Note that, if the higher order terms of $\Delta$ were neglected, equation (3.13) leads to equation (3.6). Furthermore, if the mode shape of the damaged structure, $\phi_{di}$, is replaced by the mode shape of the undamaged structure, $\phi_i$, equation (3.13) becomes equation (3.6)

# CHAPTER 4 SETUP FOR THE EXPERIMENTAL STUDY

## 4.1 Introduction

Researches in the theoretical development and the experimental study of structural damage diagnosis have been vigorously expanded during last two decades. Most objects of interest for analysis or experiment, however, were limited to simple structures [1-6], small-sized models or specimens [7-10], or bridge structures [11-17]. In the past years, despite Yao and his co-workers [18], Elkordy and his colleagues [19], and ASCE Structural Health Monitoring Committee [20], not too many researchers devoted themselves to the experiment investigation of the damage diagnosis in large-scaled building structures. As we know, the damage diagnosis for real-world civil structures is very difficult. Due to the inherent inconsistency between the model and real structure (especially when the size of the structure becomes larger), when the developed theories for the structural damage diagnosis were applied to practical cases, the results may not be as good as we expect, even though the theoretical analysis and the numerical results were perfect. Nevertheless, this work aims to investigate and exam the proposed methods through the conducted experiments to provide a full looks on the study of the structural health monitoring. Consequently, a scaled-down four-story steel frame has been employed to verify the damage detection study in this work. The conducted experiments aim to investigate the following topics.

(1) To verify the proposed ANN-based system identification model or approach；

(2) To verify the proposed damage detection/diagnosis strategies；

(3) To investigate the capabilities of the fiber Bragg grating sensors for structure monitoring；

(4) To explore the possibility of other damage related indicators；

(5) To provide a reference for the experiment investigation of the damage diagnosis of

large-scaled building structures.

Subsequently, the characterizations of the experimental specimen, the organization of the measuring instruments, the design of the simulated structural damage, the experiment layouts, and the preliminary analysis on the observed measurements are consecutively introduced in the following sections.

## 4.2 Shaking Table And Experimental Specimen

A series of shaking table tests of a steel frame structure for damage detection study was conducted in the laboratory in the department of civil engineering, National Chiao Tung University (NCTU). Table 4.1 depicts the basic description of the shaking table (or earthquake emulator) in NCTU. Figure 4.1 shows the appearance of the shaking table. This shaking table is a 3m long, 3m wide, and 5 tons uni-axial earthquake simulator. The maximum weight capacity of the experimental specimen for this table to carry is about 10 tons. The shaking table can simulated any earthquake in the world to the intensity of $\pm 1$ g.

The Kobe earthquake, of which the intensity is reduced to 0.08g, is used as the input excitations to the shaking table throughout the damage detection study. Figure 4.2 shows the time-history and spectrum of the input excitation (Kobe earthquake with PGA 0.08g).

A four-story steel frame was designed and constructed to perform the experiments of damage detection. The four-story test model is a 2m long, 2m wide, and 6.4m high steel frame. Lead blocks were piled on each floor such that the mass of each floor was approximately $120\, kg - s^2 / m$. The experimental specimen is designed to be a ‘soft structure’ for the sake of obtaining the modal parameters easily and explicitly. Figure 4.3 diagrams the four-story frame. The characterizations of the experimental specimen are listed in Table 4.2. The detailed cross sections of the members are shown in Figure 4.4.

According to the parameters listed in Table 4.2, an analytical model was established and analyzed via the ETABS software. Table 4.3 shows the modal parameters of the analytical model.

Note that, because the experiments were designed to execute along the transverse direction (i.e. *y*-axis), Table 4.3 only shows the modal parameters of the model along the *y*-axis.

Figure 4.5 shows the photo of the four-story steel frame after locked on the shaking table. The author would like to mention that, the steel frame shown in this photo which was constructed by the columns, beams, girders, and mass blocks but not installed with ‘strengthening column’ is termed as ‘clear frame’. The description about the strengthening column will be expanded later in Section 4.4.

## 4.3 Sensing Instrumentations

Three types of sensors, including accelerometers, electrical resistance strain gages (RSG), and optic fiber Bragg grating (FBG) sensors, were installed on the specimen to measure the structural responses during the shaking table tests. The basic information, such as the specifications and arrangements of the sensors, about the sensing instrumentations is briefly introduced in the followings.

Five accelerometers were designed to monitor the acceleration responses of the test specimen when subjected to the simulated earthquakes. Figure 4.6 shows the deployment of the accelerometers. According to the figure, four accelerometers were placed along the central line of the frame at each floor to measure the structural responses, and one accelerometer was placed at the foot of the column to measure the input base excitation to the structure. Figure 4.7 and 4.8 show the actual installations of the accelerometers at the 2nd floor and base, respectively. A simple description of the employed accelerometers is listed in Table 4.4 in which the symbols A1 to A4 represent the accelerometers at the 1st to 4th floor, respectively, and the symbol Abase represents the accelerometer at the base.

Fiber Bragg grating sensors are one of the most exciting developments in the field of optical fiber sensors in recent years. Since the pioneering work done by Meltz *et al.* [21], subsequent interest in FBG sensors has increased considerably. One of the probable main reasons for this is that, FBG sensors have great potential for a wide range of sensing applications for important physical quantities, such as strain, temperature, pressure, acceleration [22-24], etc. It this work, the FBG sensors are used for measuring the strain responses of the structure during earthquakes. FBG sensors have a number of distinguishing advantages which make them a promising candidate for smart structures. When compared with RSG used for strain monitoring, FBG sensor have several distinguishing advantages, including [25]

(1) much less intrusive mass and size;

(2) much better immunity to electro-magnetic interference;

(3) greater capacity of multiplexing a large number of sensors along a single fiber link, unlike RSGs which need a huge amount of wiring;

(4) greater resistance to corrosion when used in open structures, such as bridges and dams;

(5) higher temperature capacity (typically about $300^{\circ}C$);

(6) longer lifetime for long term operation.

These features have made FBG sensor very attractive for health monitoring of smart structures.

***<u>Sensing principle of FBG sensor</u>***

An FBG is written into a segment of Ge-doped single mode fiber in which a periodic modulation of the core refractive index is formed by exposure to a spatial pattern of ultraviolet light in the region of 244-248 nm. The lengths of FBG sensors are normally within the region of 1-20mm and grating reflectivities can approach ~100%. Being a recent developed technique for civil engineering, the sensing principle of FBG sensor is briefly introduced herein. When the FBG is illuminated by a broadband light source, each FBG sensor in a fiber reflects a specific wavelength that shifts slightly depending on the strain applied to the sensor. The change in wavelength is directly proportional to the change in mechanical features such as strain or temperature.

In its simplest form a fiber Bragg grating consists of a periodic modulation of the refractive index in the core of a single-mode optical fiber (Figure 4.9). According to Bragg's law, reflected Bragg wavelength, $\lambda_B$, is given by

$$\lambda_B = 2n_{\text{eff}}\Lambda \tag{4.1}$$

where $n_{\text{eff}}$ represents the effective refractive index of the fiber core and $\Lambda$ is the period of the index modulation.

The Bragg wavelength is the free space center wavelength of the input light that will be back-reflected from the Bragg grating. The Bragg grating resonance, which is the center wavelength of reflected light from a Bragg grating, depends on the effective index of refraction of the core and the periodicity of the grating. The effective index of refraction, as well as the periodic spacing between the grating planes, will be affected by changes in strain and temperature. While the strain effect, which corresponds to a change in the grating spacing and the strain-optic induced change in the refractive index, is considered (Figure 4.10), the Bragg wavelength change can be expressed as

$$\Delta\lambda_B = 2n^*_{\text{eff}}\Delta\Lambda \tag{4.2}$$

where $n^*_{\text{eff}}$ is the changed effective refractive index. Hence the wavelength shift, $\frac{\Delta\lambda_B}{\lambda_B}$, can be derived.

$$\frac{\Delta\lambda_B}{\lambda_B} = \frac{2n^*_{\text{eff}}\Delta\Lambda}{2n_{\text{eff}}\Lambda} = \frac{n^*_{\text{eff}}}{n_{\text{eff}}}\frac{\Delta\Lambda}{\Lambda} = \kappa_\varepsilon\frac{\Delta l}{l} = \kappa_\varepsilon\varepsilon \tag{4.3}$$

where $\kappa_\varepsilon$ is a strain-sensitive coefficient. Furthermore, the Bragg wavelength shift due to the temperature effect may be written as

$$\frac{\Delta\lambda_B}{\lambda_B} = (\xi + \alpha)\Delta T = \kappa_T\Delta T \tag{4.4}$$

where $\Delta T$ is the change in temperature; $\xi$ is the thermal optical coefficient; $\alpha$ is the thermal expansion coefficient; and $\kappa_T$ represents the thermal-sensitive coefficient. Combining equations

(4.3) with (4.4), the Bragg wavelength shift due to strain and thermal effects can be expressed as

$$\frac{\Delta\lambda_B}{\lambda_B} = \kappa_\varepsilon \varepsilon + \kappa_T \Delta T \quad (4.5)$$

Further details about the FBG sensor technology and its applications can be found in related books or review articles, such as Othonos and Kalli [26], Kashyap [27], and Rao [25, 28].

According to the experiments the strain-sensitive and thermal-sensitive coefficients provided by the Prime Optical Fiber Corporation (POFC, Hsinchu, Taiwan) are about 0.80 and $5.88\times10^{-6}$, respectively, which make equation (4.5) becomes

$$\frac{\Delta\lambda_B}{\lambda_B} = 0.80\varepsilon + 5.88\times10^{-6}\Delta T \quad (4.6)$$

Then the strain or temperature variation can be converted from the wavelength change by the following relationship.

$$1pm \approx 0.8\mu\,\text{strain} \approx 0.1^\circ C \quad (4.7)$$

***<u>FBG Data Acquisition System</u>***

An FBG data acquisition system, including the MOI's (Micron Optics, Inc.) Fiber Bragg Grating Swept Laser Interrogator (FBG-SLI) and a notebook (Figure 4.11), is adopted to monitor and restore the FBG wavelength data.

The FBG-SLI is a high-power, fast, multi-sensor measurement system that provides a major advancement for mechanical sensing applications. The FBG-SLI combines the speed of MOI's unique Swept Laser technology and the accuracy of the patented picoWave reference technique to resolve changes in optical wavelengths of approximately 1pm (<1 $\mu$ strain) and achieve high calibrated wavelength accuracy. It is a complete system that includes a swept source used to illuminate the FBG sensors and the four detectors, which simultaneously measure the reflected optical signals on each fiber. All sensors (maximum of 64 FBG sensors per fiber) on all channels are scanned simultaneously at a maximum rate of 108Hz. Table 4.5 lists the specification of the FBG-SLI.

A block diagram of the optical layout is shown in Figure 4.12. The swept laser illuminates the Bragg gratings and each FBG sensor reflects its corresponding wavelength. The Fiber Fabry-Perot Tunable Filter (FFP-TF) simultaneously scans the reflected wavelengths from the FBG sensors and the picoWave reference. Through the detector circuitry and software, the detected signals are converted to wavelengths. A PC or notebook provides the on-line calibration, data display/storage, and the FBG sensors under test.

***FBG sensors arrangement***

There are 12 FBG sensors along two fibers were employed in this work to monitor the strain responses of the test frame during excitations. Eight FBG sensors were arranged along one fiber link which was connected to the first channel (terms as Channel 1) of the FBG-SLI, and four FBG sensors were arranged along another fiber link which was connected to the second channel (terms as Channel 2) of the FBG-SLI. The descriptions of the specification and arrangement of the FBG sensors along Channel 1 and Channel 2 are shown in Tables 4.6 and 4.7 and Figure 4.13, respectively. Figures 4.14 and 4.15 display the transmission and reflection spectra of the FBG sensors on Channel 1 and Channel 2, respectively.

The FBG sensors were attached to the columns at each story to measure the strain responses of the test frame. The FBG sensors along Channel 1 were located near the top and the bottom of the story columns on east side; meanwhile, the FBG sensors along Channel 2 were located near the bottom of the story columns on west side. A sketch of the deployment of the FBG sensors is also demonstrated in Figure 4.5. The actual attachments of FBG1 and FBG2 on Channel 1 and FBG9 on Channel 2 are shown in Figure 4.16, Figure 4.17, and Figure 4.18, respectively. Note that, FBG1 and RSG1 in Figure 4.16 were installed near the bottom of the column of 1st story on east side, FBG2 in Figure 4.17 was installed near the top of the column of 1st story on east side, and FBG9 in Figure 4.18 was installed near the bottom of the column of 1st story on west side.

In addition to the FBG sensors, four RSGs were also adopted as a reference to the FBG sensors. Therefore, one RSG was attached right beside the FBG sensor to the bottom of the column of each story, as shown in Figure 4.16. The RSGs configuration was also depicted in Figure 4.6.

## 4.4 Damage Simulation

There are several kinds of mechanisms for damage simulation according to the study objectives of interest. By reviewing the numerical or experimental studies in damage detection or assessment during these years, the simulations of structural damage are classified into the following categories.

(1) For beams-like or bridge structures:

— decreasing the stiffness of the elements numerically [29];

— reducing the thickness or cross-section of the selected elements [4, 14, 30-34];

— support failure and/or crack degradation [2, 11, 35, 36].

(2) For truss structures:

— reducing the cross-section or Young's modulus of the bars to simulate the axial stiffness failures [31, 37, 38];

— loss of stiffness and mass of members [39].

(3) For building or frame structures:

— loosing the beam-column joints to simulate joints failures [40, 41];

— weakening the story stiffness via the reduction in bracing areas [19];

— reducing the flexural stiffness of the beams belonging to the corresponding floors [42].

### 4.4.1 Strengthening Column

The damage in a structure is assumed in this work to be the change in story stiffness. In most experimental studies of damage detection which is based on such an assumption commonly used bracing elements as simulations [19]. This work, however, employs a different type of mechanism, called the 'strengthening column (SC for short)', as simulations to the structural damage.

Most of the past experimental studies focus on high-level damage extent, and most of the successful diagnoses were usually based on the high-level damage. Small extent damage is not as easy and evident as large extent damage to be identified and assessed because of many uncertainties and errors such as boundary conditions, measurement errors, ambient noise, and computation errors. Even though, this work attempts to investigate that if the small extent (or low-level) damage as well as the large extent (high-level) damage can be successfully identified and diagnosed.

Compare with the experimental specimens in the works conducted by Elkordy [19] and Koh [7], the specimen in this work is heavier and bigger. Furthermore, according to the analysis result from ETABS software, even small cross-section of bracing can provide significant lateral stiffness which results in considerable changes in the natural frequencies of the structure. In order to investigate whether small damage in a structure can be detected and assessed, simulation on small damage scenario is also considered in this work. Consequently, instead of using the bracing, the SC is designed to provide the specimen with additional lateral stiffness. The element selected to perform as SC is the lightweight 'C' shape steel. Table 4.8 and Figure 4.19 show the detailed dimension of the SC and how the SC is connected to the beams, respectively. Note that, the symbols 'SC-A' and 'SC-B' in Table 4.8 denote the SCs whose cross sections are $C100\times50\times20\times2.3$ and $C75\times45\times15\times2.3$, respectively. The SC was fixed with 4 bolts at each end to the top and bottom of the story beams. The actual installation of the SC at the 1st story is depicted in Figure 4.20.

The clear frame that combines with 6 SCs-A at the 1st to 3rd stories (2 SCs at each floor from 1st to 3rd stories) is defined as the 'intact (or healthy) structure'. Figure 4.21 shows a photo of the intact structure. Alternatively, the frame that incorporated with smaller SCs (to simulate a slight damage scenario) or without SC (to simulate a considerable damage scenario) is treated as ‘damaged structure’.

### 4.4.2 Simulated Damage Cases

Herein, both single-site damage cases and multiple-site damage cases are simulated. Table 5.9 lists all the damage cases in studying. For convenience and simplicity, certain notations to the damage cases are assigned. Refer to Table 4.9, the notation *AAA* represents an undamaged case in which the test frame was installed with 6 SCs-A at the 1st to 3rd stories (2 SCs at each floor). The rest cases which are pre-noted with ‘*Dcase*’ represent the damage cases. Furthermore, the symbols ‘A’ , ‘B’, and ‘N’ represent SC-A, SC-B, and without SC, respectively. For example, ‘A-B-N’ of case *Dcase_ABN* means that the frame was installed with the SCs-A at the 1st story, the SCs-B at the 2nd story, and without SC at the 3rd story. It is seen from Table 4.9 that, *Dcase_BAA* and *Dcase_NAA* are damage cases in which the damage was induced by reduction in the story stiffness at the 1st story. Hence, the damage class for these cases is denoted by $Dclass\_k_1$. Similarly, if the SCs at the 1st and 2nd story were removed from the intact structure, this damage case and its corresponding damage class are denoted by *Dcase_NNA* and $Dclass\_k_1\&k_2$, respectively.

## 4.5 Experimental Scheme

Starting from the shaking table test of the intact structure, the simulated damage events, listed in Table 4.9, are then in turn implemented on the shaking table. The base excitation that inputs to the shaking table is the Kobe earthquake whose intensity is reduced to the level of PGA 0.08g. The sampling rate of the acceleration and RSG records is 200Hz. Table 4.10 shows the operation sequence of the shaking table tests and how the response records are denoted for simplicity.

## 4.6 Pre-Analysis Of The Measured Data

Some statistical properties about the acceleration measurements are listed in Table 4.11. According to the statistics, several findings are discussed as follow.

(1) Because the input excitations for each shaking table test are the same, the influence of the induced damage to the test frame can be directly discussed basing on the structural response.

(2) The effect of replacing the smaller SCs (SC-B in Table 4.8), according to Table 4.11, is much lesser than that of removing the SCs. For example, the measurements of the damage case *Dcase_BAA* are slightly higher than that of the intact case *AAA* (the max(*acc.*)= 0.001, 0.010, 0.009, 0.023); in contrast, the measurements of *Dcase_NAA* increase significantly (the max(*acc.*)= 0.012, 0.025, 0.039, 0.014). Similar situations also happen to other damage cases, such as *Dcase_ABA* and *Dcase_ANA*, *Dcase_AAB* and *Dcase_AAN*, etc. This phenomenon is welcome because it meets the requirement for studying both the low-level and high-level damage in the structure.

(3) Due to the insignificance of replacing the SC-A with SC-B to the structure, the measurement discrepancy between each other is small (i.e. the responses are similar to each other), especially when the SCs were replaced from only one story. For instance, compare the case *AAA* with *Dcase_AAB* whose SCs at the 3rd story were replaced with SCs-B, the relative increments of the maximum response for each floor are only -3.9%, 6.0%, 4.9%, and 0.8%. Similar situations also happen to *Dcase_ANA* and *Dcase_BNA*, *Dcase_NAA* and *Dcase_NBA*, and *Dcase_AAN* and *Dcase_ABN*, etc.

(4) Following with the finding 3, this phenomenon could possibly lead to similar identification results of modal parameters.

As mentioned previously, 12 FBG sensors were configured along two fiber links, Channel 1 and Channel 2. These 12 FBG sensors are further classified, according to their locations, into three groups: the sensors which located near the bottom of the story columns on east side (i.e. FBG1, FBG3, FBG5, and FBG7) will be shortly called ‘sensors at BE’; the sensors which located near the top of the story columns on east side (i.e. FBG2, FBG4, FBG6, and FBG8) will be shortly called ‘sensors at TE’; and the sensors which located near the bottom of the story columns on west side (i.e. FBG9 to FBG12) will be shortly called ‘sensors at BW’. Statistical results of the FBG sensors’ records, based on the three groups, are summarized in Tables 4.12 to 4.14, respectively. Meanwhile, statistical summaries of the RSGs’ records are shown in Table 4.15. Based on the summarized tables of the acceleration and strain measurements (Tables 4.11 to 4.15), certain findings are presented below.

(1) Compare with the acceleration responses, the strain row data (from either FBG sensors or RSGs) shows more sensitivity to the system changes. The changes in maximum measurement of the acceleration responses (column IV, Table 4.11) are smaller than that of the strain responses (column IV, Tables 4.12 to 4.15). Take the case *Dcase_NNN* for example, the maximum relative increments in acceleration and strain responses are 68.5% (4F) and 122.3% (FBG5), respectively.

(2) One of the major advantages of the FBG sensors is that they have better immunity to EM interference. Therefore, the signals of the FBG sensors is lesser noise-corrupted. This situation can be validated from two aspects. Firstly, according to the comparison between the FBG sensors’ and RSGs’ records, a number of disturbances containing in the RSGs records. Secondly, the ratio, ($\frac{\text{std}(\varepsilon)}{\max(\varepsilon)}$), between the standard deviation of the response (std($\varepsilon$)) and the maximum response (max($\varepsilon$)) for the RSGs’ records (Table 5.15) is larger than that for the FBG sensors’ records (Table 4.12).

(3) As mentioned before, one of the functions of the RSGs is to be a reference to the FBG sensors.

(4) The FBG sensors at BE were placed at the opposite position of the story columns to the FBG sensors at TE. Therefore, the measurements they obtained should be with similar magnitude but negative phase. Take the case *AAA* once again for example, the correlation coefficients between the measurements of the FBG sensors at BE and the measurements of the FBG sensors at TE are $\{-0.9993, -0.9998, -0.9998, -0.9995\}$

which mean that these two sets of data are highly correlated in negative phase.

(5) Four FBG sensors (from FBG9 to FBG12) were placed at BW to have parallel location with the FBG sensors at BE so as to check torsional effect of the specimen. The correlation coefficients between the data of these two figures are $\{0.9997, 0.9989, 0.9995, 0.9985\}$ which mean that these two sets of data are highly correlated.

# Chapter 5 Health Monitoring On The Test Frame

## 5.1 Introduction

In Chapters 3 and 4, neural network-based system identification methods and a two-stage damage assessment approach were proposed and examined by either numerical examples or laboratory measurements. The examined results have preliminarily shown their capabilities of dealing with the associated problems. By conducting a series of shaking table tests for the health monitoring study, the proposed methods and approach are further investigated by the experimental measurements.

In implementing the health monitoring of the test structure, three strategies are carried out. By using the first strategy, the acceleration measurements of each simulated damage case are first analyzed using the ANNSI model to generate the modal frequencies and displacement modal shapes of the test structure. The structural condition of the specimen can then be diagnosed based on the identified modal data change. In the second strategy, the health monitoring of the test structure is basing on the changes in strain mode shape information. The strain mode shapes are extracted from the FBG sensors and RSGs measurements by also using the ANNSI model. Moreover, the global and decentralized monitoring networks are adopted for the purpose of health monitoring using the structural acceleration and strain measurements in the third strategy. The three strategies are sequentially introduced in the subsequent sections. Notably, according to the nature of the damage detection procedure in the strategy, the first strategy is model-based; while the second and third strategies are non-model-based. Moreover, though three different strategies for structural health monitoring are utilized, they should produce similar diagnostic results.

## 5.2 Modal Analysis Using The ANNSI Model

Based on the empirical and trail-and-error methods as well as the preliminarily analysis on the Fourier spectra of the experimental measurements, the appropriate architecture of the modal analysis network (MAN) in ANNSI model is determined. The acceleration measurements are first analyzed to obtain the corresponding modal parameters. Subsequently, the strain measurements from the FBG sensors and RSGs are also analyzed to generate the strain mode shapes information. Those modal data will be further applied to monitor and assess the structural conditions.

### 5.2.1 Modal Data of the Specimen Extracted from the Acceleration Measurements

The acceleration measurements from the intact structure (i.e. AAA_acc, in Table 4.10) are first analyzed using the ANNSI model to obtain the baseline information. Figure 5.1 presents the response time-histories of the AAA_acc measurement. It is seen that, the larger responses happened to the time between 4.5 and 15 seconds. Therefore, the measurements between 5 and 12.5 seconds (i.e. 1500 records with 200Hz sampling rate) are used throughout this chapter to train the neural networks. Figure 5.2 shows the excellent correspondence between the measured responses and the computed responses from the trained MAN.

After the MAN was trained by the AAA_acc measurement, the modal parameters of the intact structure can be estimated based on the connective weights of the trained MAN. Table 5.1 presents the identified baseline modal data extracted from the acceleration measurements.

Basing on the aforementioned MAN structure, each of the rest acceleration measurements obtained from the shaking table tests on the simulated damaged structures is trained by a MAN and then extracted the corresponding modal parameters from it. Tables 5.2 to 5.25 show the modal parameters for each simulated damage case listed in Table 6.9. Note that, the *MAC* values in those tables were computed with respect to the mode shapes of the intact structure.

According to the tables, some discussions are addressed below.

(1) As discussed in section 4.6, the effect of replacing the smaller SCs is much lesser than that of removing the SCs; therefore, the modal parameters changed more when the SCs were removed from the test structure.

(2) According to Tables 5.1, 5.2, 5.4, and 5.6, the 1st modal frequencies of the low-level damage scenarios are very close to each other. In addition, the 1st and 2nd modal frequencies of *Dcase_ABA* are slightly higher than the baseline values. As known, the loss of mass and enhancement of stiffness increase the natural frequencies. Though the stiffness provided by the SC-A is more than by the SC-B, the SC-A is heavier than the SC-B. Accordingly, the reason for the above circumstance may be that the effectiveness of the stiffness to the 1st and 2nd modes of *Dcase_ABA* is lower than that of the mass.

(3) Since the structures of the cases of *Dclass_*$k_1$&$k_2$ are damaged at the 1st and 2nd stories, they should exhibit the properties of *Dclass_*$k_1$ and *Dclass_*$k_2$ mentioned in last discussion. In *Dcase_NBA*, the structure was damaged at the 1st and 2nd stories, and the damage extent at the 1st story is higher than at the 2nd story. Therefore, the amounts of changes in modal frequencies for all modes exceed 3%. Moreover, the structure damaged more seriously at the 2nd story than at the 1st story in *Dcase_BNA*, which causes changes in modal frequencies for all modes except for the 2nd mode exceed 3%. Similar situations also happen to the cases of *Dclass_*$k_1$&$k_3$ and *Dclass_*$k_2$&$k_3$.

(4) Though certain measurements produced the same identified results on the 1st modal frequency, such as *Dcase_NAA*, *Dcase_BNA*, *Dcase_NAB*, and *Dcase_NBB*, the rest modal frequencies of these cases are different from each others because they belong to different damage classes. Therefore, it is quite difficult to detect structural damage basing only on one modal frequency in the modal-based damage detection methods.

### 5.2.2 Modal Data of the Specimen Extracted from the RSGs Measurements

Since the structural strains can reflect local changes in a structure, the strain mode shapes (SMSs) would be a sensitive indicator for identifying the location of the structural damage. In the experiments of this work, two sets of strain data from the RSGs and the FBG sensors were recorded. The ANNSI model is also applied to the observed strain measurements to obtain the SMSs of the specimen.

The strain measurements from the RSGs were first analyzed. The identified modal parameters are listed in Tables 5.26 to 5.50. According to the experiences during modal analysis and these tables, some observations are discussed below.

(1) The order needed for the 1st and 2nd modes to be identified is lower than that for the 3rd and 4th modes. This may caused by the noise that contaminated in the RSGs measurements.

(2) Compare with the modes been identified from the acceleration measurements, only the first three modes can be identified from the RSGs measurements for most cases except for *Dcase_NNA*, *Dcase_BAB*, and *Dcase_ANN*.

(3) The 1st and 2nd modal frequencies been identified from acceleration and RSGs measurements are almost identical. Though the 3rd modal frequency been identified from the RSGs measurements is slight differ from that from the acceleration measurements, the maximum discrepancy between them is lesser than 1.2% (*Dcase_AAN*).

(4) The modal damping been identified from the RSGs measurements is close to the one from the acceleration measurements.

### 5.2.3 Modal Data of the Specimen Extracted from the FBG Sensors Measurements

Aforementioned, FBG sensors have much better immunity to electro-magnetic interference; therefore, the noise effect when using FBG sensors is much smaller than when using RSGs. This has been first discussed in section 4.6, and will be further examined here. Following the same procedure when analyzing the RSGs measurements, the FBG sensors measurements are also analyzed to obtain the corresponding strain mode shapes information. Only the records from the FBG sensors on Channel 1 (i.e. FBG1 to FBG8) are used for modal analysis. The identified results obtained from the FBG sensors measurements for each simulated damage case are shown in Tables 5.51 to 5.75.

Before discussing the identified results, certain important things should be noted in advance. Although the rate for sampling the FBG sensors measurements is set to be 106Hz, the sampling rate did not stay constant during the test; it fluctuated around 106Hz. While the sampling rate for the input excitation is set to be constant 200Hz. The input excitations for each damage case are re-sampled with 106Hz by using linear interpolation method before they are used for modal analysis due to the inconsistent in sampling rates of the structural responses and input excitation. Theoretically, no matter what measurements (such as structural displacement, velocity, acceleration, and strain) are used for modal analysis, the identified modal frequencies for the same structure should be identical to each other. Subject to the problems of fluctuant sampling rate and data re-sampling, however, the identified modal parameters extracted from the FBG sensors measurements could be different to those based on the RSGs measurements. According to the identifications, it can be concluded that:

(1) Generally, the signal noise increases the difficulty of system identification. More explicitly, since the signals from the FBG sensors are cleaner than those from the RSGs, the order needed for the ANNSI model when using the FBG sensors measurements is much lesser than when using the RSGs measurements. The number of order needed for identifying the lower modes is quite small. This feature is attractive in on-line system identification because smaller order implies quicker identification.

(2) Unlike the identification results obtained from the RSGs measurements, four modes in most cases can be successfully identified by using the FBG sensors measurements. This feature is advantaged in the cases of higher modes are needed. For example, it has been seen that the changes in lower modes for slight damage scenarios are not distinct enough to indicate damage, while the changes in higher modes, though their accuracies are lower, are distinguishable to signify possible damage.

## 5.3 Damage Detection With The Monitoring Networks

The global and decentralized monitoring networks were preliminarily examined by either laboratory or numerical example, respectively, in previous sections. The results had shown their potentials for applying to the practical situations. In this section, they are further investigated by the experimental data obtained from the conducted shaking table tests on a four-story steel frame structure. Acceleration measurements as well as strain measurements from FBG sensors are used for investigations.

For health monitoring purpose, the MAN that had been trained by the measurements from an intact structure is employed to play the role of monitoring unit. The trained MAN should be capable of generating the system outputs from it within a tolerable error range if the structure does not change. On the contrary, if the structural characteristics of target structure changed significantly, the trained MAN for the intact structure will no more suitable for representing the current state of the structure; as a result, the generated outputs from the trained MAN will differ from the measured responses from the damaged structure.

The health monitoring approach of using global monitoring network is applied to the acceleration and strain measurements, respectively. Notably, the strain measurements used in this section are the ones observed from the FBG sensors (FBG1 to FBG8). Start from the acceleration measurements, each set of measurements of the 24 damage cases is fed into the MAN trained by the AAA_acc measurement. The relative changes in prediction error are shown in Figure 5.3. Since the global monitoring network provides global view on structural condition, the prediction error is derived by calculating the average of MAEs of every DOF. It is seen from Figure 5.3 that the structural damage indeed increases the prediction error of the monitoring network. However, it is not easy to affirm structural damage from comparing any two of data, especially when the damage is not significant. Therefore, continuous monitoring on a structure is essential.

If the FBG sensors measurements are used for health monitoring by using global monitoring network, the prediction errors of the 24 damage cases are depicted in Figure 5.5. Likewise, the results of the six cases for simulating the degradation development in a structure are shown in Figure 5.6. Compare the results of these two figures with those of Figures 5.3 and 5.4, the results show the similar trend while the structure was damaged though there were slight difference existed between them. Moreover, the increments in prediction error of strain measurements are larger than those of acceleration in serious damage cases. For examples, the relative increments in prediction error of acceleration and strain measurements for *Dcase_NAA* are within 100% and beyond 300%, respectively; the maximum values in Figures 5.3 and 5.5 are about 175% and 870%, respectively.

# CHAPTER 6 CONCLUDING REMARKS

The main purpose of this work attempts to assemble a framework of a health monitoring system for smart structures based on ANN models. By investigating from analytical study to experimental study, the proposed framework for an ANN-based integrated system for structural monitoring and damage diagnosis is revealed adaptive and feasible. According to the study results shown in this research, they are summarized and discussed in the succeeding sections.

(1) The ANNSI model successfully identified the structural modal parameters of the specimen under various damage states from the measurements of the accelerometers, FBG sensors, and RSGs. The identified results show consistency between each of them.

(2) The induced damage can be reflected by the changes in structural modal parameters of the specimen. However, the modal parameters changes of the lower mode are not significant in the structure with slight damage.

(3) The FBG sensors do show their potentials in system identification and monitoring. The noise effect of the FBG sensors measurements is much smaller than that of the RSGs and accelerometers. This will make the identification easier when using the FBG sensors data. Furthermore, the distinguishing advantages of much less mass and great capacity of multiplexing a large number of sensors along a single fiber link make FBG sensors promising for health monitoring of practical structures.

(4) Compare with the CMS that based on the displacement mode shapes, the CSMS that based on the strain mode shapes is more sensitive to the structural damage. Moreover, the location of damage can be reflected by the sensing stations with larger value of CSMS. By using this approach, the damage location for the most simulated damage

cases can be identified.

(5) The damage detection strategy that based on the prediction errors from the monitoring networks is easy to implement without limitation on the number of sensors. The increasing prediction error from the global monitoring network in the simulation of degradation development signifies deterioration of the structural integrity. Moreover, the larger prediction errors from the decentralized neural networks indicate the locality of the structural damage.

(6) Although the damage detection method that based on the DLF and the UFN model failed to be applied to the experimental measurements due to the problem of without a suitable analytical model, the damage diagnosis of the structure can still be carried out by other proposed strategies. If a suitable analytical model is available, the damage diagnosis of the structure will be improved and enhanced.

(7) Since the methods and approaches involved in the system are mainly based on ANNs, the system is adaptive because ANNs are expected to improve their performance as they experience more episodes form the reality.

(8) The damage detection mechanism of the system was designed to integrate different diagnosis strategies to implement the similar tasks. In this way, even one of the diagnosis strategies fails to perform its duty, the system can still work properly.

(9) The system is independent of the methods used in each mechanism and is expandable. Any effective or improved method can be added to the corresponding mechanism to enhance the performance of the whole system.

# REFERENCE


[1] Salawu, O. S., "Detection of structural damage through changes in frequency: a review," Engineering Structures, 19(9), pp. 718-723, 1997.

[2] Alampalli, S. and Fu, G. K., "Full scale dynamic monitoring of highway bridges," Structural Engineering in Natural Hazards Mitigation, 1(pp. 1602-1607, 1993.

[3] Salawu, O. S. and Williams, C., "Bridge assessment using forced-vibration testing," Journal of Structural Engineering, ASCE, 121(2), pp. 161-173, 1995.

[4] West, W. M., "Illustration of the use of modal assurance criterion to detect structural changes in an orbiter test specimen," Proc., 4th International Modal Analysis Conference, 1986.

[5] Lieven, N. A. J. and Ewins, D. J., "Spatial correlation of mode shapes, the coordinate modal assurance criterion (COMAC)," Proc., 5th International Modal Analysis Conference, 1988.

[6] Biswas, M., et al., "Diagnosis experiment spectral/modal analysis of highway bridges," The International Journal of Analytical and Experimental Modal Analysis, 5(1), pp. 33-42, 1990.

[7] Cawley, P. and Adams, R. D., "The location of defects in structures from measurements of natural frequencies," Journal of Strain Analysis, 14(2), pp. 49-57, 1979.

[8] Penny, J. E. T., et al., "Damage location in structures using vibration data," Proc., 11th Internatiional Modal Analysis Conference, Kissimee, FL., 1993.

[9] Contursi, T., et al., "A multiple-damage location assurance criterion based on natural frequency changes," Journal of Vibration and Control, 4(5), pp. 619-663, 1998.

[10] Hearn, G. and Testa, R. B., "Modal analysis for damage detection in structures," Journal of Structural Engineering, ASCE, 117(10), pp. 3042-3063, 1991.

[11] Shi, Z. Y., et al., "Structural damage localization from modal strain energy change," Journal of Sound and Vibration, 218(5), pp. 825-844, 1998.

[12] Shi, Z. Y., et al., "Structural damage detection from modal strain energy change," Journal of Engineering Mechanics, ASCE, 126(12), pp. 1216-1223, 2000.

[13] Zimmermann, D. C. and Kaouk, M., "Structural damage detection using a subspace rotation algorithm," Proc. AIAA 33rd Structures, Structural Dynamics, and Materials Conference, Dallas, TX, 1992.

[14] Lim, T. W. and Kashangaki, T. A. L., "Structural damage detection of space truss structures using best achievable eigenvectors," AIAA Journal, 32(5), pp. 1049-1057, 1994.

[15] Yao, G. C., et al., "Damage diagnosis of steel frames using vibrational signature analysis," Journal of Engineering Mechanics, ASCE, 118(9), pp. 1949-1961, 1992.

[16] Stubbs, N. and Kim, J. T., "Damage localization in structures without baseline modal parameters," AIAA Journal, 34(8), pp. 1644-1649, 1996.

[17] Topole, K. G. and Stubbs, N., "Non-destructive damage evaluation of a structure from limited modal parameters," Earthquake Engineering and Structural Dynamics, 24(12), pp. 1427-1436, 1995.

[18] Messina, A., et al., "Damage detection and localisation using natural frequency changes," Proc., Identification in Engineering Systems, Swansea, Wales, 1996.

[19] Messina, A., et al., "Structural damage detection by a sensitivity and statistical-based method," Journal of Sound and Vibration, 216(5), pp. 791-808, 1998.

[20] Shi, Z. Y., et al., "Damage localization by directly using incomplete mode shapes," Journal of Engineering Mechanics, ASCE, 126(6), pp. 656-660, 2000.

[21] Lin, C. S., "Location of modeling errors using modal test data," AIAA Journal, 33(9), pp. 1650-1654, 1995.

[22] Pandey, A. K. and Biswas, M., "Damage diagnosis of truss structures by estimation of flexibity change," International Journal of Analytical and Experimental Modal Anal, 10(2), pp. 104-117, 1995.

[23] Pandey, A. K., et al., "Damage detection from chamges in curvature mode shapes," Journal of Sound and Vibration, 145(2), pp. 321-332, 1991.

[24] Cornwell, P., et al., "Application of the strain energy damage detection method to plate-like structures," Journal of Sound and Vibration, 224(2), pp. 359-374, 1999.

[25] Ratcliffe, C. P., "Damage detection using a modified Laplacian operator on mode shape data," Journal of Sound and Vibration, 204(3), pp. 505-517, 1997.

[26] Wahab, M. M. A. and Roeck, D. D., "Damage detection in bridges using modal curvatures: application to a real damage scenario," Journal of Sound and Vibration, 226(2), pp. 217-235, 1999.

[27] Ricles, J. M. and Kosmatka, J. B., "Damage detection in elastic structures using vibratory residual forces and weighted sensitivity," AIAA Journal, 30(9), pp. 2310-2316, 1992.

[28] Kosmatka, J. B. and Ricles, J. M., "Damage detection in structures by modal vibration characterization," Journal of Structural Engineering, ASCE, 125(12), pp. 1384-1392,

1999.

[29] Zimmermann, D. C. and Kaouk, M., "Structural damage detection using a minimum rank update theory," Journal of Vibration and Acoustics, ASME, 116(pp. 222-231, 1994.

[30] Kaouk, M. and Zimmermann, D. C., "Structural damage assessment using a generalized minimum rank perturbation theory," AIAA Journal, 32(4), pp. 836-842, 1994.

[31] Shi, Z. Y., et al., "Optimum sensor placement for structural damage detection," Journal of Engineering Mechanics, ASCE, 126(11), pp. 1173-1179, 2000.

[32] Koh, C. G., et al., "Damage detection of buildings: numerical and experimental studies," Journal of Structural Engineering, ASCE, 121(8), pp. 1155-1160, 1995.

[33] Shi, Z. Y., et al., "Improved damage quantification from elemental modal strain energy change," Journal of Engineering Mechanics, ASCE, 128(5), pp. 521-529, 2002.

[34] Golden, R. M., Mathematical methods for neural network analysis and design. MIT Press, Cambridge, MA., 1996.

[35] Adeli, H. and Hung, S. L., "A fuzzy neural network learning model for image recognition," Integrated Computer-Aided Engineering, 1(1), pp. 43-55, 1993.

[36] Adeli, H. and Hung, S. L., Machine Learning- Neural Networks, Genetic Algorithms, and Fuzzy Systems. John Wiley & Sons, New York, NY, 1995.

[37] Adeli, H. and Park, H. S., Neurocomputing in design automation. CRC Press, Boca Raton, FL, 1998.

[38] Haykin, S., Neural networks: a comprehensive foundation. Prentice-Hall, Englewood Cliffs, NJ., 1999.

[39] Ghaboussi, J., et al., "Knowledge-based modeling of material behavior with neural networks," Journal of Engineering Mechanics, ASCE, 117(1), pp. 132-153, 1991.

[40] Wu, X., et al., "Use of neural networks in detection of structural damage," Computers and Structures, 42(4), pp. 649-659, 1992.

[41] Elkordy, M. F., et al., "Neural networks trained by analytically simulated damage states," Journal of Computing In Civil Engineering., ASCE, 7(2), pp. 130-145, 1993.

[42] Szewezyk, P. and Hajela, P., "Damage detection in structures based on feature-sensitive neural network," Journal of Computing In Civil Engineering., ASCE, 8(2), pp. 163-178, 1994.

[43] Pandey, P. C. and Barai, S. V., "Multilayer perceptron in damage detection of bridge structures," Computers and Structures, 54(4), pp. 597-608, 1995.

[44] Pandey, P. C. and Barai, S. V., "Time-delay neural networks in damage detection of

railway bridges," Advance in Engineering Software, 28(1), pp. 1-10, 1997.

[45] Zhao, J., et al., "Structural damage detection using artificial neural networks," Journal of Infrastructure Systems, ASCE, 4(2), pp. 93-101, 1998.

[46] Masri, S. F., et al., "Application of neural networks for detection of changes in nonlinear systems," Journal of Engineering Mechanics, ASCE, 126(7), pp. 666-676, 2000.

[47] Zapico, J. L., et al., "Vibration-based damage assessment in steel frames using neural networks," Smart Materials and Structures, 10(3), pp. 553-559, 2001.

[48] Sahin, M. and Shenoi, R. A., "Quantification and localisation of damage in beam-like structures by using artificial neural networks wth experimental validation," Engineering Structures, 25(14), pp. 1785-1802, 2003.

[49] Kim, S. H., et al., "Structural monitoring system based on sensitivity analysis and a neural network," Computer-Aided Civil and Infrastructure Engineering, 15(4), pp. 309-318, 2000.

[50] Marwala, T., "Damage identification using committee of neural networks," Journal of Engineering Mechanics, ASCE, 126(1), pp. 43-50, 2000.

[51] Yun, C. B., et al., "Joint damage assessment of framed structures using a neural networks technique," Engineering Structures, 23(5), pp. 425-435, 2001.

[52] Ni, Y. Q., et al., "Constructing input vectors to nueral networks for structiral damage identification," Smart Material and Structures, 11(pp. 825-833, 2002.

[53] Tsai, C. H. and Hsu, D. S., "Diagnosis of reinforced concrete structural damage based on displacement time history using the back-propagation neural network technique," Journal of Computing In Civil Engineering., ASCE, 16(1), pp. 49-58, 2002.

[54] Wu, Z., et al., "Decentralized parameteric damage detection based on neural networks," Computer-Aided Civil and Infrastructure Engineering, 17(pp. 175-184, 2002.

[55] McCulloch, W. and Pitts, W., "A logical calculus of ideas imminent in nervous activity," Bulletin of Mathematical Biophysics, 5(pp. 115-133, 1943.

[56] Rosenblatt, F., "The perceptron: a probabilitistic model for information storage and organization in the brain," Psychological Review, 65(pp. 386-408, 1958.

[57] Rumelhart, D. E., et al., "Learning international representation by error propagation," in *Parallel Distributed Processing*, R. J. Williams, Ed. Cambridge, MA.: The MIT Press, 1986, pp. 318-362.

[58] Hecht-Nielsen, R., "Theory of the back propagation neural network," Proceedins of International Joint Conference on Neural Network, IEEE, 1989.

[59] Hung, S. L. and Lin, Y. L., "Application of an L-BFGS Neural Network Learning

Algorithm in Engineering Analysis and Design," Proc., The 2nd National Conf. on Struct. Engrg., Taiwan, R.O.C., 1994.

[60] Adeli, H., "Neural network in civil engineering: 1989-2000," Compter-Aided Civil and Infrastructure Engineering, 16(2), pp. 126-142, 2001.

[61] Hung, S. L. and Jan, J. C., "Machine learning in engineering design: an unsupervised fuzzy neural network learning model," Proc. of Intelligent Information Systems, IEEE Computer Society, California, 1997.

[62] Hung, S. L. and Jan, J. C., "Machine learning in engineering analysis and design: an integrated fuzzy neural network learning model," Computer-Aided Civil and Infrastructure Engineering, 14(pp. 207-219, 1999.

[63] Hung, S. L. and Jan, J. C., "Augmented IFN Learning Model," Journal of Computing in Civil Engineering, ASCE, 14(1), pp. 15-22, 2000.

[64] Hung, S. L. and Lai, C. M., "Unsupervised fuzzy neural network structural active pulse controller," Earthquake Engineering and Structural Dynamics, 30(4), pp. 465-484, 2001.

[65] Wen, C. M. and Hung, S. L., "Unsupervised fuzzy neural network for the damage detection of structures," (Submitted to Earthquake Engineering and Structural Dynamics), 2004.

[66] Maia, N. M. M., et al., Theoretical and experimental modal analysis. Research Studies Press, Ltd., Baldock, Hertfordshire, England, 1997.

[67] He, J. and Fu, Z. F., Modal analysis. Butterworth-Heinemann, Woburn, MA, 2001.

[68] Yun, C. B. and Bahng, E. Y., "Substructural identification using neural networks," Computers and Structures, 77(1), pp. 41-52, 2000.

[69] Huang, C. S., "Structural identification from ambient vibration measurement using the multivariate AR model," Journal of Sound and Vibration, 241(3), pp. 337-359, 2001.

[70] Huang, C. S., "A study on techniques for analyzing ambient vibration measurement (II) - time series methods," National Center for Research on Earthquake Engineering, Taiwan, R.O.C NCREE Report No. NCREE-99-018, 1999.

[71] Law, S. S., et al., "Efficient numerical model for the damage detection of large scale engineering structures," Engineering Structures, 23(5), pp. 436-451, 2001.

**Table 4.1** Specifications of the shaking table in NCTU

| **Item** | **Value** |
|---|---|
| Table size ($m^2$) | $3 \times 3$ |
| Weight of table (*kg*) | 5000 |
| Max. specimen weight (*kg*) | 10,000 |
| Max. displacement (*cm*) | $\pm 12.5$ |
| Max. velocity (*cm/sec*) | $\pm 60$ |
| Max. acceleration (*g*) | $\pm 1$ |

**Table 4.2** The characterizations of the experimental specimen

| **Item** | **Value** |
|---|---|
| Plane size ($m^2$) | $2 \times 2$ |
| Story height (*m*) | 1.6 |
| Weight (*kg*) | $\approx 5000$ |
| Cross section of the column (*mm*) | $125 \times 60 \times 6 \times 8$ |
| Cross section of the beam (*mm*) | $125 \times 60 \times 6 \times 8$ |
| Cross section of the girder (*mm*) | $100 \times 50 \times 5 \times 7$ |
| Size of the mass block (*mm*) | $1360 \times 1360 \times 32$ |
| Mass at 4th floor ($kg - s^2 / m$) | 117.06 |
| Mass at 3rd floor ($kg - s^2 / m$) | 121.21 |
| Mass at 2nd floor ($kg - s^2 / m$) | 121.21 |
| Mass at 1st floor ($kg - s^2 / m$) | 121.54 |

**Table 4.3** Analytical modal parameters of the test model in the transverse direction

| ***Mode*** | | **1** | **2** | **3** | **4** |
|---|---|---|---|---|---|
| ***Frequency (Hz)*** | | 1.18 | 3.48 | 5.45 | 6.80 |
| ***Damping ratio (%)*** | | 5 | 5 | 5 | 5 |
| ***Mode shape*** | ***4F*** | 1.000 | 1.000 | 0.664 | 0.380 |
| | ***3F*** | 0.879 | 0.011 | -0.846 | -0.903 |
| | ***2F*** | 0.648 | -0.998 | -0.348 | 1.000 |
| | ***1F*** | 0.332 | -0.976 | 1.000 | -0.659 |

**Table 4.4** Specifications of the accelerometers

| | **TYPE** | **Axes** | **Span (g)** |
|---|---|---|---|
| **A4** | *CrossBow* CXL02LF1 | X | ± 2 |
| **A3** | *CrossBow* CXL02LF1 | X | ± 2 |
| **A2** | *CrossBow* CXL01LF1 | X | ±1 |
| **A1** | *CrossBow* CXL01LF1 | X | ±1 |
| **Abase** | *CrossBow* CXL01LF1 | X | ±1 |

**Table 4.5** Specifications of the FBG-SLI

| | |
|---|---|
| **Optical** | |
| Number of Optical Channels | 4 |
| Maximum Number of FBG Sensors/Channel | 64 (256 total across 4 channels) |
| Wavelength Range | 1525 - 1565 nm |
| Absolute Accuracy | +/- 5 pm (~4.2 µ ) typ, +/- 10 pm max |
| Repeatability | +/- 2 pm (~1.7 µ ) typ, +/- 5 pm max |
| Optical Power/Channel | -10 dBm approx. |
| Dynamic Range (4 software-controlled gain settings) | 30 dB |
| Resolution | <1 pm (~0.8µ ) |
| Scan Frequency | 108 Hz max |
| Minimum FBG Spacing | 0.5 nm |
| Optical Connector | FC/APC |
| **Hardware and Software** | |
| Computer Interface Card PCI or PC CARD | (PCMCIA) |
| Interface Cable | Included |
| FBG-IS Software for Windows 95, 98, 2000, NT and XP | Included |
| **Electrical** | |
| Power Supply | 95-135 VAC or 190-265 VAC, 15W |
| Uncalibrated Analog Output - BNC Connectors | Test, sync and scan |
| **Mechanical** | |
| Operating Temperature | $10^{o}$ – $40^{o}$C |
| Dimensions | 69 x 277 x 267 mm |
| Weight | 4.1 kg |
| **Options** | |
| Test Processor | Laptop computer/data management system |
| Custom Optical Connectors | FC/SPC |
| Custom Computer Interface Cards | ISA |

**Table 4.6** Center wavelength of the FBG sensors along Channel 1

| | **FBG1** | **FBG2** | **FBG3** | **FBG4** | **FBG5** | **FBG6** | **FBG7** | **FBG8** |
|---|---|---|---|---|---|---|---|---|
| **Wavelength (nm)** | 1542 | 1545 | 1548 | 1551 | 1554 | 1557 | 1560 | 1563 |

**Table 4.7** Center wavelength of the FBG sensors along Channel 2

| | **FBG9** | **FBG10** | **FBG11** | **FBG12** |
|---|---|---|---|---|
| **Wavelength (nm)** | 1530 | 1533 | 1539 | 1536 |

**Table 4.8** Dimension of the SC

| | **Cross section (mm)** | **Area ($cm^2$)** | **Mass (kg/m)** | **$I_x$ ($cm^4$)** |
|---|---|---|---|---|
| SC-A | $100\times50\times20\times2.3$ | 5.14 | 4.06 | 80.7 |
| SC-B | $75\times45\times15\times2.3$ | 4.14 | 3.25 | 37.1 |

**Table 4.9** Characterizations of the simulated damage cases

| No. | Notation of the damage case | SC arrangement (1F-2F-3F) | Notation of the damage class |
|---|---|---|---|
| 1 | *AAA* | A-A-A | *Intact* |
| 2 | *Dcase_BAA* | B-A-A | $Dclass\_k_1$ |
| 3 | *Dcase_NAA* | N-A-A | $Dclass\_k_1$ |
| 4 | *Dcase_ABA* | A-B-A | $Dclass\_k_2$ |
| 5 | *Dcase_ANA* | A-N-A | $Dclass\_k_2$ |
| 6 | *Dcase_AAB* | A-A-B | $Dclass\_k_3$ |
| 7 | *Dcase_AAN* | A-A-N | $Dclass\_k_3$ |
| 8 | *Dcase_BBA* | B-B-A | $Dclass\_k_1\&k_2$ |
| 9 | *Dcase_BNA* | B-N-A | $Dclass\_k_1\&k_2$ |
| 10 | *Dcase_NBA* | N-B-A | $Dclass\_k_1\&k_2$ |
| 11 | *Dcase_NNA* | N-N-A | $Dclass\_k_1\&k_2$ |
| 12 | *Dcase_BAB* | B-A-B | $Dclass\_k_1\&k_3$ |
| 13 | *Dcase_BAN* | B-A-N | $Dclass\_k_1\&k_3$ |
| 14 | *Dcase_NAB* | N-A-B | $Dclass\_k_1\&k_3$ |
| 15 | *Dcase_NAN* | N-A-N | $Dclass\_k_1\&k_3$ |
| 16 | *Dcase_ABB* | A-B-B | $Dclass\_k_2\&k_3$ |
| 17 | *Dcase_ABN* | A-B-N | $Dclass\_k_2\&k_3$ |
| 18 | *Dcase_ANB* | A-N-B | $Dclass\_k_2\&k_3$ |
| 19 | *Dcase_ANN* | A-N-N | $Dclass\_k_2\&k_3$ |
| 20 | *Dcase_BBB* | B-B-B | $Dclass\_k_1\&k_2\&k_3$ |
| 21 | *Dcase_BBN* | B-B-N | $Dclass\_k_1\&k_2\&k_3$ |
| 22 | *Dcase_NBB* | N-B-B | $Dclass\_k_1\&k_2\&k_3$ |
| 23 | *Dcase_BNN* | B-N-N | $Dclass\_k_1\&k_2\&k_3$ |
| 24 | *Dcase_NNB* | N-N-B | $Dclass\_k_1\&k_2\&k_3$ |
| 25 | *Dcase_NNN* | N-N-N | $Dclass\_k_1\&k_2\&k_3$ |

**Table 4.10** Operation sequence of the shaking table tests

| Case | Save acc. data as | Save RSG data as | Save FBG data as |
|---|---|---|---|
| *AAA* | AAA_acc | AAA_RSG | AAA_FBG |
| *Dcase_BAA* | BAA_acc | BAA_RSG | BAA_FBG |
| *Dcase_NAA* | NAA_acc | NAA_RSG | NAA_FBG |
| *Dcase_ABA* | ABA_acc | ABA_RSG | ABA_FBG |
| *Dcase_ANA* | ANA_acc | ANA_RSG | ANA_FBG |
| *Dcase_AAB* | AAB_acc | AAB_RSG | AAB_FBG |
| *Dcase_AAN* | AAN_acc | AAN_RSG | AAN_FBG |
| *Dcase_BBA* | BBA_acc | BBA_RSG | BBA_FBG |
| *Dcase_BNA* | BNA_acc | BNA_RSG | BNA_FBG |
| *Dcase_NBA* | NBA_acc | NBA_RSG | NBA_FBG |
| *Dcase_NNA* | NNA_acc | NNA_RSG | NNA_FBG |
| *Dcase_BAB* | BAB_acc | BAB_RSG | BAB_FBG |
| *Dcase_BAN* | BAN_acc | BAN_RSG | BAN_FBG |
| *Dcase_NAB* | NAB_acc | NAB_RSG | NAB_FBG |
| *Dcase_NAN* | NAN_acc | NAN_RSG | NAN_FBG |
| *Dcase_ABB* | ABB_acc | ABB_RSG | ABB_FBG |
| *Dcase_ABN* | ABN_acc | ABN_RSG | ABN_FBG |
| *Dcase_ANB* | ANB_acc | ANB_RSG | ANB_FBG |
| *Dcase_ANN* | ANN_acc | ANN_RSG | ANN_FBG |
| *Dcase_BBB* | BBB_acc | BBB_RSG | BBB_FBG |
| *Dcase_BBN* | BBN_acc | BBN_RSG | BBN_FBG |
| *Dcase_NBB* | NBB_acc | NBB_RSG | NBB_FBG |
| *Dcase_BNN* | BNN_acc | BNN_RSG | BNN_FBG |
| *Dcase_NNB* | NNB_acc | NNB_RSG | NNB_FBG |
| *Dcase_NNN* | NNN_acc | NNN_RSG | NNN_FBG |

**Table 4.11** Statistical summaries of the acceleration records

| Case | I. Max. response (g) max(*acc.*) | | | | II. Standard deviation (g) std(*acc.*) | | | |
|---|---|---|---|---|---|---|---|---|
| | **1F** | **2F** | **3F** | **4F** | **1F** | **2F** | **3F** | **4F** |
| *AAA* | 0.095 | 0.119 | 0.131 | 0.177 | 0.016 | 0.023 | 0.028 | 0.035 |
| *Dcase_BAA* | 0.096 | 0.129 | 0.140 | 0.200 | 0.018 | 0.027 | 0.034 | 0.041 |
| *Dcase_NAA* | 0.107 | 0.144 | 0.170 | 0.191 | 0.028 | 0.038 | 0.046 | 0.057 |
| *Dcase_ABA* | 0.093 | 0.124 | 0.142 | 0.181 | 0.020 | 0.030 | 0.036 | 0.045 |
| *Dcase_ANA* | 0.095 | 0.145 | 0.160 | 0.204 | 0.021 | 0.038 | 0.047 | 0.056 |
| *Dcase_AAB* | 0.091 | 0.126 | 0.137 | 0.178 | 0.019 | 0.028 | 0.034 | 0.042 |
| *Dcase_AAN* | 0.117 | 0.149 | 0.157 | 0.180 | 0.021 | 0.030 | 0.037 | 0.045 |
| *Dcase_BBA* | 0.094 | 0.123 | 0.144 | 0.175 | 0.019 | 0.030 | 0.038 | 0.045 |
| *Dcase_BNA* | 0.093 | 0.143 | 0.167 | 0.202 | 0.021 | 0.037 | 0.048 | 0.056 |
| *Dcase_NBA* | 0.106 | 0.143 | 0.166 | 0.207 | 0.028 | 0.042 | 0.052 | 0.062 |
| *Dcase_NNA* | 0.102 | 0.156 | 0.184 | 0.244 | 0.033 | 0.058 | 0.074 | 0.085 |
| *Dcase_BAB* | 0.102 | 0.138 | 0.160 | 0.184 | 0.022 | 0.032 | 0.039 | 0.048 |
| *Dcase_BAN* | 0.137 | 0.172 | 0.159 | 0.218 | 0.028 | 0.036 | 0.04 | 0.052 |
| *Dcase_NAB* | 0.104 | 0.148 | 0.192 | 0.216 | 0.027 | 0.043 | 0.054 | 0.063 |
| *Dcase_NAN* | 0.143 | 0.189 | 0.188 | 0.235 | 0.036 | 0.048 | 0.056 | 0.070 |
| *Dcase_ABB* | 0.097 | 0.131 | 0.141 | 0.184 | 0.022 | 0.033 | 0.039 | 0.048 |
| *Dcase_ABN* | 0.115 | 0.150 | 0.152 | 0.181 | 0.023 | 0.034 | 0.043 | 0.052 |
| *Dcase_ANB* | 0.095 | 0.161 | 0.171 | 0.225 | 0.023 | 0.040 | 0.051 | 0.060 |
| *Dcase_ANN* | 0.100 | 0.158 | 0.162 | 0.230 | 0.026 | 0.043 | 0.055 | 0.066 |
| *Dcase_BBB* | 0.089 | 0.129 | 0.152 | 0.184 | 0.024 | 0.035 | 0.042 | 0.051 |
| *Dcase_BBN* | 0.130 | 0.170 | 0.160 | 0.221 | 0.030 | 0.041 | 0.046 | 0.058 |
| *Dcase_NBB* | 0.103 | 0.159 | 0.201 | 0.227 | 0.036 | 0.059 | 0.074 | 0.087 |
| *Dcase_BNN* | 0.135 | 0.171 | 0.179 | 0.265 | 0.034 | 0.053 | 0.065 | 0.078 |
| *Dcase_NNB* | 0.098 | 0.148 | 0.193 | 0.248 | 0.043 | 0.079 | 0.099 | 0.115 |
| *Dcase_NNN* | 0.133 | 0.184 | 0.210 | 0.298 | 0.050 | 0.084 | 0.109 | 0.127 |

**Table 4.11 (*Continue*)**

| Case | III. $\Delta\max(acc.)$ (g) (=*damage case – baseline*) | | | | IV. $\Delta\max(acc.)/baseline$ (%) | | | |
|---|---|---|---|---|---|---|---|---|
| | **1F** | **2F** | **3F** | **4F** | **1F** | **2F** | **3F** | **4F** |
| *AAA* | / | / | / | / | / | / | / | / |
| *Dcase_BAA* | 0.001 | 0.010 | 0.009 | 0.023 | 0.6 | 8.3 | 6.9 | 13.0 |
| *Dcase_NAA* | 0.012 | 0.025 | 0.039 | 0.014 | 12.3 | 21.0 | 29.5 | 7.9 |
| *Dcase_ABA* | -0.002 | 0.005 | 0.011 | 0.004 | -1.8 | 4.3 | 8.0 | 2.0 |
| *Dcase_ANA* | 0.000 | 0.026 | 0.029 | 0.027 | 0.2 | 21.7 | 22.1 | 15.0 |
| *Dcase_AAB* | -0.004 | 0.007 | 0.006 | 0.001 | -3.9 | 6.0 | 4.9 | 0.8 |
| *Dcase_AAN* | 0.022 | 0.030 | 0.026 | 0.003 | 23.6 | 24.8 | 19.8 | 1.5 |
| *Dcase_BBA* | -0.001 | 0.004 | 0.013 | -0.002 | -1.6 | 3.0 | 10.2 | -1.4 |
| *Dcase_BNA* | -0.002 | 0.024 | 0.036 | 0.025 | -1.9 | 20.0 | 27.5 | 13.9 |
| *Dcase_NBA* | 0.011 | 0.024 | 0.035 | 0.030 | 11.2 | 20.1 | 27.0 | 16.9 |
| *Dcase_NNA* | 0.007 | 0.037 | 0.053 | 0.067 | 7.4 | 31.1 | 40.5 | 37.9 |
| *Dcase_BAB* | 0.007 | 0.019 | 0.029 | 0.007 | 7.5 | 15.9 | 22.1 | 4.1 |
| *Dcase_BAN* | 0.042 | 0.053 | 0.028 | 0.041 | 44.7 | 44.8 | 21.4 | 23.4 |
| *Dcase_NAB* | 0.009 | 0.029 | 0.061 | 0.039 | 9.2 | 24.5 | 46.9 | 22.2 |
| *Dcase_NAN* | 0.048 | 0.070 | 0.057 | 0.058 | 50.5 | 58.7 | 43.3 | 32.6 |
| *Dcase_ABB* | 0.002 | 0.012 | 0.010 | 0.007 | 2.6 | 10.3 | 7.3 | 3.7 |
| *Dcase_ABN* | 0.020 | 0.031 | 0.021 | 0.004 | 21.4 | 25.7 | 15.8 | 2.1 |
| *Dcase_ANB* | 0.000 | 0.042 | 0.040 | 0.048 | 0.4 | 35.4 | 30.5 | 26.9 |
| *Dcase_ANN* | 0.005 | 0.039 | 0.031 | 0.053 | 5.3 | 32.8 | 23.7 | 29.9 |
| *Dcase_BBB* | -0.006 | 0.010 | 0.021 | 0.007 | -6.3 | 8.4 | 16.0 | 4.0 |
| *Dcase_BBN* | 0.035 | 0.051 | 0.029 | 0.044 | 36.7 | 43.2 | 22.1 | 25.0 |
| *Dcase_NBB* | 0.008 | 0.040 | 0.070 | 0.050 | 8.0 | 33.6 | 53.5 | 28.1 |
| *Dcase_BNN* | 0.040 | 0.052 | 0.048 | 0.088 | 42.1 | 43.7 | 36.6 | 49.7 |
| *Dcase_NNB* | 0.003 | 0.029 | 0.062 | 0.071 | 2.7 | 24.6 | 47.5 | 40.0 |
| *Dcase_NNN* | 0.038 | 0.065 | 0.079 | 0.121 | 40.0 | 54.5 | 60.2 | 68.5 |

**Table 4.12** Statistical summaries of the strain records from the FBG sensors at BE

| **Case** | **I. Max. response ( $\mu$ strain)** max($\varepsilon$) | | | | **II. Standard deviation ( $\mu$ strain)** std($\varepsilon$) | | | |
|---|---|---|---|---|---|---|---|---|
| | **FBG1** | **FBG3** | **FBG5** | **FBG7** | **FBG1** | **FBG3** | **FBG5** | **FBG7** |
| *AAA* | 238.1 | 184.2 | 143.1 | 109.6 | 44.5 | 36.8 | 28.2 | 20.5 |
| *Dcase_BAA* | 256.4 | 197.7 | 155.2 | 121.2 | 56.9 | 47.1 | 35.7 | 25.1 |
| *Dcase_NAA* | 337.4 | 245.2 | 173.4 | 121.5 | 92.0 | 64.4 | 50.2 | 34.2 |
| *Dcase_ABA* | 272.0 | 215.7 | 135.6 | 117.2 | 62.8 | 53.3 | 33.2 | 27.6 |
| *Dcase_ANA* | 296.9 | 296.7 | 154.3 | 134.8 | 83.9 | 89.4 | 44.6 | 36.0 |
| *Dcase_AAB* | 264.7 | 212.4 | 144.2 | 114.4 | 52.8 | 45.3 | 31.6 | 23.5 |
| *Dcase_AAN* | 285.5 | 209.7 | 196.3 | 114.6 | 65.5 | 55.9 | 52.5 | 28.5 |
| *Dcase_BBA* | 293.0 | 219.3 | 155.0 | 113.0 | 69.7 | 55.3 | 38.8 | 26.7 |
| *Dcase_BNA* | 296.0 | 296.6 | 175.8 | 136.2 | 81.5 | 86.5 | 49.8 | 34.6 |
| *Dcase_NBA* | 349.3 | 275.7 | 192.6 | 131.9 | 105.9 | 79.9 | 56.4 | 38.1 |
| *Dcase_NNA* | 376.5 | 350.5 | 222.4 | 164.3 | 132.4 | 118.2 | 69.1 | 46.2 |
| *Dcase_BAB* | 302.1 | 230.9 | 152.0 | 117.1 | 75.2 | 59.1 | 40.5 | 29.7 |
| *Dcase_BAN* | 332.0 | 242.9 | 233.0 | 140.4 | 75.9 | 59.8 | 55.7 | 30.9 |
| *Dcase_NAB* | 370.2 | 283.6 | 182.7 | 134.5 | 112.4 | 83.5 | 56.0 | 39.3 |
| *Dcase_NAN* | 392.9 | 281.5 | 242.5 | 143.5 | 112.6 | 83.0 | 77.0 | 41.3 |
| *Dcase_ABB* | 274.6 | 212.6 | 148.4 | 118.1 | 65.7 | 55.8 | 39.0 | 28.9 |
| *Dcase_ABN* | 298.3 | 227.0 | 200.3 | 114.4 | 72.8 | 62.1 | 59.0 | 32.2 |
| *Dcase_ANB* | 312.3 | 306.0 | 177.9 | 138.0 | 87.4 | 93.0 | 52.1 | 37.5 |
| *Dcase_ANN* | 315.0 | 315.0 | 262.2 | 150.6 | 94.6 | 100.4 | 76.7 | 40.5 |
| *Dcase_BBB* | 313.2 | 246.1 | 163.0 | 121.5 | 78.8 | 62.5 | 42.8 | 30.5 |
| *Dcase_BBN* | 350.8 | 255.7 | 243.7 | 140.1 | 86.3 | 67.9 | 62.2 | 34.5 |
| *Dcase_NBB* | 421.1 | 304.2 | 212.4 | 152.2 | 152.5 | 108.6 | 77.4 | 54.1 |
| *Dcase_BNN* | 353.8 | 335.5 | 293.1 | 174.4 | 113.0 | 107.6 | 81.4 | 43.3 |
| *Dcase_NNB* | 419.7 | 385.1 | 230.2 | 171.5 | 220.5 | 196.9 | 107.1 | 75.4 |
| *Dcase_NNN* | 427.8 | 385.8 | 318.0 | 187.0 | 195.7 | 176.9 | 129.8 | 66.9 |

**Table 4.12 (*Continue*)**

| Case | III. $\frac{\text{std}(\varepsilon)}{\max(\varepsilon)}$ (%) | | | | IV. $\Delta\max(\varepsilon)/baseline$ (%) | | | |
|---|---|---|---|---|---|---|---|---|
| | **FBG1** | **FBG3** | **FBG5** | **FBG7** | **FBG1** | **FBG3** | **FBG5** | **FBG7** |
| *AAA* | 18.7 | 20.0 | 19.7 | 18.7 | / | / | / | / |
| *Dcase_BAA* | 22.2 | 23.8 | 23.0 | 20.7 | 7.7 | 7.4 | 8.5 | 10.6 |
| *Dcase_NAA* | 27.3 | 26.3 | 28.9 | 28.1 | 41.7 | 33.1 | 21.2 | 10.9 |
| *Dcase_ABA* | 23.1 | 24.7 | 24.5 | 23.6 | 14.2 | 17.1 | -5.2 | 6.9 |
| *Dcase_ANA* | 28.3 | 30.1 | 28.9 | 26.7 | 24.7 | 61.1 | 7.9 | 23.0 |
| *Dcase_AAB* | 19.9 | 21.3 | 21.9 | 20.5 | 11.2 | 15.3 | 0.8 | 4.4 |
| *Dcase_AAN* | 23.0 | 26.7 | 26.8 | 24.8 | 19.9 | 13.8 | 37.2 | 4.6 |
| *Dcase_BBA* | 23.8 | 25.2 | 25.0 | 23.7 | 23.1 | 19.1 | 8.4 | 3.1 |
| *Dcase_BNA* | 27.5 | 29.2 | 28.3 | 25.4 | 24.3 | 61.1 | 22.9 | 24.3 |
| *Dcase_NBA* | 30.3 | 29.0 | 29.3 | 28.9 | 46.7 | 49.7 | 34.6 | 20.4 |
| *Dcase_NNA* | 35.2 | 33.7 | 31.1 | 28.1 | 58.1 | 90.3 | 55.4 | 49.9 |
| *Dcase_BAB* | 24.9 | 25.6 | 26.6 | 25.4 | 26.9 | 25.4 | 6.3 | 6.9 |
| *Dcase_BAN* | 22.9 | 24.6 | 23.9 | 22.0 | 39.4 | 31.9 | 62.9 | 28.1 |
| *Dcase_NAB* | 30.4 | 29.4 | 30.6 | 29.3 | 55.5 | 54.0 | 27.7 | 22.7 |
| *Dcase_NAN* | 28.7 | 29.5 | 31.8 | 28.8 | 65.0 | 52.9 | 69.5 | 30.9 |
| *Dcase_ABB* | 23.9 | 26.3 | 26.3 | 24.5 | 15.3 | 15.4 | 3.7 | 7.7 |
| *Dcase_ABN* | 24.4 | 27.3 | 29.4 | 28.1 | 25.3 | 23.2 | 40.0 | 4.4 |
| *Dcase_ANB* | 28.0 | 30.4 | 29.3 | 27.2 | 31.2 | 66.1 | 24.4 | 25.9 |
| *Dcase_ANN* | 30.0 | 31.9 | 29.2 | 26.9 | 32.3 | 71.0 | 83.3 | 37.4 |
| *Dcase_BBB* | 25.2 | 25.4 | 26.3 | 25.1 | 31.5 | 33.6 | 14.0 | 10.9 |
| *Dcase_BBN* | 24.6 | 26.5 | 25.5 | 24.6 | 47.4 | 38.8 | 70.3 | 27.8 |
| *Dcase_NBB* | 36.2 | 35.7 | 36.4 | 35.5 | 76.9 | 65.2 | 48.4 | 38.9 |
| *Dcase_BNN* | 31.9 | 32.1 | 27.8 | 24.8 | 48.6 | 82.2 | 104.8 | 59.1 |
| *Dcase_NNB* | 52.5 | 51.1 | 46.5 | 44.0 | 76.3 | 109.1 | 60.9 | 56.5 |
| *Dcase_NNN* | 45.7 | 45.9 | 40.8 | 35.8 | 79.7 | 109.5 | 122.3 | 70.6 |

**Table 4.13** Statistical summaries of the strain records from FBG the sensors at TE

| Case | I. Max. response ($\mu$ strain) max($\varepsilon$) | | | | II. Standard deviation ($\mu$ strain) std($\varepsilon$) | | | |
|---|---|---|---|---|---|---|---|---|
| | **FBG2** | **FBG4** | **FBG6** | **FBG8** | **FBG2** | **FBG4** | **FBG6** | **FBG8** |
| *AAA* | 241.5 | 188.2 | 151.5 | 111.6 | 46.1 | 37.8 | 30.1 | 20.9 |
| *Dcase_BAA* | 266.8 | 202.7 | 163.5 | 122.5 | 60.1 | 48.3 | 38.1 | 25.5 |
| *Dcase_NAA* | 350.3 | 251.7 | 186.6 | 124.2 | 95.9 | 66.8 | 53.5 | 34.7 |
| *Dcase_ABA* | 277.1 | 219.3 | 146.0 | 119.2 | 64.8 | 54.3 | 35.9 | 28.2 |
| *Dcase_ANA* | 299.0 | 300.2 | 169.0 | 136.1 | 85.2 | 90.7 | 49.4 | 36.4 |
| *Dcase_AAB* | 269.4 | 216.7 | 154.7 | 117.6 | 54.6 | 46.1 | 34.2 | 24.0 |
| *Dcase_AAN* | 287.3 | 210.9 | 208.8 | 119.6 | 67.7 | 56.3 | 55.6 | 29.9 |
| *Dcase_BBA* | 298.9 | 224.3 | 166.3 | 115.1 | 71.5 | 56.4 | 41.8 | 27.3 |
| *Dcase_BNA* | 300.8 | 294.6 | 193.6 | 138.5 | 83.7 | 86.2 | 54.7 | 35.2 |
| *Dcase_NBA* | 358.1 | 280.3 | 209.4 | 133.3 | 109.2 | 81.7 | 60.8 | 38.7 |
| *Dcase_NNA* | 384.2 | 350.1 | 243.3 | 167.2 | 135.5 | 118.2 | 75.8 | 47.2 |
| *Dcase_BAB* | 307.5 | 236.6 | 163.4 | 118.8 | 77.4 | 60.9 | 43.6 | 30.3 |
| *Dcase_BAN* | 331.2 | 245.0 | 245.6 | 147.1 | 77.9 | 60.8 | 58.7 | 32.5 |
| *Dcase_NAB* | 379.7 | 291.9 | 196.4 | 137.0 | 116.6 | 86.3 | 60.4 | 39.9 |
| *Dcase_NAN* | 397.6 | 286.1 | 254.7 | 150.5 | 116.5 | 84.8 | 80.7 | 43.5 |
| *Dcase_ABB* | 277.9 | 215.9 | 159.2 | 120.6 | 67.7 | 56.7 | 42.0 | 29.7 |
| *Dcase_ABN* | 302.6 | 226.7 | 211.3 | 118.9 | 75.3 | 62.3 | 62.6 | 33.8 |
| *Dcase_ANB* | 314.0 | 307.7 | 195.5 | 140.1 | 88.8 | 94.0 | 57.3 | 38.1 |
| *Dcase_ANN* | 315.8 | 317.0 | 279.4 | 159.1 | 96.2 | 100.7 | 81.7 | 42.7 |
| *Dcase_BBB* | 319.8 | 249.5 | 174.6 | 126.0 | 81.0 | 63.9 | 45.9 | 31.3 |
| *Dcase_BBN* | 353.6 | 258.2 | 257.5 | 147.0 | 88.7 | 68.7 | 65.7 | 36.2 |
| *Dcase_NBB* | 427.0 | 314.4 | 229.6 | 153.4 | 155.8 | 113.2 | 83.5 | 54.5 |
| *Dcase_BNN* | 354.9 | 336.9 | 312.2 | 183.1 | 114.8 | 108.0 | 86.9 | 45.7 |
| *Dcase_NNB* | 429.7 | 387.2 | 251.8 | 174.6 | 226.1 | 198.1 | 118.1 | 76.8 |
| *Dcase_NNN* | 434.72 | 384.2 | 338.5 | 196.8 | 201.2 | 176.7 | 138.7 | 70.8 |

**Table 4.13 (*Continue*)**

| Case | III. $\frac{\text{std}(\varepsilon)}{\max(\varepsilon)}$ (%) | | | | IV. $\Delta\max(\varepsilon)/baseline$ (%) | | | |
|---|---|---|---|---|---|---|---|---|
| | **FBG2** | **FBG4** | **FBG6** | **FBG8** | **FBG2** | **FBG4** | **FBG6** | **FBG8** |
| *AAA* | 19.1 | 20.1 | 19.8 | 18.7 | / | / | / | / |
| *Dcase_BAA* | 22.5 | 23.8 | 23.3 | 20.8 | 10.5 | 7.7 | 7.9 | 9.8 |
| *Dcase_NAA* | 27.4 | 26.6 | 28.7 | 28.0 | 45.0 | 33.7 | 23.2 | 11.3 |
| *Dcase_ABA* | 23.4 | 24.8 | 24.6 | 23.6 | 14.7 | 16.5 | -3.6 | 6.9 |
| *Dcase_ANA* | 28.5 | 30.2 | 29.3 | 26.7 | 23.8 | 59.5 | 11.5 | 22.0 |
| *Dcase_AAB* | 20.3 | 21.3 | 22.1 | 20.4 | 11.5 | 15.1 | 2.1 | 5.5 |
| *Dcase_AAN* | 23.6 | 26.7 | 26.6 | 25.0 | 18.9 | 12.0 | 37.8 | 7.2 |
| *Dcase_BBA* | 23.9 | 25.1 | 25.2 | 23.7 | 23.8 | 19.2 | 9.8 | 3.2 |
| *Dcase_BNA* | 27.8 | 29.3 | 28.2 | 25.4 | 24.6 | 56.5 | 27.8 | 24.2 |
| *Dcase_NBA* | 30.5 | 29.1 | 29.0 | 29.0 | 48.3 | 48.9 | 38.2 | 19.5 |
| *Dcase_NNA* | 35.3 | 33.8 | 31.2 | 28.2 | 59.1 | 86.0 | 60.6 | 49.9 |
| *Dcase_BAB* | 25.2 | 25.7 | 26.7 | 25.5 | 27.3 | 25.7 | 7.9 | 6.5 |
| *Dcase_BAN* | 23.5 | 24.8 | 23.9 | 22.1 | 37.1 | 30.2 | 62.1 | 31.9 |
| *Dcase_NAB* | 30.7 | 29.6 | 30.8 | 29.1 | 57.2 | 55.1 | 29.6 | 22.8 |
| *Dcase_NAN* | 29.3 | 29.6 | 31.7 | 28.9 | 64.6 | 52.0 | 68.1 | 34.9 |
| *Dcase_ABB* | 24.4 | 26.3 | 26.3 | 24.6 | 15.0 | 14.7 | 5.1 | 8.1 |
| *Dcase_ABN* | 24.9 | 27.5 | 29.6 | 28.4 | 25.3 | 20.4 | 39.5 | 6.6 |
| *Dcase_ANB* | 28.3 | 30.5 | 29.3 | 27.2 | 30.0 | 63.4 | 29.0 | 25.6 |
| *Dcase_ANN* | 30.5 | 31.8 | 29.2 | 26.8 | 30.7 | 68.4 | 84.4 | 42.6 |
| *Dcase_BBB* | 25.3 | 25.6 | 26.3 | 24.9 | 32.4 | 32.6 | 15.3 | 13.0 |
| *Dcase_BBN* | 25.1 | 26.6 | 25.5 | 24.6 | 46.4 | 37.2 | 70.0 | 31.8 |
| *Dcase_NBB* | 36.5 | 36.0 | 36.4 | 35.5 | 76.8 | 67.0 | 51.5 | 37.5 |
| *Dcase_BNN* | 32.3 | 32.0 | 27.8 | 24.9 | 46.9 | 79.0 | 106.1 | 64.2 |
| *Dcase_NNB* | 52.6 | 51.2 | 46.9 | 44.0 | 77.9 | 105.7 | 66.2 | 56.5 |
| *Dcase_NNN* | 46.3 | 46.0 | 41.0 | 36.0 | 80.0 | 104.1 | 123.4 | 76.4 |

**Table 4.14** Statistical summaries of the strain records from the FBG sensors at BW

| Case | I. Max. response ($\mu$ strain) max($\varepsilon$) | | | | II. Standard deviation ($\mu$ strain) std($\varepsilon$) | | | |
|---|---|---|---|---|---|---|---|---|
| | **FBG9** | **FBG10** | **FBG11** | **FBG12** | **FBG9** | **FBG10** | **FBG11** | **FBG12** |
| *AAA* | 250.0 | 190.1 | 142.8 | 98.1 | 47.0 | 38.2 | 28.5 | 19.2 |
| *Dcase_BAA* | 275.6 | 205.4 | 155.8 | 108.1 | 61.2 | 48.8 | 36.1 | 23.4 |
| *Dcase_NAA* | 362.6 | 256.5 | 179.5 | 111.2 | 99.5 | 65.9 | 50.3 | 31.5 |
| *Dcase_ABA* | 285.4 | 221.7 | 136.5 | 109.7 | 66.1 | 54.9 | 33.9 | 26.4 |
| *Dcase_ANA* | 314.2 | 306.3 | 154.4 | 127.0 | 89.0 | 92.2 | 44.7 | 33.8 |
| *Dcase_AAB* | 278.2 | 219.8 | 144.6 | 106.9 | 55.8 | 46.8 | 32.0 | 22.4 |
| *Dcase_AAN* | 299.1 | 217.2 | 195.7 | 112.5 | 69.4 | 58.0 | 52.7 | 26.2 |
| *Dcase_BBA* | 310.6 | 227.3 | 159.4 | 108.4 | 73.8 | 57.1 | 40.4 | 25.0 |
| *Dcase_BNA* | 315.1 | 307.3 | 178.6 | 129.0 | 86.9 | 89.4 | 50.5 | 31.4 |
| *Dcase_NBA* | 371.6 | 277.5 | 198.5 | 126.1 | 113.2 | 80.7 | 57.6 | 34.9 |
| *Dcase_NNA* | 402.2 | 355.0 | 225.7 | 156.1 | 141.3 | 119.7 | 70.5 | 41.8 |
| *Dcase_BAB* | 322.4 | 239.6 | 154.4 | 114.3 | 80.4 | 61.4 | 41.1 | 28.3 |
| *Dcase_BAN* | 352.2 | 252.2 | 236.4 | 138.4 | 81.1 | 62.4 | 56.2 | 28.6 |
| *Dcase_NAB* | 398.3 | 287.4 | 181.6 | 130.8 | 121.1 | 84.8 | 56.0 | 37.0 |
| *Dcase_NAN* | 418.1 | 286.3 | 240.8 | 141.3 | 120.9 | 84.4 | 76.4 | 38.4 |
| *Dcase_ABB* | 287.4 | 220.2 | 149.7 | 108.7 | 69.2 | 57.7 | 39.6 | 26.7 |
| *Dcase_ABN* | 313.6 | 236.7 | 201.9 | 104.9 | 77.0 | 64.4 | 59.2 | 29.6 |
| *Dcase_ANB* | 330.6 | 315.5 | 179.3 | 129.3 | 92.8 | 96.0 | 52.1 | 33.9 |
| *Dcase_ANN* | 332.7 | 325.6 | 260.5 | 150.1 | 100.7 | 103.7 | 76.1 | 37.4 |
| *Dcase_BBB* | 332.2 | 254.0 | 169.2 | 124.2 | 83.6 | 64.2 | 44.4 | 29.8 |
| *Dcase_BBN* | 371.2 | 264.9 | 248.0 | 138.8 | 91.9 | 70.5 | 63.7 | 31.9 |
| *Dcase_NBB* | 449.3 | 313.1 | 212.3 | 143.4 | 163.1 | 112.3 | 76.8 | 49.3 |
| *Dcase_BNN* | 375.5 | 348.2 | 290.1 | 172.1 | 121.2 | 111.7 | 80.8 | 40.2 |
| *Dcase_NNB* | 449.3 | 389.6 | 233.2 | 167.7 | 235.9 | 199.2 | 108.1 | 70.6 |
| *Dcase_NNN* | 455.1 | 390.6 | 316.5 | 185.3 | 209.9 | 179.1 | 129.5 | 62.7 |

**Table 4.14 (*Continue*)**

| Case | III. $\frac{\mathrm{std}(\varepsilon)}{\max(\varepsilon)}$ (%) | | | | IV. $\Delta\max(\varepsilon)/baseline$ (%) | | | |
|---|---|---|---|---|---|---|---|---|
| | **FBG9** | **FBG10** | **FBG11** | **FBG12** | **FBG9** | **FBG10** | **FBG11** | **FBG12** |
| *AAA* | 18.8 | 20.1 | 20.0 | 19.5 | / | / | / | / |
| *Dcase_BAA* | 22.2 | 23.7 | 23.2 | 21.7 | 10.2 | 8.0 | 9.1 | 10.2 |
| *Dcase_NAA* | 27.5 | 25.7 | 28.0 | 28.3 | 45.0 | 34.9 | 25.7 | 13.3 |
| *Dcase_ABA* | 23.1 | 24.8 | 24.8 | 24.1 | 14.2 | 16.6 | -4.4 | 11.8 |
| *Dcase_ANA* | 28.3 | 30.1 | 28.9 | 26.6 | 25.7 | 61.1 | 8.1 | 29.4 |
| *Dcase_AAB* | 20.1 | 21.3 | 22.1 | 21.0 | 11.3 | 15.6 | 1.3 | 8.9 |
| *Dcase_AAN* | 23.2 | 26.7 | 26.9 | 23.3 | 19.7 | 14.2 | 37.1 | 14.6 |
| *Dcase_BBA* | 23.8 | 25.1 | 25.3 | 23.0 | 24.3 | 19.6 | 11.6 | 10.4 |
| *Dcase_BNA* | 27.6 | 29.1 | 28.3 | 24.3 | 26.0 | 61.6 | 25.1 | 31.4 |
| *Dcase_NBA* | 30.5 | 29.1 | 29.0 | 27.7 | 48.7 | 46.0 | 39.0 | 28.4 |
| *Dcase_NNA* | 35.1 | 33.7 | 31.2 | 26.8 | 60.9 | 86.7 | 58.0 | 59.0 |
| *Dcase_BAB* | 24.9 | 25.6 | 26.6 | 24.8 | 29.0 | 26.0 | 8.1 | 16.4 |
| *Dcase_BAN* | 23.0 | 24.7 | 23.8 | 20.7 | 40.9 | 32.7 | 65.5 | 41.0 |
| *Dcase_NAB* | 30.4 | 29.5 | 30.8 | 28.3 | 59.3 | 51.2 | 27.2 | 33.3 |
| *Dcase_NAN* | 28.9 | 29.5 | 31.7 | 27.2 | 67.2 | 50.6 | 68.6 | 44.0 |
| *Dcase_ABB* | 24.1 | 26.2 | 26.5 | 24.6 | 15.0 | 15.8 | 4.8 | 10.8 |
| *Dcase_ABN* | 24.5 | 27.2 | 29.3 | 28.2 | 25.5 | 24.5 | 41.4 | 6.9 |
| *Dcase_ANB* | 28.1 | 30.4 | 29.1 | 26.2 | 32.2 | 66.0 | 25.6 | 31.8 |
| *Dcase_ANN* | 30.2 | 31.8 | 29.2 | 24.9 | 33.1 | 71.3 | 82.4 | 52.9 |
| *Dcase_BBB* | 25.2 | 25.3 | 26.2 | 24.0 | 32.9 | 33.6 | 18.5 | 26.5 |
| *Dcase_BBN* | 24.7 | 26.6 | 25.7 | 23.0 | 48.5 | 39.4 | 73.7 | 41.4 |
| *Dcase_NBB* | 36.3 | 35.9 | 36.2 | 34.4 | 79.7 | 64.7 | 48.7 | 46.1 |
| *Dcase_BNN* | 32.3 | 32.1 | 27.8 | 23.3 | 50.2 | 83.2 | 103.1 | 75.3 |
| *Dcase_NNB* | 52.5 | 51.1 | 46.3 | 42.1 | 79.7 | 104.9 | 63.3 | 70.9 |
| *Dcase_NNN* | 46.1 | 45.9 | 40.9 | 33.8 | 82.1 | 105.4 | 121.6 | 88.8 |

**Table 4.15** Statistical summaries of the strain records from the RSGs

| Case | I. Max. response ($\mu$ strain) max($\varepsilon$) | | | | II. Standard deviation ($\mu$ strain) std($\varepsilon$) | | | |
|---|---|---|---|---|---|---|---|---|
| | **RSG1** | **RSG2** | **RSG3** | **RSG4** | **RSG1** | **RSG2** | **RSG3** | **RSG4** |
| *AAA* | 166.4 | 144.9 | 121.3 | 96.2 | 36.6 | 33.5 | 27.5 | 21.1 |
| *Dcase_BAA* | 185.4 | 156.3 | 129.1 | 103.9 | 45.4 | 41.5 | 33.8 | 25.3 |
| *Dcase_NAA* | 236.7 | 196.3 | 152.0 | 112.6 | 73.8 | 57.1 | 47.8 | 34.0 |
| *Dcase_ABA* | 192.3 | 169.1 | 116.0 | 113.7 | 48.9 | 45.5 | 31.1 | 27.2 |
| *Dcase_ANA* | 214.7 | 235.9 | 139.4 | 123.9 | 63.5 | 73.7 | 39.9 | 33.6 |
| *Dcase_AAB* | 188.6 | 167.6 | 121.9 | 107.8 | 45.7 | 43.1 | 32.5 | 25.5 |
| *Dcase_AAN* | 203.1 | 167.2 | 169.0 | 112.8 | 49.4 | 46.3 | 46.5 | 26.7 |
| *Dcase_BBA* | 210.1 | 179.5 | 137.6 | 117.6 | 56.9 | 49.6 | 37.5 | 27.3 |
| *Dcase_BNA* | 210.9 | 232.8 | 164.2 | 119.6 | 64.9 | 75.2 | 46.4 | 33.9 |
| *Dcase_NBA* | 246.4 | 215.3 | 175.2 | 131.8 | 83.5 | 69.5 | 52.5 | 37.1 |
| *Dcase_NNA* | 266.8 | 273.6 | 188.8 | 136.9 | 119.3 | 114.7 | 73.4 | 50.6 |
| *Dcase_BAB* | 213.6 | 184.3 | 135.4 | 105.5 | 58.1 | 50.1 | 36.8 | 28.7 |
| *Dcase_BAN* | 240.7 | 188.6 | 194.1 | 123.8 | 60.1 | 52.0 | 51.9 | 30.3 |
| *Dcase_NAB* | 266.3 | 221.2 | 165.4 | 137.5 | 86.7 | 70.9 | 51.1 | 37.6 |
| *Dcase_NAN* | 278.4 | 221.1 | 201.9 | 134.5 | 89.4 | 72.6 | 72.0 | 40.5 |
| *Dcase_ABB* | 195.7 | 171.4 | 128.2 | 102.9 | 52.3 | 48.8 | 36.9 | 28.7 |
| *Dcase_ABN* | 210.7 | 186.2 | 171.5 | 105.8 | 55.7 | 52.2 | 53.1 | 30.6 |
| *Dcase_ANB* | 222.9 | 240.5 | 151.1 | 131.8 | 68.6 | 79.4 | 47.9 | 36.1 |
| *Dcase_ANN* | 225.4 | 243.4 | 212.1 | 129.0 | 73.9 | 85.1 | 69.5 | 38.4 |
| *Dcase_BBB* | 223.6 | 191.6 | 148.2 | 114.6 | 63.3 | 55.1 | 40.8 | 30.6 |
| *Dcase_BBN* | 253.7 | 205.6 | 208.3 | 129.7 | 68.7 | 59.3 | 58.2 | 33.9 |
| *Dcase_NBB* | 302.4 | 234.4 | 186.6 | 145.6 | 121.5 | 94.7 | 72.5 | 52.8 |
| *Dcase_BNN* | 255.0 | 260.0 | 244.2 | 147.9 | 96.7 | 99.8 | 81.0 | 45.0 |
| *Dcase_NNB* | 298.8 | 300.9 | 207.0 | 148.0 | 162.8 | 158.3 | 92.3 | 67.6 |
| *Dcase_NNN* | 307.1 | 302.7 | 273.2 | 171.8 | 173.4 | 170.7 | 134.2 | 72.6 |

**Table 4.15 (*Continue*)**

| Case | III. $\frac{\mathrm{std}(\varepsilon)}{\max(\varepsilon)}$ (%) | | | | IV. $\Delta\max(\varepsilon)/baseline$ (%) | | | |
|---|---|---|---|---|---|---|---|---|
| | **RSG1** | **RSG2** | **RSG3** | **RSG4** | **RSG1** | **RSG2** | **RSG3** | **RSG4** |
| *AAA* | 22.0 | 23.1 | 22.7 | 21.9 | / | / | / | / |
| *Dcase_BAA* | 24.5 | 26.5 | 26.2 | 24.4 | 11.4 | 7.9 | 6.4 | 8.0 |
| *Dcase_NAA* | 31.2 | 29.1 | 31.4 | 30.2 | 42.3 | 35.5 | 25.4 | 17.0 |
| *Dcase_ABA* | 25.4 | 26.9 | 26.8 | 23.9 | 15.6 | 16.7 | -4.3 | 18.3 |
| *Dcase_ANA* | 29.6 | 31.2 | 28.6 | 27.1 | 29.1 | 62.8 | 15.0 | 28.9 |
| *Dcase_AAB* | 24.2 | 25.7 | 26.6 | 23.6 | 13.4 | 15.7 | 0.6 | 12.1 |
| *Dcase_AAN* | 24.3 | 27.7 | 27.5 | 23.7 | 22.1 | 15.4 | 39.3 | 17.3 |
| *Dcase_BBA* | 27.1 | 27.6 | 27.3 | 23.2 | 26.3 | 23.9 | 13.5 | 22.3 |
| *Dcase_BNA* | 30.8 | 32.3 | 28.3 | 28.4 | 26.8 | 60.7 | 35.4 | 24.4 |
| *Dcase_NBA* | 33.9 | 32.3 | 30.0 | 28.1 | 48.1 | 48.6 | 44.5 | 37.1 |
| *Dcase_NNA* | 44.7 | 41.9 | 38.9 | 37.0 | 60.4 | 88.9 | 55.7 | 42.4 |
| *Dcase_BAB* | 27.2 | 27.2 | 27.2 | 27.2 | 28.4 | 27.2 | 11.7 | 9.7 |
| *Dcase_BAN* | 25.0 | 27.6 | 26.7 | 24.5 | 44.7 | 30.2 | 60.1 | 28.8 |
| *Dcase_NAB* | 32.5 | 32.0 | 30.9 | 27.3 | 60.0 | 52.7 | 36.4 | 43.0 |
| *Dcase_NAN* | 32.1 | 32.9 | 35.7 | 30.1 | 67.3 | 52.6 | 66.5 | 39.8 |
| *Dcase_ABB* | 26.7 | 28.5 | 28.8 | 27.9 | 17.7 | 18.3 | 5.7 | 7.0 |
| *Dcase_ABN* | 26.4 | 28.1 | 31.0 | 28.9 | 26.7 | 28.5 | 41.4 | 10.0 |
| *Dcase_ANB* | 30.8 | 33.0 | 31.7 | 27.4 | 34.0 | 66.0 | 24.6 | 37.0 |
| *Dcase_ANN* | 32.8 | 35.0 | 32.8 | 29.8 | 35.5 | 68.0 | 74.9 | 34.2 |
| *Dcase_BBB* | 28.3 | 28.7 | 27.5 | 26.7 | 34.4 | 32.3 | 22.2 | 19.2 |
| *Dcase_BBN* | 27.1 | 28.8 | 27.9 | 26.1 | 52.5 | 41.9 | 71.8 | 34.8 |
| *Dcase_NBB* | 40.2 | 40.4 | 38.8 | 36.3 | 81.8 | 61.8 | 53.9 | 51.4 |
| *Dcase_BNN* | 37.9 | 38.4 | 33.2 | 30.4 | 53.3 | 79.5 | 101.4 | 53.8 |
| *Dcase_NNB* | 54.5 | 52.6 | 44.6 | 45.7 | 79.6 | 107.7 | 70.7 | 53.8 |
| *Dcase_NNN* | 56.5 | 56.4 | 49.1 | 42.3 | 84.6 | 108.9 | 125.3 | 78.6 |

**Table 5.1** Modal parameters of the test structure in healthy condition (*AAA*)

| ***Mode*** | | **1** | **2** | **3** | **4** |
|---|---|---|---|---|---|
| ***Frequency (Hz)*** | | 1.69 | 5.04 | 8.14 | 10.22 |
| ***Damping ratio (%)*** | | 3.32 | 1.38 | 1.40 | 2.01 |
| ***Mode shape*** | **A4** | 1.000 | 1.000 | 0.427 | 0.288 |
| | **A3** | 0.846 | -0.130 | -0.729 | -0.729 |
| | **A2** | 0.628 | -0.914 | -0.137 | 1.000 |
| | **A1** | 0.336 | -0.830 | 1.000 | -0.705 |

**Table 5.2** Modal parameters of *Dcase_BAA*

| ***Mode*** | | **1** | **2** | **3** | **4** |
|---|---|---|---|---|---|
| ***Frequency (Hz)*** | | 1.68 | 4.94 | 7.89 | 10.17 |
| ***Damping ratio (%)*** | | 2.54 | 1.23 | 0.54 | 3.04 |
| ***Mode shape*** | **A4** | 1.000 | 1.000 | 0.557 | 0.254 |
| | **A3** | 0.844 | -0.100 | -0.893 | -0.775 |
| | **A2** | 0.629 | -0.935 | -0.206 | 1.000 |
| | **A1** | 0.340 | -0.887 | 1.000 | -0.672 |
| ***MAC*** | | 1.000 | 0.999 | 0.989 | 0.998 |

**Table 5.3** Modal parameters of *Dcase_NAA*

| ***Mode*** | | **1** | **2** | **3** | **4** |
|---|---|---|---|---|---|
| ***Frequency (Hz)*** | | 1.60 | 4.78 | 7.77 | 9.88 |
| ***Damping ratio (%)*** | | 1.80 | 0.28 | 0.49 | 2.53 |
| ***Mode shape*** | **A4** | 1.000 | 1.000 | 0.582 | 0.317 |
| | **A3** | 0.857 | -0.035 | -0.870 | -0.809 |
| | **A2** | 0.649 | -0.879 | -0.303 | 1.000 |
| | **A1** | 0.370 | -0.932 | 1.000 | -0.618 |
| ***MAC*** | | 1.000 | 0.992 | 0.979 | 0.993 |

**Table 5.4** Modal parameters of *Dcase_ABA*

| ***Mode*** | | **1** | **2** | **3** | **4** |
|---|---|---|---|---|---|
| ***Frequency (Hz)*** | | 1.70 | 5.09 | 7.93 | 10.15 |
| ***Damping ratio (%)*** | | 2.11 | 0.50 | 1.27 | 2.68 |
| ***Mode shape*** | **A4** | 1.000 | 1.000 | 0.449 | 0.249 |
| | **A3** | 0.843 | -0.149 | -0.769 | -0.871 |
| | **A2** | 0.648 | -0.835 | -0.197 | 1.000 |
| | **A1** | 0.344 | -0.786 | 1.000 | -0.757 |
| ***MAC*** | | 1.000 | 0.998 | 0.998 | 0.993 |

**Table 5.5** Modal parameters of *Dcase_ANA*

| ***Mode*** | | **1** | **2** | **3** | **4** |
|---|---|---|---|---|---|
| ***Frequency (Hz)*** | | 1.63 | 5.02 | 7.84 | 9.85 |
| ***Damping ratio (%)*** | | 1.78 | 0.69 | 4.64 | 4.26 |
| ***Mode shape*** | **A4** | 1.000 | 1.000 | 0.415 | 0.388 |
| | **A3** | 0.856 | -0.121 | -0.614 | -0.923 |
| | **A2** | 0.671 | -0.823 | -0.214 | 1.000 |
| | **A1** | 0.326 | -0.829 | 1.000 | -0.640 |
| ***MAC*** | | 0.999 | 0.998 | 0.989 | 0.982 |

**Table 5.6** Modal parameters of *Dcase_AAB*

| ***Mode*** | | **1** | **2** | **3** | **4** |
|---|---|---|---|---|---|
| ***Frequency (Hz)*** | | 1.68 | 5.03 | 7.97 | 10.10 |
| ***Damping ratio (%)*** | | 2.80 | 0.33 | 2.23 | 1.32 |
| ***Mode shape*** | **A4** | 1.000 | 1.000 | 0.609 | 0.277 |
| | **A3** | 0.852 | -0.119 | -0.951 | -0.836 |
| | **A2** | 0.638 | -0.885 | -0.176 | 1.000 |
| | **A1** | 0.337 | -0.827 | 1.000 | -0.709 |
| ***MAC*** | | 1.000 | 1.000 | 0.981 | 0.996 |

**Table 5.7** Modal parameters of *Dcase_AAN*

| ***Mode*** | | **1** | **2** | **3** | **4** |
|---|---|---|---|---|---|
| ***Frequency (Hz)*** | | 1.63 | 4.84 | 7.70 | 9.65 |
| ***Damping ratio (%)*** | | 2.92 | 0.28 | 1.22 | 1.64 |
| ***Mode shape*** | **A4** | 1.000 | 0.955 | 0.692 | 0.284 |
| | **A3** | 0.852 | -0.042 | -1.000 | -0.723 |
| | **A2** | 0.602 | -1.000 | -0.134 | 1.000 |
| | **A1** | 0.317 | -0.909 | 0.928 | -0.866 |
| ***MAC*** | | 1.000 | 0.993 | 0.955 | 0.991 |

**Table 5.8** Modal parameters of *Dcase_BBA*

| ***Mode*** | | **1** | **2** | **3** | **4** |
|---|---|---|---|---|---|
| ***Frequency (Hz)*** | | 1.62 | 4.89 | 7.72 | 10.08 |
| ***Damping ratio (%)*** | | 2.50 | 1.64 | 0.53 | 2.52 |
| ***Mode shape*** | **A4** | 1.000 | 1.000 | 0.558 | 0.351 |
| | **A3** | 0.855 | -0.075 | -0.829 | -0.807 |
| | **A2** | 0.649 | -0.855 | -0.252 | 1.000 |
| | **A1** | 0.354 | -0.832 | 1.000 | -0.565 |
| ***MAC*** | | 1.000 | 0.998 | 0.988 | 0.986 |

**Table 5.9** Modal parameters of *Dcase_BNA*

| ***Mode*** | | **1** | **2** | **3** | **4** |
|---|---|---|---|---|---|
| ***Frequency (Hz)*** | | 1.60 | 4.91 | 7.49 | 9.68 |
| ***Damping ratio (%)*** | | 1.75 | 1.03 | 0.56 | 1.32 |
| ***Mode shape*** | **A4** | 1.000 | 1.000 | 0.532 | 0.361 |
| | **A3** | 0.859 | -0.086 | -0.755 | -0.954 |
| | **A2** | 0.654 | -0.934 | -0.294 | 1.000 |
| | **A1** | 0.319 | -0.855 | 1.000 | -0.547 |
| ***MAC*** | | 1.000 | 0.999 | 0.985 | 0.967 |

**Table 5.10** Modal parameters of *Dcase_NBA*

| ***Mode*** | | **1** | **2** | **3** | **4** |
|---|---|---|---|---|---|
| ***Frequency (Hz)*** | | 1.58 | 4.76 | 7.59 | 9.49 |
| ***Damping ratio (%)*** | | 1.47 | 0.50 | 0.65 | 3.27 |
| ***Mode shape*** | **A4** | 1.000 | 1.000 | 0.564 | 0.312 |
| | **A3** | 0.863 | -0.025 | -0.807 | -0.826 |
| | **A2** | 0.657 | -0.883 | -0.336 | 1.000 |
| | **A1** | 0.363 | -0.957 | 1.000 | -0.685 |
| ***MAC*** | | 1.000 | 0.990 | 0.977 | 0.996 |

**Table 5.11** Modal parameters of *Dcase_NNA*

| ***Mode*** | | **1** | **2** | **3** | **4** |
|---|---|---|---|---|---|
| ***Frequency (Hz)*** | | 1.55 | 4.72 | 7.38 | 9.62 |
| ***Damping ratio (%)*** | | 0.72 | 0.66 | 0.34 | 0.62 |
| ***Mode shape*** | **A4** | 1.000 | 1.000 | 0.520 | 0.352 |
| | **A3** | 0.868 | -0.014 | -0.682 | -0.982 |
| | **A2** | 0.668 | -0.918 | -0.382 | 1.000 |
| | **A1** | 0.349 | -0.934 | 1.000 | -0.546 |
| ***MAC*** | | 1.000 | 0.992 | 0.964 | 0.962 |

**Table 5.12** Modal parameters of *Dcase_BAB*

| ***Mode*** | | **1** | **2** | **3** | **4** |
|---|---|---|---|---|---|
| ***Frequency (Hz)*** | | 1.63 | 4.90 | 7.81 | 10.04 |
| ***Damping ratio (%)*** | | 2.31 | 0.25 | 0.88 | 1.08 |
| ***Mode shape*** | **A4** | 1.000 | 1.000 | 0.610 | 0.294 |
| | **A3** | 0.855 | -0.063 | -0.920 | -0.808 |
| | **A2** | 0.653 | -0.844 | -0.205 | 1.000 |
| | **A1** | 0.355 | -0.824 | 1.000 | -0.671 |
| ***MAC*** | | 1.000 | 0.997 | 0.983 | 0.997 |

**Table 5.13** Modal parameters of *Dcase_BAN*

| ***Mode*** | | **1** | **2** | **3** | **4** |
|---|---|---|---|---|---|
| ***Frequency (Hz)*** | | 1.59 | 4.72 | 7.74 | 9.70 |
| ***Damping ratio (%)*** | | 2.58 | 0.11 | 0.31 | 2.17 |
| ***Mode shape*** | **A4** | 1.000 | 0.985 | 0.675 | 0.246 |
| | **A3** | 0.859 | -0.014 | -1.000 | -0.948 |
| | **A2** | 0.619 | -1.000 | -0.094 | 1.000 |
| | **A1** | 0.335 | -0.946 | 0.863 | -0.847 |
| ***MAC*** | | 1.000 | 0.991 | 0.941 | 0.985 |

**Table 5.14** Modal parameters of *Dcase_NAB*

| ***Mode*** | | **1** | **2** | **3** | **4** |
|---|---|---|---|---|---|
| ***Frequency (Hz)*** | | 1.60 | 4.84 | 7.71 | 9.99 |
| ***Damping ratio (%)*** | | 1.49 | 0.21 | 0.79 | 0.62 |
| ***Mode shape*** | **A4** | 1.000 | 1.000 | 0.632 | 0.289 |
| | **A3** | 0.860 | -0.044 | -0.942 | -0.808 |
| | **A2** | 0.667 | -0.835 | -0.273 | 1.000 |
| | **A1** | 0.371 | -0.889 | 1.000 | -0.603 |
| ***MAC*** | | 0.999 | 0.993 | 0.975 | 0.992 |

**Table 5.15** Modal parameters of *Dcase_NAN*

| ***Mode*** | | **1** | **2** | **3** | **4** |
|---|---|---|---|---|---|
| ***Frequency (Hz)*** | | 1.56 | 4.63 | 7.67 | 9.65 |
| ***Damping ratio (%)*** | | 1.42 | 0.04 | 0.20 | 2.33 |
| ***Mode shape*** | **A4** | 1.000 | 0.978 | 0.698 | 0.282 |
| | **A3** | 0.862 | 0.026 | -1.000 | -0.703 |
| | **A2** | 0.627 | -0.959 | -0.163 | 1.000 |
| | **A1** | 0.348 | -1.000 | 0.803 | -0.771 |
| ***MAC*** | | 1.000 | 0.983 | 0.923 | 0.998 |

**Table 5.16** Modal parameters of *Dcase_ABB*

| *Mode* | | 1 | 2 | 3 | 4 |
|---|---|---|---|---|---|
| *Frequency (Hz)* | | 1.68 | 5.02 | 7.86 | 10.07 |
| *Damping ratio (%)* | | 2.31 | 0.31 | 1.67 | 1.12 |
| *Mode shape* | A4 | 1.000 | 1.000 | 0.559 | 0.262 |
| | A3 | 0.848 | -0.118 | -0.871 | -0.832 |
| | A2 | 0.637 | -0.888 | -0.171 | 1.000 |
| | A1 | 0.337 | -0.815 | 1.000 | -0.680 |
| *MAC* | | 1.000 | 1.000 | 0.991 | 0.995 |

**Table 5.17** Modal parameters of *Dcase_ABN*

| *Mode* | | 1 | 2 | 3 | 4 |
|---|---|---|---|---|---|
| *Frequency (Hz)* | | 1.64 | 4.84 | 7.77 | 9.58 |
| *Damping ratio (%)* | | 2.08 | 0.16 | 0.24 | 1.76 |
| *Mode shape* | A4 | 1.000 | 0.953 | 0.660 | 0.332 |
| | A3 | 0.853 | -0.049 | -1.000 | -0.760 |
| | A2 | 0.598 | -1.000 | -0.068 | 1.000 |
| | A1 | 0.313 | -0.876 | 0.890 | -0.780 |
| *MAC* | | 0.999 | 0.994 | 0.952 | 0.998 |

**Table 5.18** Modal parameters of *Dcase_ANB*

| *Mode* | | 1 | 2 | 3 | 4 |
|---|---|---|---|---|---|
| *Frequency (Hz)* | | 1.61 | 4.90 | 7.68 | 9.76 |
| *Damping ratio (%)* | | 1.59 | 0.21 | 1.65 | 0.70 |
| *Mode shape* | A4 | 1.000 | 1.000 | 0.483 | 0.277 |
| | A3 | 0.859 | -0.075 | -0.702 | -0.826 |
| | A2 | 0.660 | -0.858 | -0.211 | 1.000 |
| | A1 | 0.321 | -0.867 | 1.000 | -0.492 |
| *MAC* | | 1.000 | 0.997 | 0.995 | 0.974 |

**Table 5.19** Modal parameters of *Dcase_ANN*

| *Mode* | | 1 | 2 | 3 | 4 |
|---|---|---|---|---|---|
| *Frequency (Hz)* | | 1.57 | 4.74 | 7.59 | 9.26 |
| *Damping ratio (%)* | | 1.51 | 0.31 | 0.28 | 0.43 |
| *Mode shape* | A4 | 1.000 | 0.987 | 0.626 | 0.411 |
| | A3 | 0.861 | -0.027 | -0.853 | -0.929 |
| | A2 | 0.623 | -1.000 | -0.182 | 1.000 |
| | A1 | 0.303 | -0.920 | 1.000 | -0.670 |
| *MAC* | | 0.999 | 0.993 | 0.985 | 0.982 |

**Table 5.20** Modal parameters of *Dcase_BBB*

| *Mode* | | 1 | 2 | 3 | 4 |
|---|---|---|---|---|---|
| *Frequency (Hz)* | | 1.62 | 4.88 | 7.79 | 9.90 |
| *Damping ratio (%)* | | 2.24 | 0.36 | 0.76 | 1.40 |
| *Mode shape* | A4 | 1.000 | 1.000 | 0.559 | 0.304 |
| | A3 | 0.856 | -0.061 | -0.895 | -0.919 |
| | A2 | 0.653 | -0.845 | -0.198 | 1.000 |
| | A1 | 0.355 | -0.840 | 1.000 | -0.642 |
| *MAC* | | 1.000 | 0.997 | 0.989 | 0.985 |

**Table 5.21** Modal parameters of *Dcase_BBN*

| *Mode* | | 1 | 2 | 3 | 4 |
|---|---|---|---|---|---|
| *Frequency (Hz)* | | 1.58 | 4.72 | 7.74 | 9.60 |
| *Damping ratio (%)* | | 2.05 | 0.24 | 0.08 | 2.96 |
| *Mode shape* | A4 | 1.000 | 0.990 | 0.669 | 0.309 |
| | A3 | 0.860 | -0.025 | -1.000 | -0.713 |
| | A2 | 0.620 | -1.000 | -0.098 | 1.000 |
| | A1 | 0.337 | -0.929 | 0.934 | -0.795 |
| *MAC* | | 1.000 | 0.993 | 0.958 | 0.997 |

**Table 5.22** Modal parameters of *Dcase_NBB*

| ***Mode*** | | **1** | **2** | **3** | **4** |
|---|---|---|---|---|---|
| ***Frequency (Hz)*** | | 1.60 | 4.82 | 7.63 | 9.92 |
| ***Damping ratio (%)*** | | 0.81 | 0.29 | 0.50 | 0.57 |
| ***Mode shape*** | **A4** | 1.000 | 1.000 | 0.608 | 0.342 |
| | **A3** | 0.859 | -0.044 | -0.893 | -0.796 |
| | **A2** | 0.662 | -0.837 | -0.301 | 1.000 |
| | **A1** | 0.373 | -0.874 | 1.000 | -0.578 |
| ***MAC*** | | 0.999 | 0.994 | 0.977 | 0.989 |

**Table 5.23** Modal parameters of *Dcase_BNN*

| ***Mode*** | | **1** | **2** | **3** | **4** |
|---|---|---|---|---|---|
| ***Frequency (Hz)*** | | 1.54 | 4.65 | 7.54 | 9.25 |
| ***Damping ratio (%)*** | | 0.98 | 0.08 | 0.28 | 0.41 |
| ***Mode shape*** | **A4** | 1.000 | 1.000 | 0.612 | 0.391 |
| | **A3** | 0.867 | 0.019 | -0.866 | -0.934 |
| | **A2** | 0.636 | -0.985 | -0.195 | 1.000 |
| | **A1** | 0.324 | -0.970 | 1.000 | -0.671 |
| ***MAC*** | | 1.000 | 0.987 | 0.986 | 0.983 |

**Table 5.24** Modal parameters of *Dcase_NNB*

| ***Mode*** | | **1** | **2** | **3** | **4** |
|---|---|---|---|---|---|
| ***Frequency (Hz)*** | | 1.56 | 4.81 | 7.36 | 9.81 |
| ***Damping ratio (%)*** | | 0.38 | 0.10 | 0.12 | 1.86 |
| ***Mode shape*** | **A4** | 1.000 | 1.000 | 0.568 | 0.370 |
| | **A3** | 0.866 | -0.042 | -0.745 | -0.985 |
| | **A2** | 0.678 | -0.850 | -0.380 | 1.000 |
| | **A1** | 0.355 | -0.890 | 1.000 | -0.473 |
| ***MAC*** | | 0.999 | 0.994 | 0.966 | 0.946 |

**Table 5.25** Modal parameters of *Dcase_NNN*

| ***Mode*** | | **1** | **2** | **3** | **4** |
|---|---|---|---|---|---|
| ***Frequency (Hz)*** | | 1.52 | 4.64 | 7.33 | 9.23 |
| ***Damping ratio (%)*** | | 0.23 | 0.10 | 0.17 | 0.50 |
| ***Mode shape*** | **A4** | 1.000 | 1.000 | 0.656 | 0.368 |
| | **A3** | 0.870 | 0.025 | -0.845 | -0.924 |
| | **A2** | 0.643 | -0.980 | -0.360 | 1.000 |
| | **A1** | 0.334 | -0.970 | 1.000 | -0.640 |
| ***MAC*** | | 1.000 | 0.987 | 0.964 | 0.983 |

**Table 5.26** Modal parameters of *Dcase_AAA* using RSGs measurements

| ***Mode*** | | **1** | **2** | **3** | **4** |
|---|---|---|---|---|---|
| ***Frequency (Hz)*** | | 1.69 | 5.04 | 8.15 | / |
| ***Damping ratio (%)*** | | 3.72 | 1.87 | 2.53 | / |
| ***SMS*** | ***RSG4*** | 0.524 | 1.000 | 1.000 | / |
| | ***RSG3*** | 0.731 | 0.594 | -0.478 | / |
| | ***RSG2*** | 0.914 | -0.110 | -0.842 | / |
| | ***RSG1*** | 1.000 | -0.740 | 0.805 | / |

**Table 5.27** Modal parameters of *Dcase_BAA* using RSGs measurements

| ***Mode*** | | **1** | **2** | **3** | **4** |
|---|---|---|---|---|---|
| ***Frequency (Hz)*** | | 1.68 | 4.96 | 7.97 | / |
| ***Damping ratio (%)*** | | 2.77 | 1.83 | 2.57 | / |
| ***SMS*** | ***RSG4*** | 0.521 | 1.000 | 1.000 | / |
| | ***RSG3*** | 0.733 | 0.633 | -0.328 | / |
| | ***RSG2*** | 0.922 | -0.130 | -0.580 | / |
| | ***RSG1*** | 1.000 | -0.724 | 0.629 | / |

**Table 5.28** Modal parameters of *Dcase_NAA* using RSGs measurements

| ***Mode*** | | **1** | **2** | **3** | **4** |
|---|---|---|---|---|---|
| ***Frequency (Hz)*** | | 1.60 | 4.79 | 7.76 | / |
| ***Damping ratio (%)*** | | 1.91 | 0.40 | 1.07 | / |
| ***SMS*** | ***RSG4*** | 0.431 | 1.000 | 1.000 | / |
| | ***RSG3*** | 0.651 | 0.771 | -0.446 | / |
| | ***RSG2*** | 0.793 | 0.033 | -0.828 | / |
| | ***RSG1*** | 1.000 | -0.881 | 0.647 | / |

**Table 5.29** Modal parameters of *Dcase_ABA* using RSGs measurements

| ***Mode*** | | **1** | **2** | **3** | **4** |
|---|---|---|---|---|---|
| ***Frequency (Hz)*** | | 1.70 | 5.09 | 7.92 | / |
| ***Damping ratio (%)*** | | 2.24 | 0.61 | 1.82 | / |
| ***SMS*** | ***RSG4*** | 0.505 | 1.000 | 1.000 | / |
| | ***RSG3*** | 0.607 | 0.551 | -0.553 | / |
| | ***RSG2*** | 0.934 | -0.069 | -0.806 | / |
| | ***RSG1*** | 1.000 | -0.729 | 0.762 | / |

**Table 5.30** Modal parameters of *Dcase_ANA* using RSGs measurements

| ***Mode*** | | 1 | 2 | 3 | 4 |
|---|---|---|---|---|---|
| ***Frequency (Hz)*** | | 1.63 | 5.01 | / | / |
| ***Damping ratio (%)*** | | 1.79 | 0.85 | / | / |
| ***SMS*** | ***RSG4*** | 0.437 | 1.000 | / | / |
| | ***RSG3*** | 0.535 | 0.550 | / | / |
| | ***RSG2*** | 1.000 | -0.031 | / | / |
| | ***RSG1*** | 0.868 | -0.779 | / | / |

**Table 5.31** Modal parameters of *Dcase_AAB* using RSGs measurements

| ***Mode*** | | **1** | **2** | **3** | **4** |
|---|---|---|---|---|---|
| ***Frequency (Hz)*** | | 1.68 | 5.03 | / | / |
| ***Damping ratio (%)*** | | 2.98 | 0.33 | / | / |
| ***SMS*** | ***RSG4*** | 0.510 | 1.000 | / | / |
| | ***RSG3*** | 0.688 | 0.621 | / | / |
| | ***RSG2*** | 0.947 | -0.083 | / | / |
| | ***RSG1*** | 1.000 | -0.763 | / | / |

**Table 5.32** Modal parameters of *Dcase_AAN* using RSGs measurements

| ***Mode*** | | **1** | **2** | **3** | **4** |
|---|---|---|---|---|---|
| ***Frequency (Hz)*** | | 1.63 | 4.81 | 7.79 | / |
| ***Damping ratio (%)*** | | 3.04 | 0.18 | 2.27 | / |
| ***SMS*** | ***RSG4*** | 0.504 | 1.000 | 1.000 | / |
| | ***RSG3*** | 0.929 | 0.922 | -0.548 | / |
| | ***RSG2*** | 0.947 | -0.149 | -0.523 | / |
| | ***RSG1*** | 1.000 | -0.964 | 0.443 | / |

**Table 5.33** Modal parameters of *Dcase_BBA* using RSGs measurements

| ***Mode*** | | **1** | **2** | **3** | **4** |
|---|---|---|---|---|---|
| ***Frequency (Hz)*** | | 1.62 | 4.88 | 7.74 | / |
| ***Damping ratio (%)*** | | 2.42 | 2.03 | 1.04 | / |
| ***SMS*** | ***RSG4*** | 0.454 | 1.000 | 1.000 | / |
| | ***RSG3*** | 0.648 | 0.684 | -0.395 | / |
| | ***RSG2*** | 0.871 | -0.050 | -0.729 | / |
| | ***RSG1*** | 1.000 | -0.845 | 0.662 | / |

**Table 5.34** Modal parameters of *Dcase_BNA* using RSGs measurements

| ***Mode*** | | **1** | **2** | **3** | **4** |
|---|---|---|---|---|---|
| ***Frequency (Hz)*** | | 1.60 | 4.90 | 7.52 | / |
| ***Damping ratio (%)*** | | 1.72 | 1.36 | 2.01 | / |
| ***SMS*** | ***RSG4*** | 0.437 | 1.000 | 1.000 | / |
| | ***RSG3*** | 0.623 | 0.704 | -0.259 | / |
| | ***RSG2*** | 1.000 | -0.097 | -0.985 | / |
| | ***RSG1*** | 0.872 | -0.784 | 0.745 | / |

**Table 5.35** Modal parameters of *Dcase_NBA* using RSGs measurements

| ***Mode*** | | **1** | **2** | **3** | **4** |
|---|---|---|---|---|---|
| ***Frequency (Hz)*** | | 1.58 | 4.76 | 7.61 | / |
| ***Damping ratio (%)*** | | 1.56 | 0.56 | 3.84 | / |
| ***SMS*** | ***RSG4*** | 0.428 | 1.000 | 1.000 | / |
| | ***RSG3*** | 0.638 | 0.780 | -0.525 | / |
| | ***RSG2*** | 0.852 | 0.051 | -0.974 | / |
| | ***RSG1*** | 1.000 | -0.927 | 0.921 | / |

**Table 5.36** Modal parameters of *Dcase_NNA* using RSGs measurements

| ***Mode*** | | **1** | **2** | **3** | **4** |
|---|---|---|---|---|---|
| ***Frequency (Hz)*** | | 1.55 | 4.72 | 7.39 | 9.65 |
| ***Damping ratio (%)*** | | 0.79 | 0.77 | 0.90 | 1.74 |
| ***SMS*** | ***RSG4*** | 0.420 | 1.000 | 0.929 | -0.614 |
| | ***RSG3*** | 0.627 | 0.869 | -0.207 | 1.000 |
| | ***RSG2*** | 0.966 | -0.023 | -1.000 | -0.652 |
| | ***RSG1*** | 1.000 | -0.887 | 0.696 | 0.277 |

**Table 5.37** Modal parameters of *Dcase_BAB* using RSGs measurements

| ***Mode*** | | **1** | **2** | **3** | **4** |
|---|---|---|---|---|---|
| ***Frequency (Hz)*** | | 1.63 | 4.90 | 7.89 | 10.08 |
| ***Damping ratio (%)*** | | 2.52 | 0.55 | 1.40 | 2.79 |
| ***SMS*** | ***RSG4*** | 0.452 | 1.000 | 1.000 | -0.728 |
| | ***RSG3*** | 0.617 | 0.686 | -0.582 | 1.000 |
| | ***RSG2*** | 0.870 | -0.048 | -0.689 | -0.810 |
| | ***RSG1*** | 1.000 | -0.780 | 0.652 | 0.263 |

**Table 5.38** Modal parameters of *Dcase_BAN* using RSGs measurements

| ***Mode*** | | **1** | **2** | **3** | **4** |
|---|---|---|---|---|---|
| ***Frequency (Hz)*** | | 1.59 | 4.72 | 7.80 | / |
| ***Damping ratio (%)*** | | 2.62 | 0.35 | 1.18 | / |
| ***SMS*** | ***RSG4*** | 0.446 | 1.000 | 1.000 | / |
| | ***RSG3*** | 0.843 | 0.960 | -0.503 | / |
| | ***RSG2*** | 0.881 | -0.080 | -0.525 | / |
| | ***RSG1*** | 1.000 | -0.975 | 0.486 | / |

**Table 5.39** Modal parameters of *Dcase_NAB* using RSGs measurements

| ***Mode*** | | **1** | **2** | **3** | **4** |
|---|---|---|---|---|---|
| ***Frequency (Hz)*** | | 1.60 | 4.84 | 7.74 | / |
| ***Damping ratio (%)*** | | 1.51 | 0.71 | 1.44 | / |
| ***SMS*** | ***RSG4*** | 0.421 | 1.000 | 1.000 | / |
| | ***RSG3*** | 0.586 | 0.641 | -0.432 | / |
| | ***RSG2*** | 0.838 | 0.027 | -0.734 | / |
| | ***RSG1*** | 1.000 | -0.832 | 0.571 | / |

**Table 5.40** Modal parameters of *Dcase_NAN* using RSGs measurements

| ***Mode*** | | **1** | **2** | **3** | **4** |
|---|---|---|---|---|---|
| ***Frequency (Hz)*** | | 1.56 | 4.63 | 7.68 | / |
| ***Damping ratio (%)*** | | 1.37 | 0.02 | 1.12 | / |
| ***SMS*** | ***RSG4*** | 0.419 | 0.936 | 1.000 | / |
| | ***RSG3*** | 0.797 | 0.937 | -0.398 | / |
| | ***RSG2*** | 0.846 | 0.055 | -0.549 | / |
| | ***RSG1*** | 1.000 | -1.000 | 0.438 | / |

**Table 5.41** Modal parameters of *Dcase_ABB* using RSGs measurements

| ***Mode*** | | **1** | **2** | **3** | **4** |
|---|---|---|---|---|---|
| ***Frequency (Hz)*** | | 1.68 | 5.02 | 7.90 | / |
| ***Damping ratio (%)*** | | 2.30 | 0.17 | 2.93 | / |
| ***SMS*** | ***RSG4*** | 0.503 | 1.000 | 1.000 | / |
| | ***RSG3*** | 0.687 | 0.618 | -0.404 | / |
| | ***RSG2*** | 0.939 | -0.094 | -0.698 | / |
| | ***RSG1*** | 1.000 | -0.738 | 0.646 | / |

**Table 5.42** Modal parameters of *Dcase_ABN* using RSGs measurements

| ***Mode*** | | **1** | **2** | **3** | **4** |
|---|---|---|---|---|---|
| ***Frequency (Hz)*** | | 1.64 | 4.83 | 7.77 | / |
| ***Damping ratio (%)*** | | 2.04 | 0.26 | 0.93 | / |
| ***SMS*** | ***RSG4*** | 0.510 | 1.000 | 1.000 | / |
| | ***RSG3*** | 0.939 | 0.894 | -0.532 | / |
| | ***RSG2*** | 0.946 | -0.145 | -0.531 | / |
| | ***RSG1*** | 1.000 | -0.906 | 0.463 | / |

**Table 5.43** Modal parameters of *Dcase_ANB* using RSGs measurements

| ***Mode*** | | **1** | **2** | **3** | **4** |
|---|---|---|---|---|---|
| ***Frequency (Hz)*** | | 1.62 | 4.91 | 7.69 | / |
| ***Damping ratio (%)*** | | 1.58 | 0.73 | 3.62 | / |
| ***SMS*** | ***RSG4*** | 0.439 | 1.000 | 0.986 | / |
| | ***RSG3*** | 0.598 | 0.659 | -0.336 | / |
| | ***RSG2*** | 1.000 | -0.033 | -1.000 | / |
| | ***RSG1*** | 0.872 | -0.841 | 0.759 | / |

**Table 5.44** Modal parameters of *Dcase_ANN* using RSGs measurements

| ***Mode*** | | **1** | **2** | **3** | **4** |
|---|---|---|---|---|---|
| ***Frequency (Hz)*** | | 1.57 | 4.75 | 7.58 | 9.29 |
| ***Damping ratio (%)*** | | 1.53 | 0.30 | 1.49 | 1.84 |
| ***SMS*** | ***RSG4*** | 0.429 | 1.000 | 1.000 | -0.780 |
| | ***RSG3*** | 0.808 | 0.956 | -0.442 | 1.000 |
| | ***RSG2*** | 1.000 | -0.085 | -0.792 | -0.854 |
| | ***RSG1*** | 0.878 | -0.919 | 0.654 | 0.312 |

**Table 5.45** Modal parameters of *Dcase_BBB* using RSGs measurements

| ***Mode*** | | **1** | **2** | **3** | **4** |
|---|---|---|---|---|---|
| ***Frequency (Hz)*** | | 1.62 | 4.87 | 7.82 | / |
| ***Damping ratio (%)*** | | 2.28 | 0.65 | 2.28 | / |
| ***SMS*** | ***RSG4*** | 0.443 | 1.000 | 1.000 | / |
| | ***RSG3*** | 0.628 | 0.687 | -0.409 | / |
| | ***RSG2*** | 0.875 | -0.027 | -0.812 | / |
| | ***RSG1*** | 1.000 | -0.822 | 0.770 | / |

**Table 5.46** Modal parameters of *Dcase_BBN* using RSGs measurements

| ***Mode*** | | **1** | **2** | **3** | **4** |
|---|---|---|---|---|---|
| ***Frequency (Hz)*** | | 1.58 | 4.72 | 7.76 | / |
| ***Damping ratio (%)*** | | 2.12 | 0.29 | 0.86 | / |
| ***SMS*** | ***RSG4*** | 0.440 | 1.000 | 1.000 | / |
| | ***RSG3*** | 0.823 | 0.991 | -0.530 | / |
| | ***RSG2*** | 0.875 | -0.081 | -0.541 | / |
| | ***RSG1*** | 1.000 | -0.956 | 0.496 | / |

**Table 5.47** Modal parameters of *Dcase_NBB* using RSGs measurements

| ***Mode*** | | **1** | **2** | **3** | **4** |
|---|---|---|---|---|---|
| ***Frequency (Hz)*** | | 1.60 | 4.82 | 7.60 | / |
| ***Damping ratio (%)*** | | 0.80 | 0.29 | 1.37 | / |
| ***SMS*** | ***RSG4*** | 0.429 | 1.000 | 1.000 | / |
| | ***RSG3*** | 0.604 | 0.696 | -0.398 | / |
| | ***RSG2*** | 0.791 | -0.036 | -0.789 | / |
| | ***RSG1*** | 1.000 | -0.837 | 0.576 | / |

**Table 5.48** Modal parameters of *Dcase_BNN* using RSGs measurements

| ***Mode*** | | **1** | **2** | **3** | **4** |
|---|---|---|---|---|---|
| ***Frequency (Hz)*** | | 1.54 | 4.63 | 7.58 | / |
| ***Damping ratio (%)*** | | 1.13 | 0.13 | 1.64 | / |
| ***SMS*** | ***RSG4*** | 0.425 | 0.981 | 1.000 | / |
| | ***RSG3*** | 0.799 | 0.983 | -0.343 | / |
| | ***RSG2*** | 1.000 | -0.032 | -0.806 | / |
| | ***RSG1*** | 0.972 | -1.000 | 0.633 | / |

**Table 5.49** Modal parameters of *Dcase_NNB* using RSGs measurements

| ***Mode*** | | **1** | **2** | **3** | **4** |
|---|---|---|---|---|---|
| ***Frequency (Hz)*** | | 1.56 | 4.81 | 7.38 | / |
| ***Damping ratio (%)*** | | 0.41 | 0.60 | 0.68 | / |
| ***SMS*** | ***RSG4*** | 0.414 | 1.000 | 0.942 | / |
| | ***RSG3*** | 0.573 | 0.659 | -0.195 | / |
| | ***RSG2*** | 0.977 | 0.018 | -1.000 | / |
| | ***RSG1*** | 1.000 | -0.831 | 0.679 | / |

**Table 5.50** Modal parameters of *Dcase_NNN* using RSGs measurements

| ***Mode*** | | **1** | **2** | **3** | **4** |
|---|---|---|---|---|---|
| ***Frequency (Hz)*** | | 1.53 | 4.64 | 7.34 | / |
| ***Damping ratio (%)*** | | 0.31 | 0.12 | 0.63 | / |
| ***SMS*** | ***RSG4*** | 0.412 | 1.000 | 1.000 | / |
| | ***RSG3*** | 0.776 | 0.985 | -0.296 | / |
| | ***RSG2*** | 0.992 | -0.038 | -0.864 | / |
| | ***RSG1*** | 1.000 | -0.986 | 0.624 | / |

**Table 5.51** Modal parameters of *Dcase_AAA* using FBG sensors measurements

| ***Mode*** | | **1** | **2** | **3** | **4** |
|---|---|---|---|---|---|
| ***Frequency (Hz)*** | | 1.71 | 5.29 | 8.37 | 10.66 |
| ***Damping ratio (%)*** | | 2.89 | 2.26 | 2.43 | 3.13 |
| ***SMS*** | ***FBG8*** | 0.416 | -0.996 | -0.962 | -0.901 |
| | ***FBG7*** | -0.406 | 1.000 | 1.000 | 1.000 |
| | ***FBG6*** | 0.635 | -0.678 | 0.517 | 0.348 |
| | ***FBG5*** | -0.594 | 0.650 | -0.481 | -0.265 |
| | ***FBG4*** | 0.814 | 0.087 | 0.751 | -0.587 |
| | ***FBG3*** | -0.793 | -0.128 | -0.828 | 0.767 |
| | ***FBG2*** | 1.000 | 0.710 | -0.733 | 0.769 |
| | ***FBG1*** | -0.966 | -0.859 | 0.789 | -0.600 |

**Table 5.52** Modal parameters of *Dcase_BAA* using FBG sensors measurements

| ***Mode*** | | **1** | **2** | **3** | **4** |
|---|---|---|---|---|---|
| ***Frequency (Hz)*** | | 1.70 | 5.21 | 8.18 | / |
| ***Damping ratio (%)*** | | 2.57 | 3.85 | 2.06 | / |
| ***SMS*** | ***FBG8*** | 0.404 | -1.000 | -0.973 | / |
| | ***FBG7*** | -0.397 | 0.994 | 1.000 | / |
| | ***FBG6*** | 0.623 | -0.736 | 0.548 | / |
| | ***FBG5*** | -0.583 | 0.702 | -0.522 | / |
| | ***FBG4*** | 0.802 | 0.080 | 0.787 | / |
| | ***FBG3*** | -0.782 | -0.107 | -0.864 | / |
| | ***FBG2*** | 1.000 | 0.731 | -0.601 | / |
| | ***FBG1*** | -0.946 | -0.883 | 0.665 | / |

**Table 5.53** Modal parameters of *Dcase_NAA* using FBG sensors measurements

| ***Mode*** | | **1** | **2** | **3** | **4** |
|---|---|---|---|---|---|
| ***Frequency (Hz)*** | | 1.65 | 4.97 | 8.11 | / |
| ***Damping ratio (%)*** | | 1.76 | 0.89 | 0.95 | / |
| ***SMS*** | ***FBG8*** | 0.340 | -1.000 | -0.991 | / |
| | ***FBG7*** | -0.334 | 0.999 | 1.000 | / |
| | ***FBG6*** | 0.553 | -0.788 | 0.486 | / |
| | ***FBG5*** | -0.519 | 0.759 | -0.450 | / |
| | ***FBG4*** | 0.699 | -0.086 | 0.831 | / |
| | ***FBG3*** | -0.674 | 0.071 | -0.905 | / |
| | ***FBG2*** | 1.000 | 0.820 | -0.687 | / |
| | ***FBG1*** | 0.957 | -0.959 | 0.715 | / |

**Table 5.54** Modal parameters of *Dcase_ABA* using FBG sensors measurements

| ***Mode*** | | **1** | **2** | **3** | **4** |
|---|---|---|---|---|---|
| ***Frequency (Hz)*** | | 1.73 | 5.35 | 8.27 | / |
| ***Damping ratio (%)*** | | 2.88 | 0.54 | 1.96 | / |
| ***SMS*** | ***FBG8*** | 0.401 | -1.000 | -0.932 | / |
| | ***FBG7*** | -0.392 | 0.999 | 0.978 | / |
| | ***FBG6*** | 0.538 | -0.588 | 0.571 | / |
| | ***FBG5*** | -0.497 | 0.550 | -0.510 | / |
| | ***FBG4*** | 0.832 | -0.018 | 0.919 | / |
| | ***FBG3*** | -0.817 | -0.051 | -1.000 | / |
| | ***FBG2*** | 1.000 | 0.584 | -0.753 | / |
| | ***FBG1*** | -0.967 | -0.771 | 0.816 | / |

**Table 5.55** Modal parameters of *Dcase_ANA* using FBG sensors measurements

| ***Mode*** | | **1** | **2** | **3** | **4** |
|---|---|---|---|---|---|
| ***Frequency (Hz)*** | | 1.67 | 5.19 | / | / |
| ***Damping ratio (%)*** | | 1.82 | 0.77 | / | / |
| ***SMS*** | ***FBG8*** | 0.391 | -1.000 | / | / |
| | ***FBG7*** | -0.387 | 1.000 | / | / |
| | ***FBG6*** | 0.542 | -0.629 | / | / |
| | ***FBG5*** | -0.489 | 0.593 | / | / |
| | ***FBG4*** | 1.000 | -0.105 | / | / |
| | ***FBG3*** | -0.986 | 0.069 | / | / |
| | ***FBG2*** | 0.941 | 0.668 | / | / |
| | ***FBG1*** | -0.926 | -0.843 | / | / |

**Table 5.56** Modal parameters of *Dcase_AAB* using FBG sensors measurements

| ***Mode*** | | **1** | **2** | **3** | **4** |
|---|---|---|---|---|---|
| ***Frequency (Hz)*** | | 1.71 | 5.21 | 8.27 | 10.48 |
| ***Damping ratio (%)*** | | 2.91 | 1.26 | 3.78 | 2.25 |
| ***SMS*** | ***FBG8*** | 0.408 | -0.998 | -0.944 | -0.548 |
| | ***FBG7*** | -0.398 | 1.000 | 1.000 | 0.616 |
| | ***FBG6*** | 0.612 | -0.699 | 0.673 | 0.960 |
| | ***FBG5*** | -0.566 | 0.667 | -0.629 | -1.000 |
| | ***FBG4*** | 0.841 | 0.063 | 0.856 | -0.838 |
| | ***FBG3*** | -0.826 | -0.081 | -0.960 | 0.872 |
| | ***FBG2*** | 1.000 | 0.664 | -0.522 | 0.347 |
| | ***FBG1*** | -0.964 | -0.828 | 0.628 | -0.497 |

**Table 5.57** Modal parameters of *Dcase_AAN* using FBG sensors measurements

| ***Mode*** | | **1** | **2** | **3** | **4** |
|---|---|---|---|---|---|
| ***Frequency (Hz)*** | | 1.64 | 4.96 | 7.98 | 10.00 |
| ***Damping ratio (%)*** | | 3.28 | 0.92 | 1.99 | 2.56 |
| ***SMS*** | ***FBG8*** | 0.414 | -1.000 | -0.962 | -0.291 |
| | ***FBG7*** | -0.392 | 0.982 | 1.000 | 0.340 |
| | ***FBG6*** | 0.803 | -0.990 | 0.686 | 1.000 |
| | ***FBG5*** | -0.757 | 0.970 | -0.662 | -0.983 |
| | ***FBG4*** | 0.829 | 0.092 | 0.635 | -0.836 |
| | ***FBG3*** | -0.825 | -0.110 | -0.721 | 0.875 |
| | ***FBG2*** | 1.000 | 0.818 | -0.446 | 0.257 |
| | ***FBG1*** | -0.967 | -0.975 | 0.489 | -0.263 |

**Table 5.58** Modal parameters of *Dcase_BBA* using FBG sensors measurements

| ***Mode*** | | **1** | **2** | **3** | **4** |
|---|---|---|---|---|---|
| ***Frequency (Hz)*** | | 1.64 | 5.09 | 8.04 | 10.52 |
| ***Damping ratio (%)*** | | 2.41 | 3.64 | 2.62 | 2.86 |
| ***SMS*** | ***FBG8*** | 0.366 | -0.998 | -0.968 | -0.443 |
| | ***FBG7*** | -0.358 | 1.000 | 1.000 | 0.557 |
| | ***FBG6*** | 0.576 | -0.754 | 0.521 | 1.000 |
| | ***FBG5*** | -0.533 | 0.723 | -0.469 | -0.955 |
| | ***FBG4*** | 0.783 | -0.090 | 0.854 | -0.525 |
| | ***FBG3*** | -0.767 | 0.078 | -0.940 | 0.639 |
| | ***FBG2*** | 1.000 | 0.704 | -0.696 | 0.373 |
| | ***FBG1*** | -0.976 | -0.851 | 0.753 | -0.526 |

**Table 5.59** Modal parameters of *Dcase_BNA* using FBG sensors measurements

| ***Mode*** | | **1** | **2** | **3** | **4** |
|---|---|---|---|---|---|
| ***Frequency (Hz)*** | | 1.65 | 5.19 | 7.75 | 10.00 |
| ***Damping ratio (%)*** | | 1.29 | 3.81 | 1.50 | 1.57 |
| ***SMS*** | ***FBG8*** | 0.399 | -1.000 | -0.795 | -0.607 |
| | ***FBG7*** | -0.393 | 0.998 | 0.818 | 0.656 |
| | ***FBG6*** | 0.632 | -0.747 | 0.338 | 0.963 |
| | ***FBG5*** | -0.575 | 0.710 | -0.299 | -1.000 |
| | ***FBG4*** | 0.997 | 0.073 | 0.893 | -0.901 |
| | ***FBG3*** | -1.000 | -0.087 | -1.000 | 0.914 |
| | ***FBG2*** | 0.975 | 0.706 | -0.607 | 0.004 |
| | ***FBG1*** | -0.949 | -0.871 | 0.617 | -0.009 |

**Table 5.60** Modal parameters of *Dcase_NBA* using FBG sensors measurements

| ***Mode*** | | **1** | **2** | **3** | **4** |
|---|---|---|---|---|---|
| ***Frequency (Hz)*** | | 1.63 | 4.90 | 7.86 | / |
| ***Damping ratio (%)*** | | 1.07 | 0.74 | 2.30 | / |
| ***SMS*** | ***FBG8*** | 0.342 | -0.981 | -0.966 | / |
| | ***FBG7*** | -0.336 | 0.979 | 0.998 | / |
| | ***FBG6*** | 0.554 | -0.841 | 0.344 | / |
| | ***FBG5*** | -0.513 | 0.808 | -0.304 | / |
| | ***FBG4*** | 0.749 | -0.102 | 0.886 | / |
| | ***FBG3*** | -0.733 | 0.098 | -1.000 | / |
| | ***FBG2*** | 1.000 | 0.860 | -0.732 | / |
| | ***FBG1*** | -0.968 | -1.000 | 0.778 | / |

**Table 5.61** Modal parameters of *Dcase_NNA* using FBG sensors measurements

| ***Mode*** | | **1** | **2** | **3** | **4** |
|---|---|---|---|---|---|
| ***Frequency (Hz)*** | | 1.59 | 4.79 | 7.60 | 9.96 |
| ***Damping ratio (%)*** | | 0.34 | 2.18 | 1.25 | 1.79 |
| ***SMS*** | ***FBG8*** | 0.344 | -0.961 | -0.779 | -0.583 |
| | ***FBG7*** | -0.337 | 0.954 | 0.800 | 0.620 |
| | ***FBG6*** | 0.567 | -0.922 | 0.262 | 0.977 |
| | ***FBG5*** | -0.517 | 0.894 | -0.217 | -1.000 |
| | ***FBG4*** | 0.872 | -0.075 | 0.900 | -0.841 |
| | ***FBG3*** | -0.873 | 0.082 | -1.000 | 0.854 |
| | ***FBG2*** | 1.000 | 0.855 | -0.494 | 0.104 |
| | ***FBG1*** | -0.977 | -1.000 | 0.505 | -0.126 |

**Table 5.62** Modal parameters of *Dcase_BAB* using FBG sensors measurements

| ***Mode*** | | **1** | **2** | **3** | **4** |
|---|---|---|---|---|---|
| ***Frequency (Hz)*** | | 1.66 | 5.05 | 8.09 | 10.35 |
| ***Damping ratio (%)*** | | 2.31 | 1.56 | 1.36 | 1.47 |
| ***SMS*** | ***FBG8*** | 0.365 | -1.000 | -0.976 | -0.630 |
| | ***FBG7*** | -0.357 | 0.999 | 1.000 | 0.666 |
| | ***FBG6*** | 0.551 | -0.741 | 0.502 | 1.000 |
| | ***FBG5*** | -0.510 | 0.716 | -0.479 | -0.999 |
| | ***FBG4*** | 0.783 | -0.070 | 0.687 | -0.834 |
| | ***FBG3*** | -0.760 | -0.072 | -0.768 | 0.870 |
| | ***FBG2*** | 1.000 | 0.722 | -0.644 | 0.331 |
| | ***FBG1*** | -0.970 | -0.880 | 0.682 | -0.355 |

**Table 5.63** Modal parameters of *Dcase_BAN* using FBG sensors measurements

| ***Mode*** | | **1** | **2** | **3** | **4** |
|---|---|---|---|---|---|
| ***Frequency (Hz)*** | | 1.63 | 4.85 | 8.03 | 10.02 |
| ***Damping ratio (%)*** | | 2.24 | 0.34 | 0.42 | 3.17 |
| ***SMS*** | ***FBG8*** | 0.375 | -0.961 | -0.974 | -0.804 |
| | ***FBG7*** | -0.355 | 0.941 | 1.000 | 0.855 |
| | ***FBG6*** | 0.733 | -0.987 | 0.452 | 0.699 |
| | ***FBG5*** | -0.694 | 0.968 | -0.443 | -0.739 |
| | ***FBG4*** | 0.785 | 0.057 | 0.437 | -0.940 |
| | ***FBG3*** | -0.773 | -0.067 | -0.503 | 1.000 |
| | ***FBG2*** | 1.000 | 0.851 | -0.468 | 0.693 |
| | ***FBG1*** | -0.969 | -1.000 | 0.488 | -0.788 |

**Table 5.64** Modal parameters of *Dcase_NAB* using FBG sensors measurements

| ***Mode*** | | **1** | **2** | **3** | **4** |
|---|---|---|---|---|---|
| ***Frequency (Hz)*** | | 1.64 | 4.91 | 8.05 | 10.38 |
| ***Damping ratio (%)*** | | 0.94 | 2.77 | 0.85 | 3.01 |
| ***SMS*** | ***FBG8*** | 0.336 | -1.000 | -0.970 | -0.665 |
| | ***FBG7*** | -0.331 | 0.999 | 1.000 | 0.707 |
| | ***FBG6*** | 0.515 | -0.788 | 0.563 | 0.993 |
| | ***FBG5*** | -0.477 | 0.754 | -0.527 | -1.000 |
| | ***FBG4*** | 0.744 | -0.212 | 0.839 | -0.867 |
| | ***FBG3*** | -0.720 | 0.201 | -0.927 | 0.910 |
| | ***FBG2*** | 1.000 | 0.786 | -0.482 | 0.278 |
| | ***FBG1*** | -0.964 | -0.924 | 0.514 | -0.350 |

**Table 5.65** Modal parameters of *Dcase_NAN* using FBG sensors measurements

| ***Mode*** | | **1** | **2** | **3** | **4** |
|---|---|---|---|---|---|
| ***Frequency (Hz)*** | | 1.61 | 4.78 | 8.00 | 10.00 |
| ***Damping ratio (%)*** | | 0.82 | 0.32 | 1.26 | 1.62 |
| ***SMS*** | ***FBG8*** | 0.346 | -0.885 | -0.970 | -0.397 |
| | ***FBG7*** | -0.327 | 0.865 | 1.000 | 0.439 |
| | ***FBG6*** | 0.681 | -0.933 | 0.549 | 1.000 |
| | ***FBG5*** | -0.649 | 0.912 | -0.536 | -0.986 |
| | ***FBG4*** | 0.740 | -0.066 | 0.512 | -0.621 |
| | ***FBG3*** | -0.725 | 0.071 | -0.605 | 0.639 |
| | ***FBG2*** | 1.000 | 0.865 | -0.475 | 0.347 |
| | ***FBG1*** | -0.963 | -1.000 | 0.490 | -0.364 |

**Table 5.66** Modal parameters of *Dcase_ABB* using FBG sensors measurements

| ***Mode*** | | **1** | **2** | **3** | **4** |
|---|---|---|---|---|---|
| ***Frequency (Hz)*** | | 1.71 | 5.22 | 8.22 | 10.47 |
| ***Damping ratio (%)*** | | 2.31 | 1.15 | 2.24 | 1.93 |
| ***SMS*** | ***FBG8*** | 0.405 | -1.000 | -0.954 | -0.265 |
| | ***FBG7*** | -0.393 | 1.000 | 1.000 | 0.293 |
| | ***FBG6*** | 0.604 | -0.695 | 0.614 | 0.986 |
| | ***FBG5*** | -0.561 | 0.667 | -0.571 | -1.000 |
| | ***FBG4*** | 0.835 | 0.025 | 0.836 | -0.630 |
| | ***FBG3*** | -0.822 | -0.066 | -0.932 | 0.657 |
| | ***FBG2*** | 1.000 | 0.663 | -0.612 | 0.158 |
| | ***FBG1*** | -0.968 | -0.827 | 0.646 | -0.096 |

**Table 5.67** Modal parameters of *Dcase_ABN* using FBG sensors measurements

| ***Mode*** | | **1** | **2** | **3** | **4** |
|---|---|---|---|---|---|
| ***Frequency (Hz)*** | | 1.66 | 4.97 | 8.04 | 9.88 |
| ***Damping ratio (%)*** | | 1.67 | 0.66 | 0.46 | 2.00 |
| ***SMS*** | ***FBG8*** | 0.423 | -1.000 | -0.954 | -0.279 |
| | ***FBG7*** | -0.401 | 0.983 | 1.000 | 0.300 |
| | ***FBG6*** | 0.815 | -0.977 | 0.628 | 0.978 |
| | ***FBG5*** | -0.767 | 0.960 | -0.609 | -1.000 |
| | ***FBG4*** | 0.827 | 0.102 | 0.568 | -0.784 |
| | ***FBG3*** | -0.824 | -0.127 | -0.646 | 0.812 |
| | ***FBG2*** | 1.000 | 0.824 | -0.440 | 0.174 |
| | ***FBG1*** | -0.964 | -0.986 | 0.473 | -0.161 |

**Table 5.68** Modal parameters of *Dcase_ANB* using FBG sensors measurements

| ***Mode*** | | **1** | **2** | **3** | **4** |
|---|---|---|---|---|---|
| ***Frequency (Hz)*** | | 1.66 | 5.03 | 7.82 | 10.21 |
| ***Damping ratio (%)*** | | 1.67 | 2.48 | 3.82 | 3.84 |
| ***SMS*** | ***FBG8*** | 0.396 | -1.000 | -0.920 | -0.724 |
| | ***FBG7*** | -0.390 | 0.996 | 0.941 | 0.695 |
| | ***FBG6*** | 0.607 | -0.748 | 0.373 | 1.000 |
| | ***FBG5*** | -0.551 | 0.719 | -0.354 | -0.937 |
| | ***FBG4*** | 1.000 | -0.096 | 0.899 | -0.734 |
| | ***FBG3*** | -0.989 | 0.079 | -1.000 | 0.779 |
| | ***FBG2*** | 0.954 | 0.772 | -0.807 | 0.685 |
| | ***FBG1*** | -0.939 | -0.938 | 0.834 | -0.694 |

**Table 5.69** Modal parameters of *Dcase_ANN* using FBG sensors measurements

| ***Mode*** | | **1** | **2** | **3** | **4** |
|---|---|---|---|---|---|
| ***Frequency (Hz)*** | | 1.62 | 4.87 | 7.85 | 9.68 |
| ***Damping ratio (%)*** | | 1.29 | 0.64 | 1.54 | 1.64 |
| ***SMS*** | ***FBG8*** | 0.409 | -0.958 | -0.970 | -0.755 |
| | ***FBG7*** | -0.387 | 0.939 | 1.000 | 0.800 |
| | ***FBG6*** | 0.802 | -0.981 | 0.359 | 0.981 |
| | ***FBG5*** | -0.752 | 0.961 | -0.335 | -0.995 |
| | ***FBG4*** | 1.000 | 0.044 | 0.732 | -0.976 |
| | ***FBG3*** | -0.997 | -0.045 | -0.845 | 1.000 |
| | ***FBG2*** | 0.962 | 0.839 | -0.555 | 0.300 |
| | ***FBG1*** | -0.946 | -1.000 | 0.533 | -0.291 |

**Table 5.70** Modal parameters of *Dcase_BBB* using FBG sensors measurements

| ***Mode*** | | **1** | **2** | **3** | **4** |
|---|---|---|---|---|---|
| ***Frequency (Hz)*** | | 1.67 | 5.05 | 8.08 | 10.26 |
| ***Damping ratio (%)*** | | 2.14 | 1.37 | 1.38 | 2.03 |
| ***SMS*** | ***FBG8*** | 0.361 | -1.000 | -0.961 | -0.442 |
| | ***FBG7*** | -0.351 | 0.998 | 1.000 | 0.434 |
| | ***FBG6*** | 0.554 | -0.748 | 0.560 | 1.000 |
| | ***FBG5*** | -0.516 | 0.725 | -0.524 | -0.982 |
| | ***FBG4*** | 0.787 | -0.037 | 0.858 | -0.640 |
| | ***FBG3*** | -0.769 | 0.016 | -0.943 | 0.667 |
| | ***FBG2*** | 1.000 | 0.742 | -0.526 | 0.169 |
| | ***FBG1*** | -0.971 | -0.898 | 0.567 | -0.240 |

**Table 5.71** Modal parameters of *Dcase_BBN* using FBG sensors measurements

| ***Mode*** | | **1** | **2** | **3** | **4** |
|---|---|---|---|---|---|
| ***Frequency (Hz)*** | | 1.62 | 4.88 | 8.02 | 9.97 |
| ***Damping ratio (%)*** | | 1.91 | 0.48 | 0.97 | 2.79 |
| ***SMS*** | ***FBG8*** | 0.369 | -0.970 | -0.953 | -0.793 |
| | ***FBG7*** | -0.350 | 0.950 | 1.000 | 0.775 |
| | ***FBG6*** | 0.720 | -0.989 | 0.635 | 0.904 |
| | ***FBG5*** | -0.680 | 0.972 | -0.612 | -0.902 |
| | ***FBG4*** | 0.778 | 0.055 | 0.574 | -0.944 |
| | ***FBG3*** | -0.768 | -0.070 | -0.650 | 1.000 |
| | ***FBG2*** | 1.000 | 0.849 | -0.555 | 0.880 |
| | ***FBG1*** | -0.969 | -1.000 | 0.575 | -0.926 |

**Table 5.72** Modal parameters of *Dcase_NBB* using FBG sensors measurements

| ***Mode*** | | **1** | **2** | **3** | **4** |
|---|---|---|---|---|---|
| ***Frequency (Hz)*** | | 1.65 | 4.92 | 7.92 | 10.32 |
| ***Damping ratio (%)*** | | 0.63 | 1.27 | 0.89 | 1.66 |
| ***SMS*** | ***FBG8*** | 0.346 | -1.000 | -0.981 | -0.568 |
| | ***FBG7*** | -0.343 | 0.997 | 1.000 | 0.633 |
| | ***FBG6*** | 0.536 | -0.801 | 0.437 | 1.000 |
| | ***FBG5*** | -0.496 | 0.777 | -0.389 | -0.987 |
| | ***FBG4*** | 0.730 | -0.113 | 0.789 | -0.717 |
| | ***FBG3*** | -0.700 | 0.100 | -0.876 | 0.822 |
| | ***FBG2*** | 1.000 | 0.768 | -0.675 | 0.275 |
| | ***FBG1*** | -0.979 | -0.909 | 0.685 | -0.179 |

**Table 5.73** Modal parameters of *Dcase_BNN* using FBG sensors measurements

| ***Mode*** | | **1** | **2** | **3** | **4** |
|---|---|---|---|---|---|
| ***Frequency (Hz)*** | | 1.58 | 4.76 | 7.78 | 9.59 |
| ***Damping ratio (%)*** | | 0.42 | 0.74 | 1.09 | 0.89 |
| ***SMS*** | ***FBG8*** | 0.376 | -0.922 | -0.958 | -0.618 |
| | ***FBG7*** | -0.356 | 0.902 | 1.000 | 0.666 |
| | ***FBG6*** | 0.741 | -0.981 | 0.506 | 1.000 |
| | ***FBG5*** | -0.693 | 0.959 | -0.462 | -0.994 |
| | ***FBG4*** | 0.936 | -0.031 | 0.814 | -0.682 |
| | ***FBG3*** | -0.932 | 0.031 | -0.940 | 0.696 |
| | ***FBG2*** | 1.000 | 0.853 | -0.676 | 0.490 |
| | ***FBG1*** | -0.983 | -1.000 | 0.704 | -0.479 |

**Table 5.74** Modal parameters of *Dcase_NNB* using FBG sensors measurements

| ***Mode*** | | **1** | **2** | **3** | **4** |
|---|---|---|---|---|---|
| ***Frequency (Hz)*** | | 1.60 | 4.88 | 7.63 | / |
| ***Damping ratio (%)*** | | 0.27 | 2.58 | 0.66 | / |
| ***SMS*** | ***FBG8*** | 0.338 | -1.000 | -0.946 | / |
| | ***FBG7*** | -0.332 | 0.997 | 0.967 | / |
| | ***FBG6*** | 0.525 | -0.869 | 0.252 | / |
| | ***FBG5*** | -0.476 | 0.837 | -0.214 | / |
| | ***FBG4*** | 0.875 | -0.189 | 0.880 | / |
| | ***FBG3*** | -0.870 | 0.196 | -1.000 | / |
| | ***FBG2*** | 1.000 | 0.722 | -0.743 | / |
| | ***FBG1*** | -0.976 | -0.843 | 0.743 | / |

**Table 5.75** Modal parameters of *Dcase_NNN* using FBG sensors measurements

| ***Mode*** | | **1** | **2** | **3** | **4** |
|---|---|---|---|---|---|
| ***Frequency (Hz)*** | | 1.57 | 4.80 | 7.59 | 9.52 |
| ***Damping ratio (%)*** | | 0.20 | 0.86 | 0.80 | 0.91 |
| ***SMS*** | ***FBG8*** | 0.349 | -0.919 | -0.979 | -0.704 |
| | ***FBG7*** | -0.329 | 0.897 | 1.000 | 0.783 |
| | ***FBG6*** | 0.688 | -0.968 | 0.362 | 1.000 |
| | ***FBG5*** | -0.644 | 0.949 | -0.321 | -0.973 |
| | ***FBG4*** | 0.879 | -0.020 | 0.876 | -0.919 |
| | ***FBG3*** | -0.880 | 0.019 | -0.988 | 0.951 |
| | ***FBG2*** | 1.000 | 0.860 | -0.615 | 0.260 |
| | ***FBG1*** | -0.973 | -1.000 | 0.605 | -0.267 |

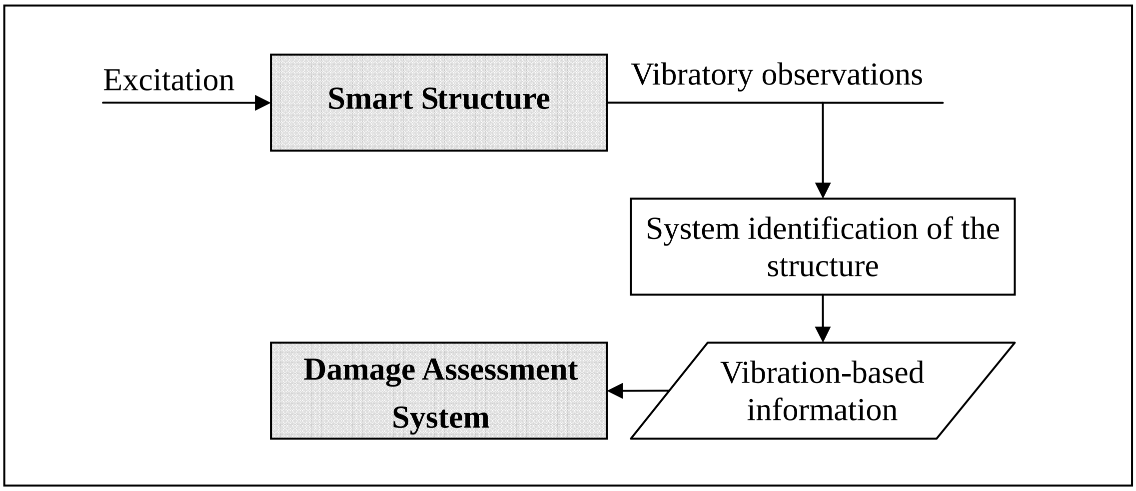


**Figure 1.1** Relationship between system identification and damage assessment techniques

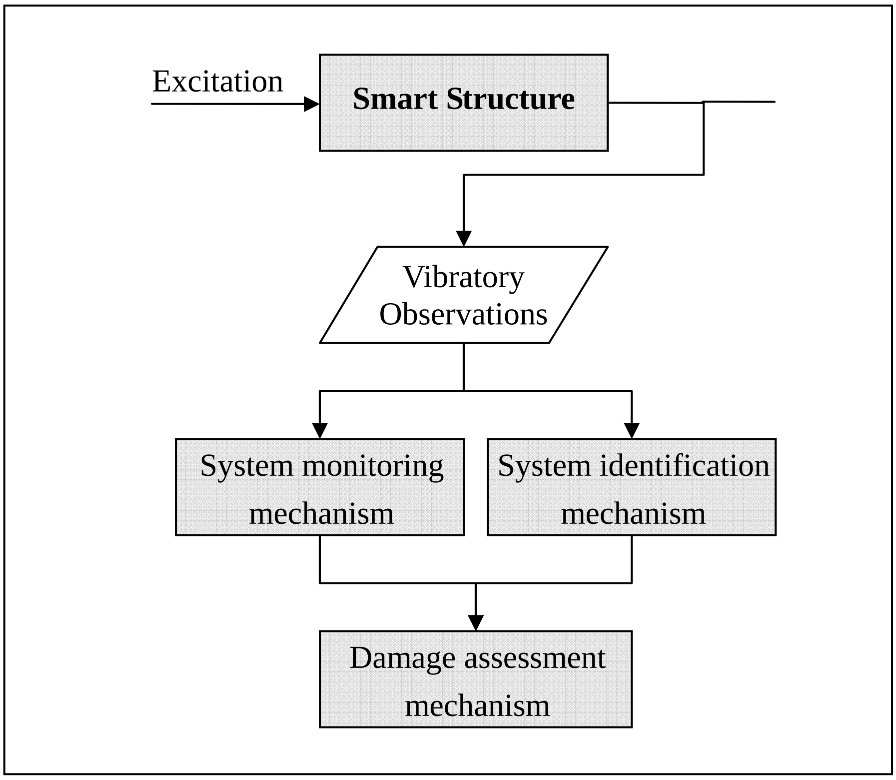


**Figure 1.2** The frame of the health monitoring system

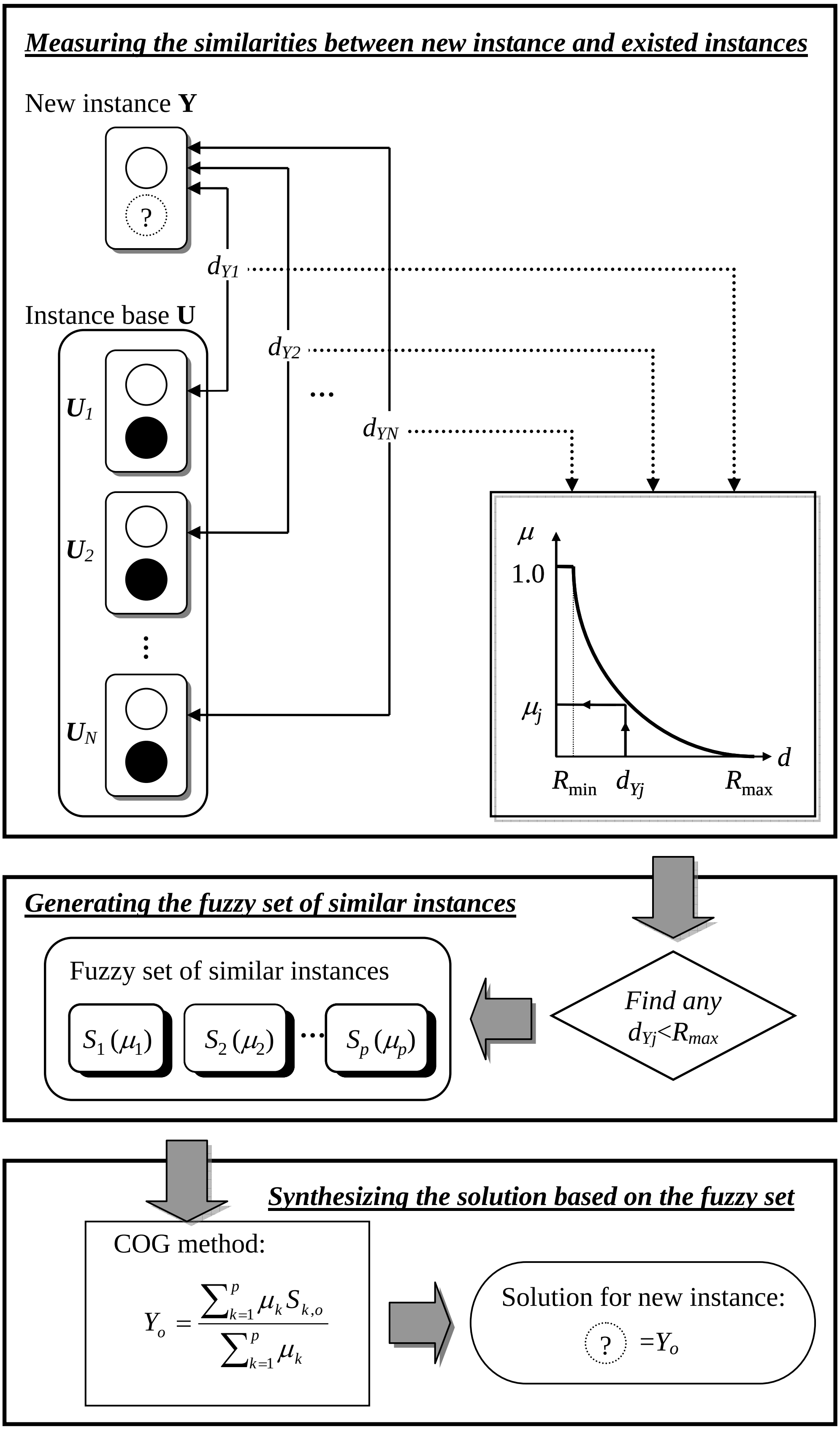


$$Y_o = \frac{\sum_{k=1}^{p} \mu_k S_{k,o}}{\sum_{k=1}^{p} \mu_k}$$

**Figure 3.1** Process of the UFN reasoning

**Figure 4.1** Earthquake simulator- the shaking table system in NCTU

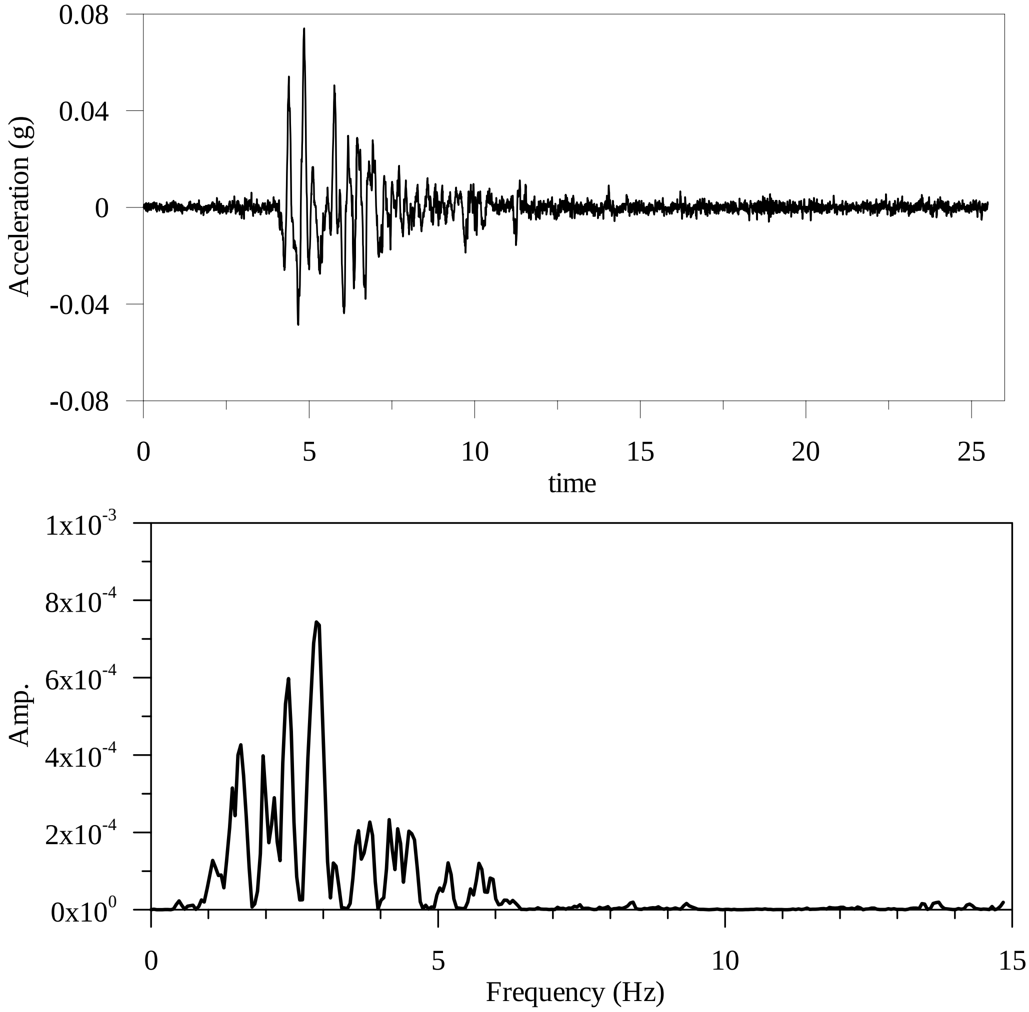


**Figure 4.2** Time-history and frequency spectrum of the 0.08g Kobe earthquake

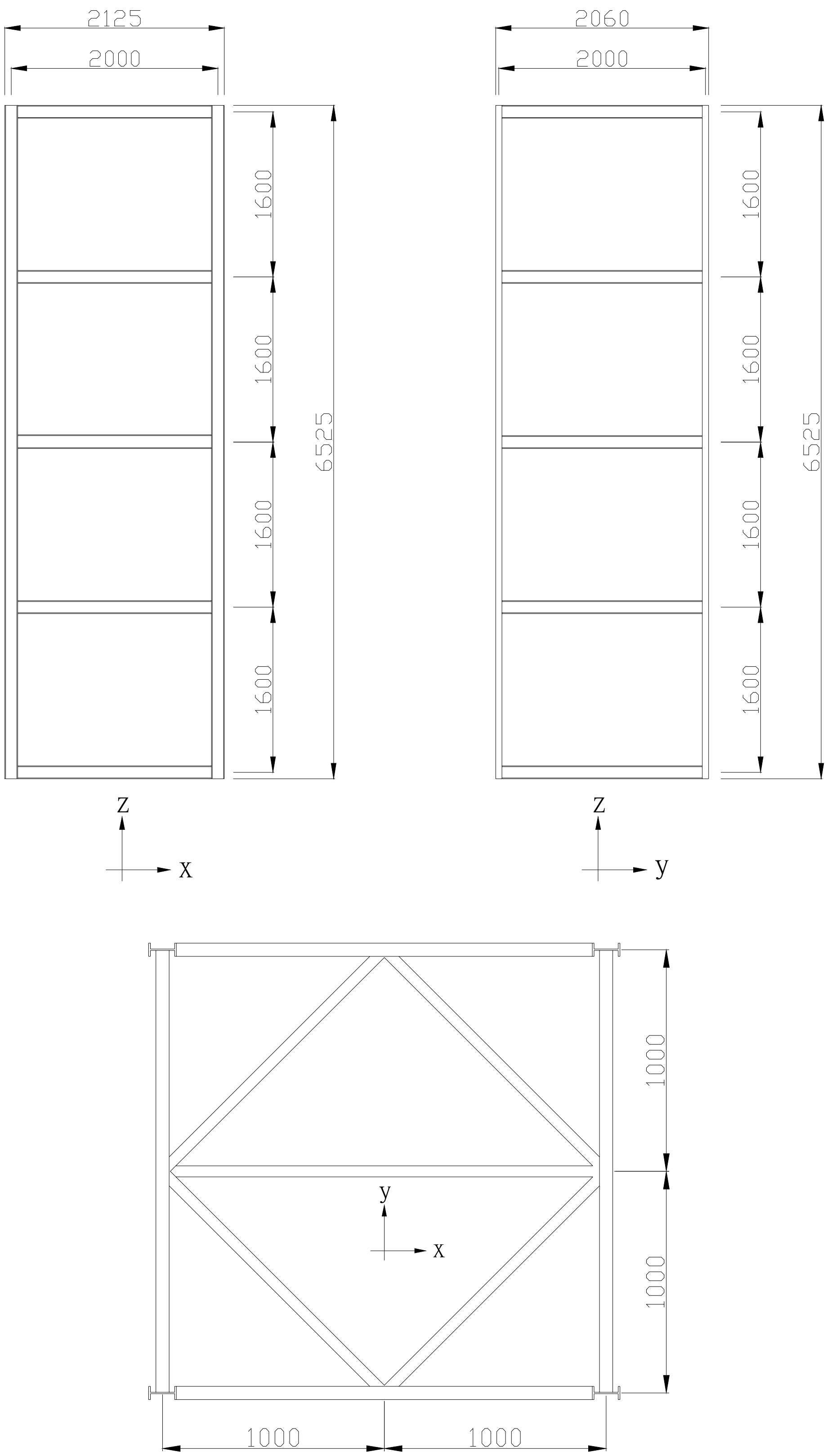


**Figure 4.3** Schematic diagrams of the four-story frame (unit: mm)

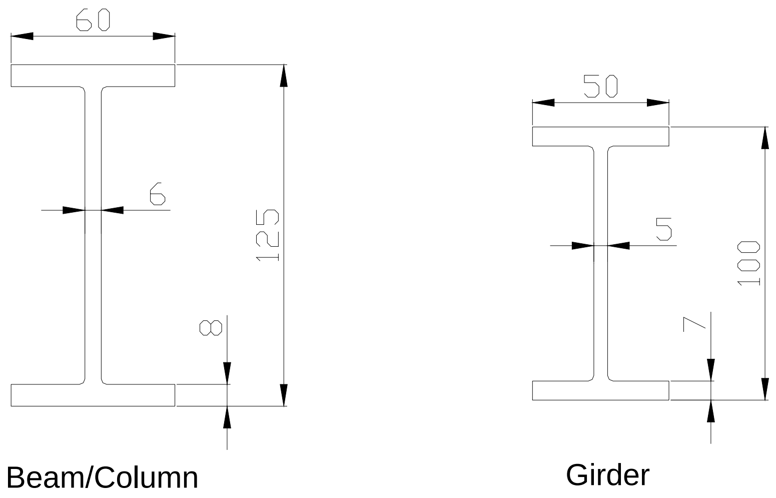


**Figure 4.4** Member cross section of the test model (unit: mm)

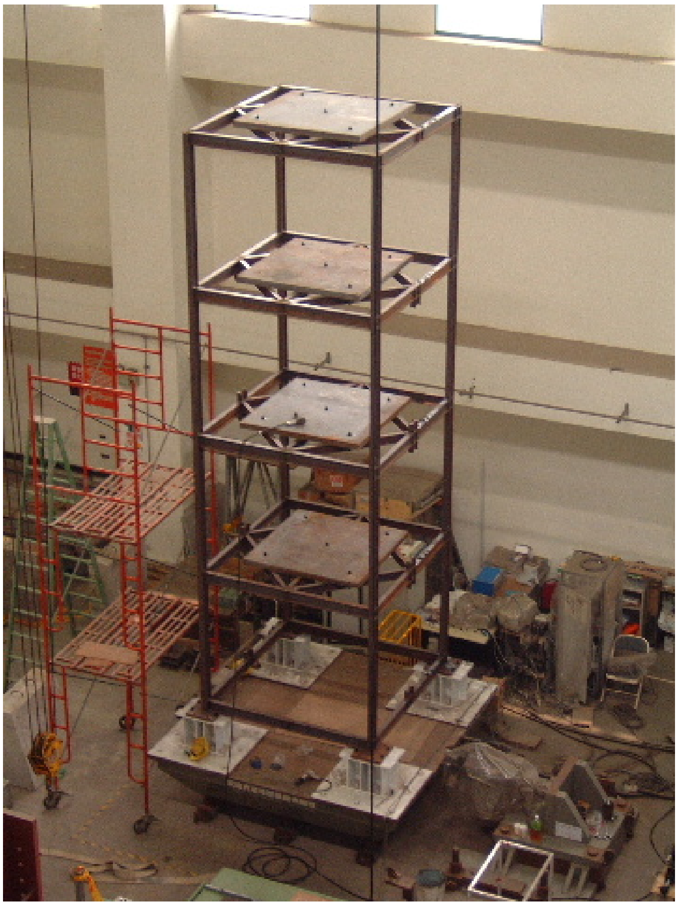

**Figure 4.5** A photo of the four-story clear frame

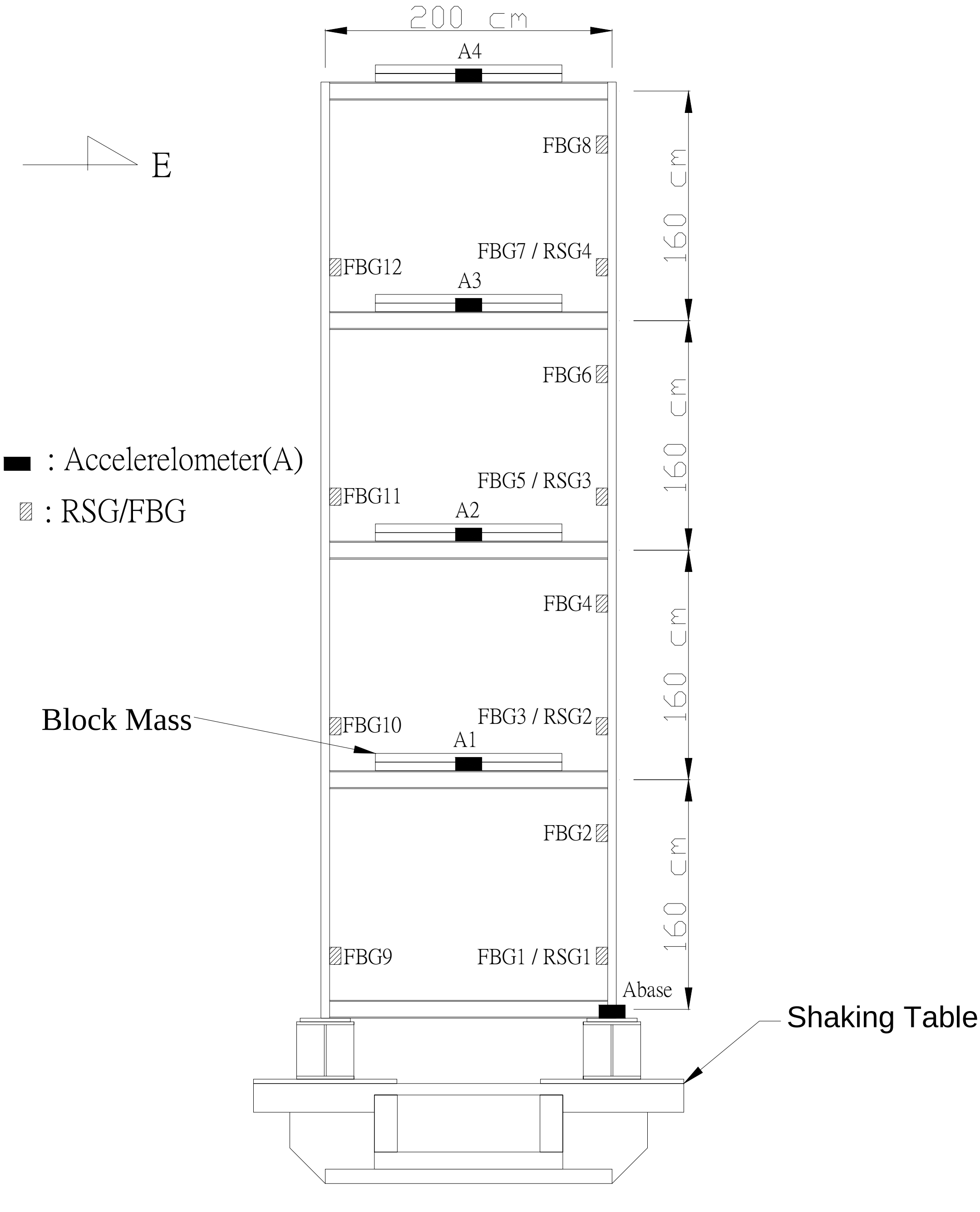


**Figure 4.6** Displacement of the sensing instrumentations

**Figure 4.7** Accelerometer at the 2nd floor of the test frame

**Figure 4.8** Accelerometer at the base of the test frame

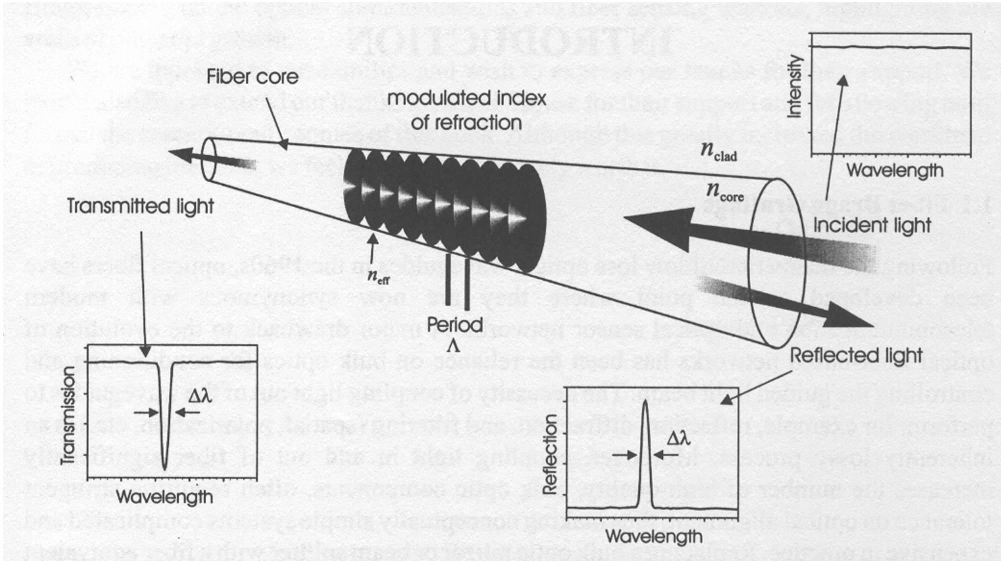


**Figure 4.9** A schematic representation of a fiber Bragg grating (extracted from Othonos and Kalli, 1999 [26])

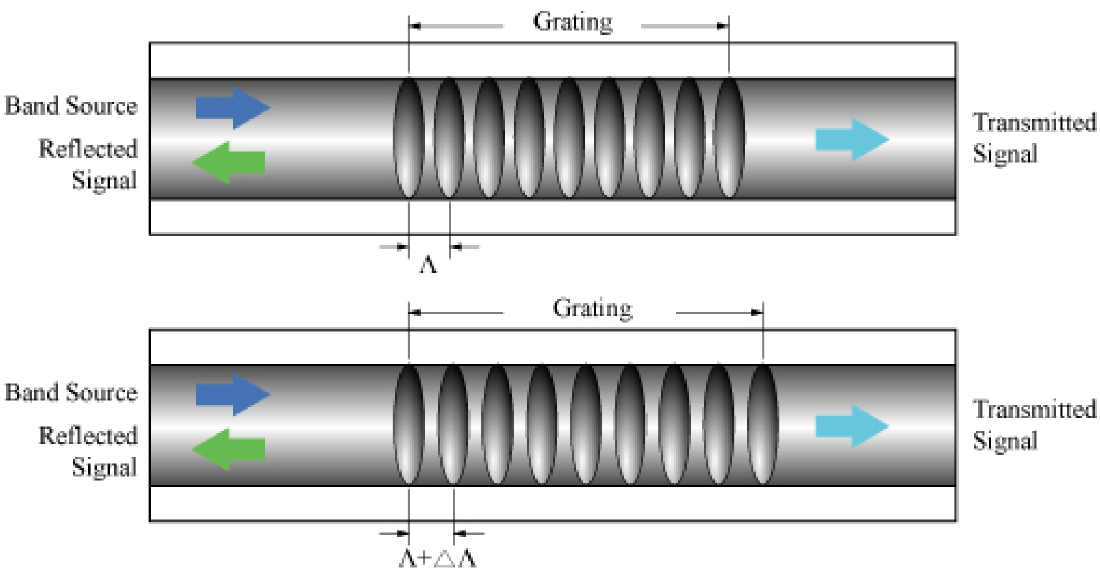


**Figure 4.10** Illustration of a fiber Bragg grating with strain effect


**Figure 4.11** FBG data acquisition system

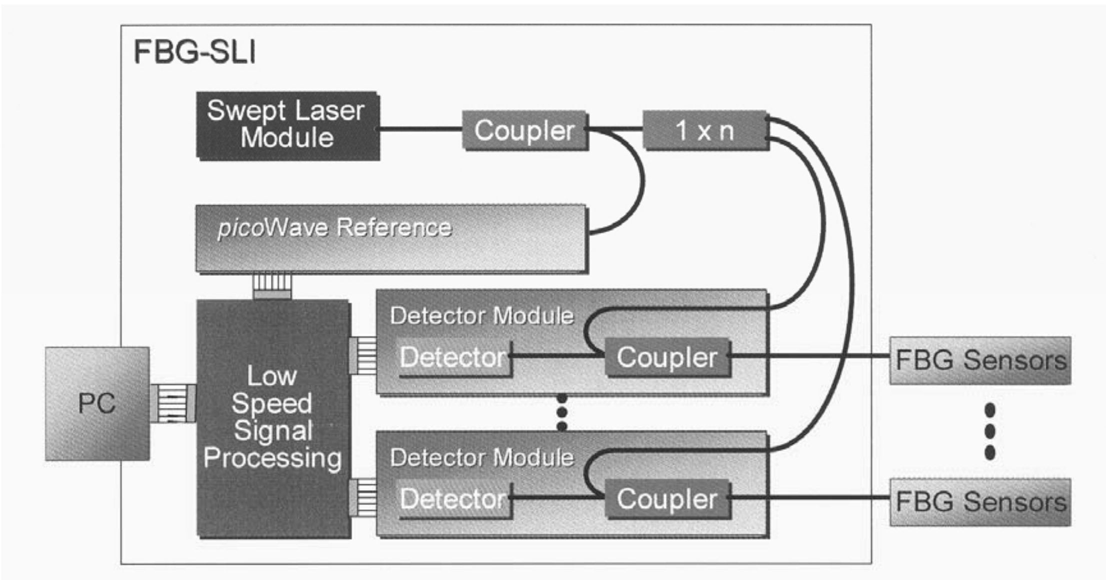


**Figure 4.12** Block diagram of the optical layout (extracted from *FBG-SLI Instruction Manual*, *Version 4.0*)

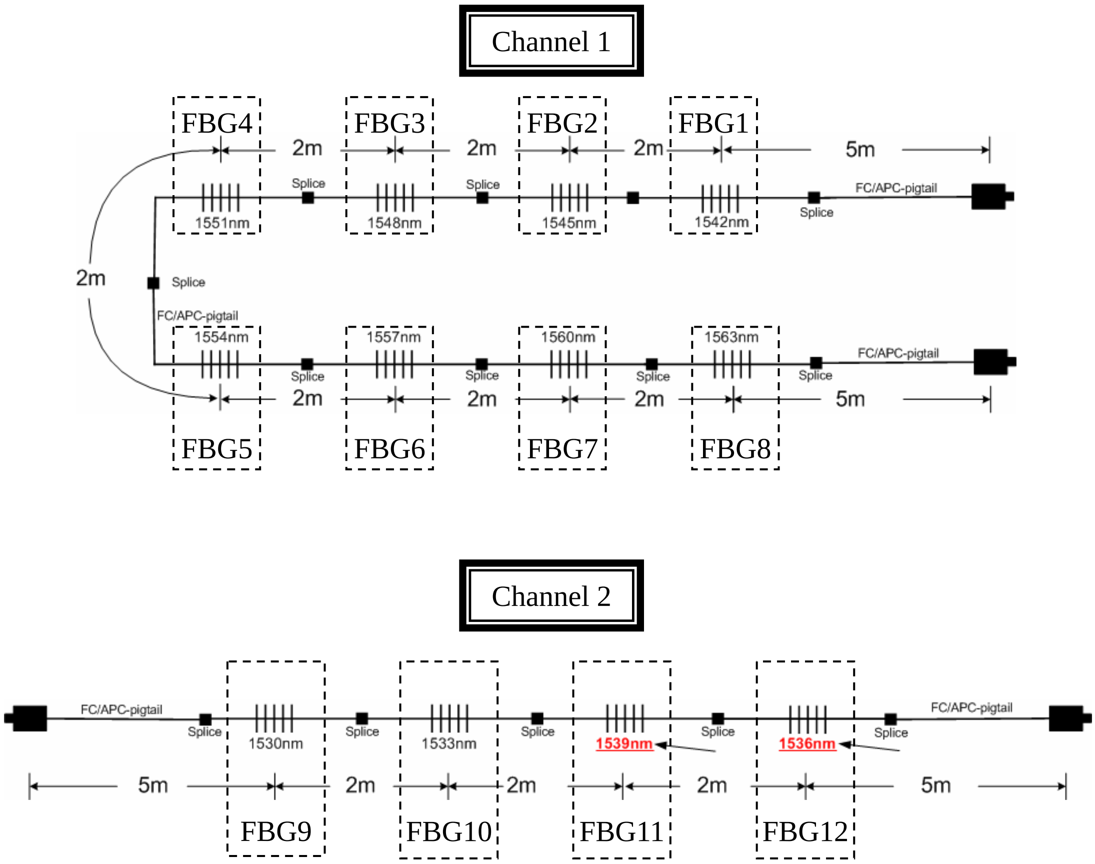


**Figure 4.13** Configurations of the FBG sensors

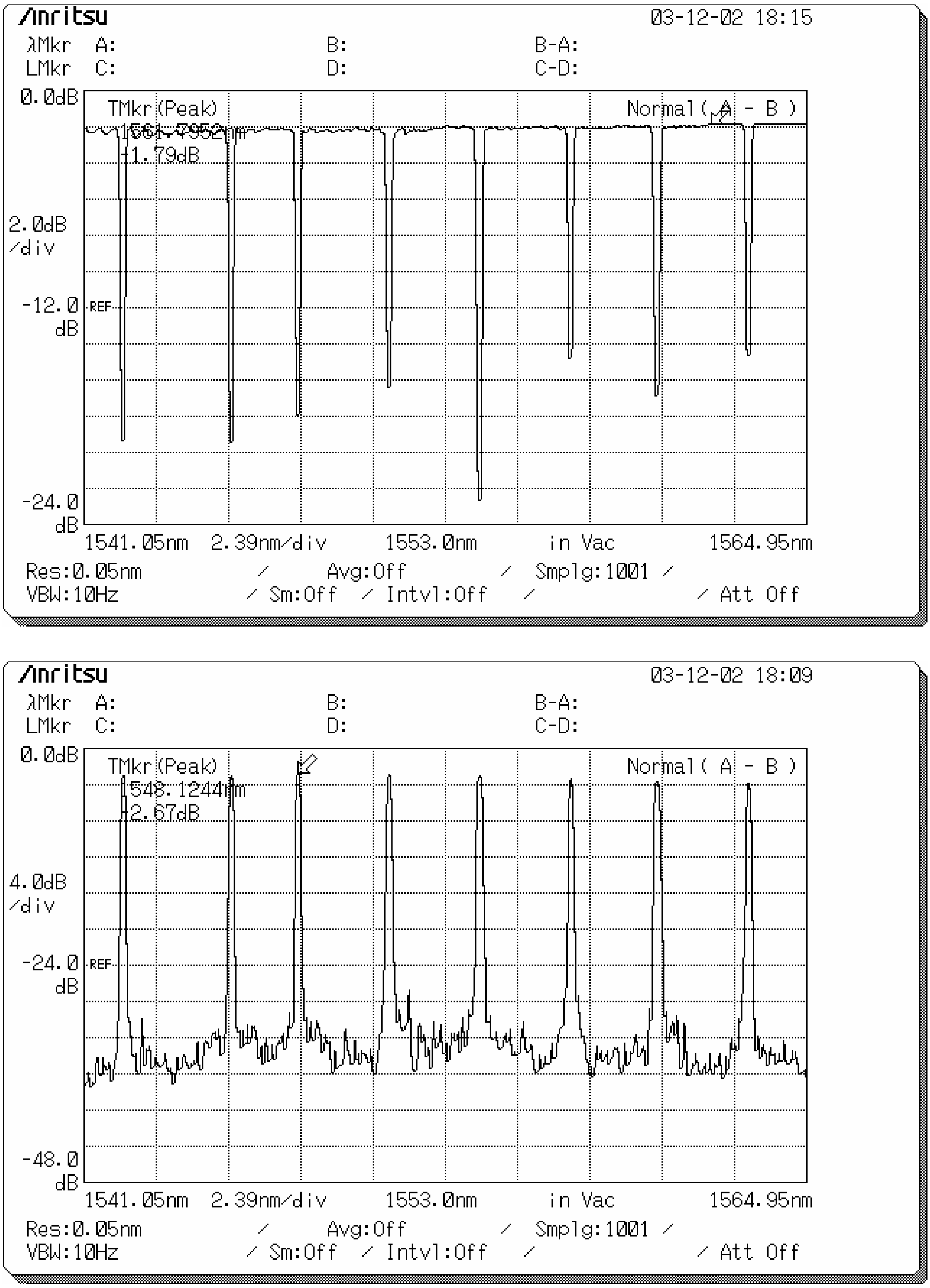


**Figure 4.14** Transmission and reflection spectra of Channel 1 (POFC provided)

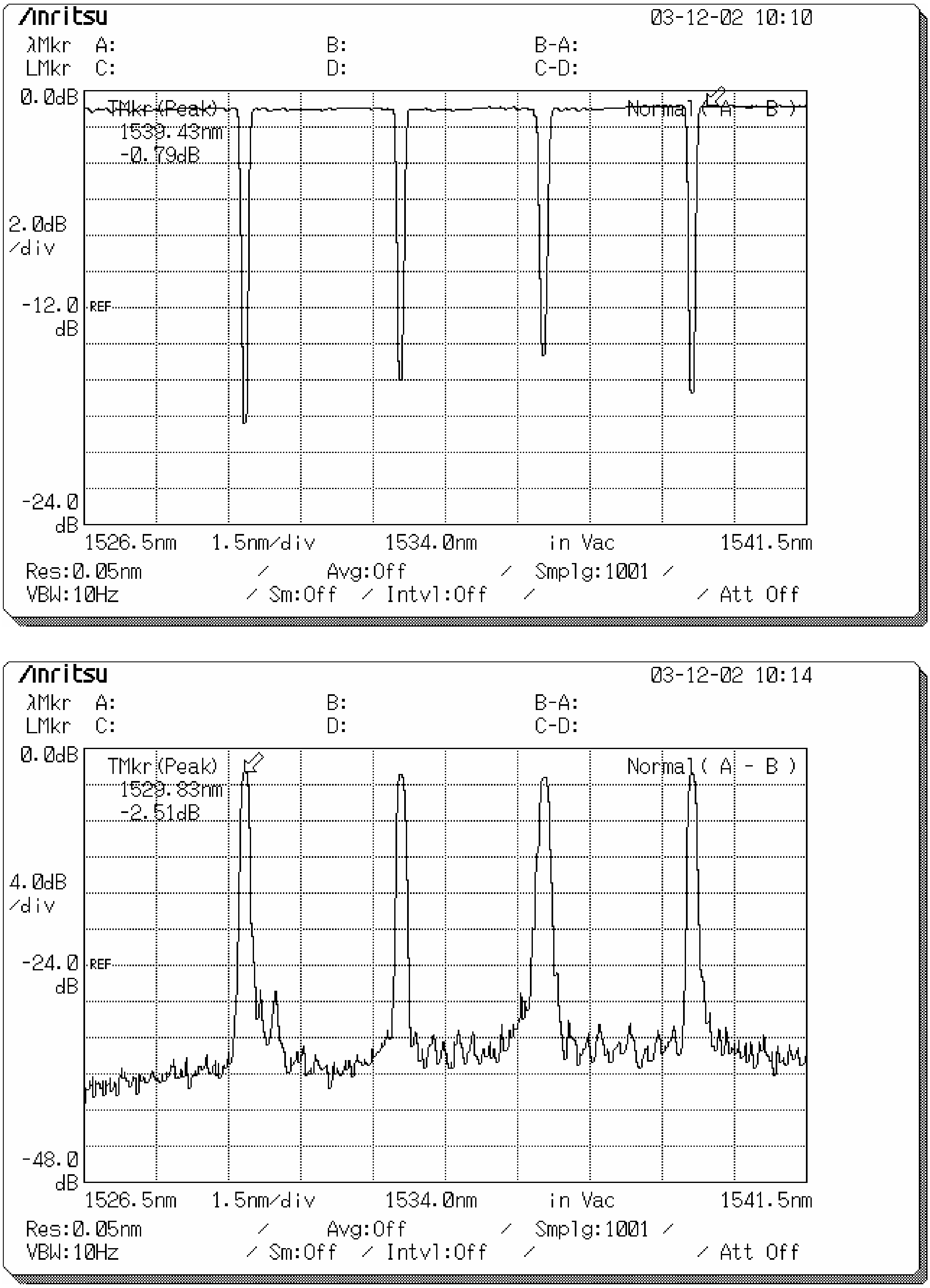


**Figure 4.15** Transmission and reflection spectra of Channel 2 (POFC provided)

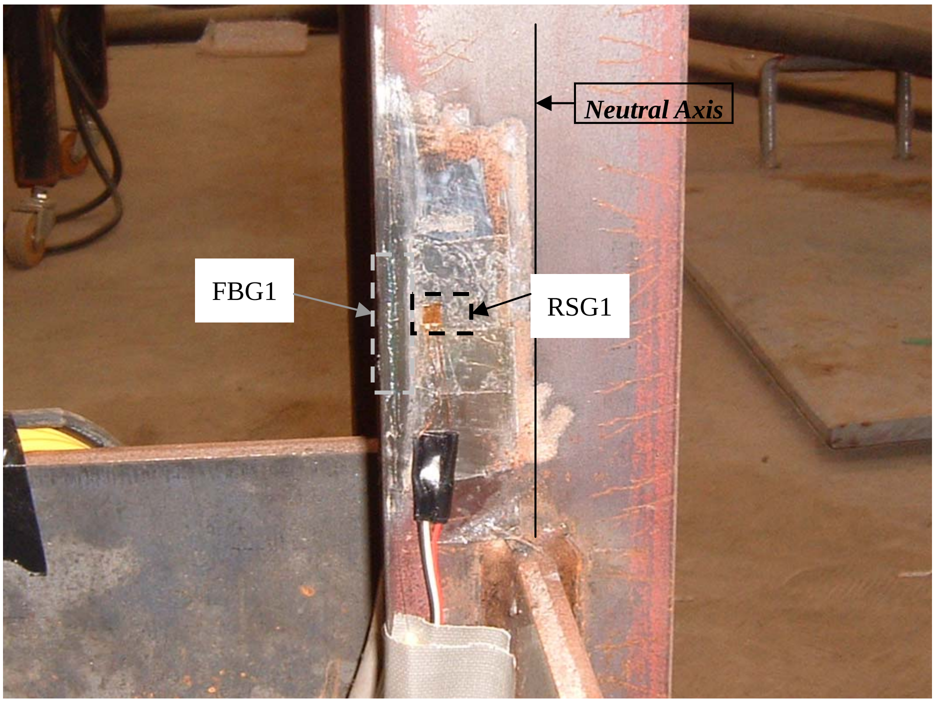


**Figure 4.16** Locations of the FBG1 and RSG1

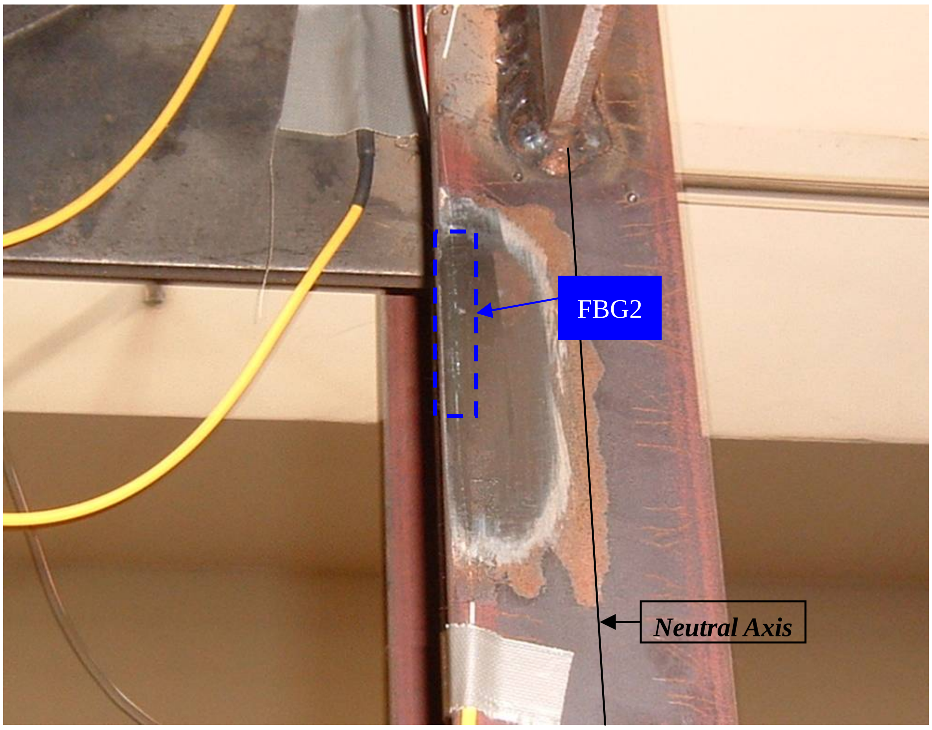


**Figure 4.17** Location of the FBG2

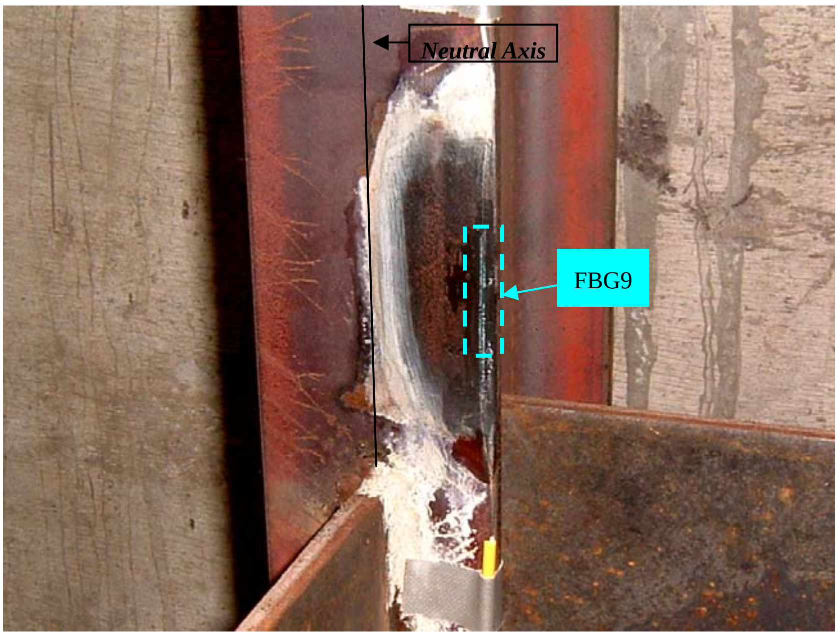


**Figure 4.18** Location of the FBG9

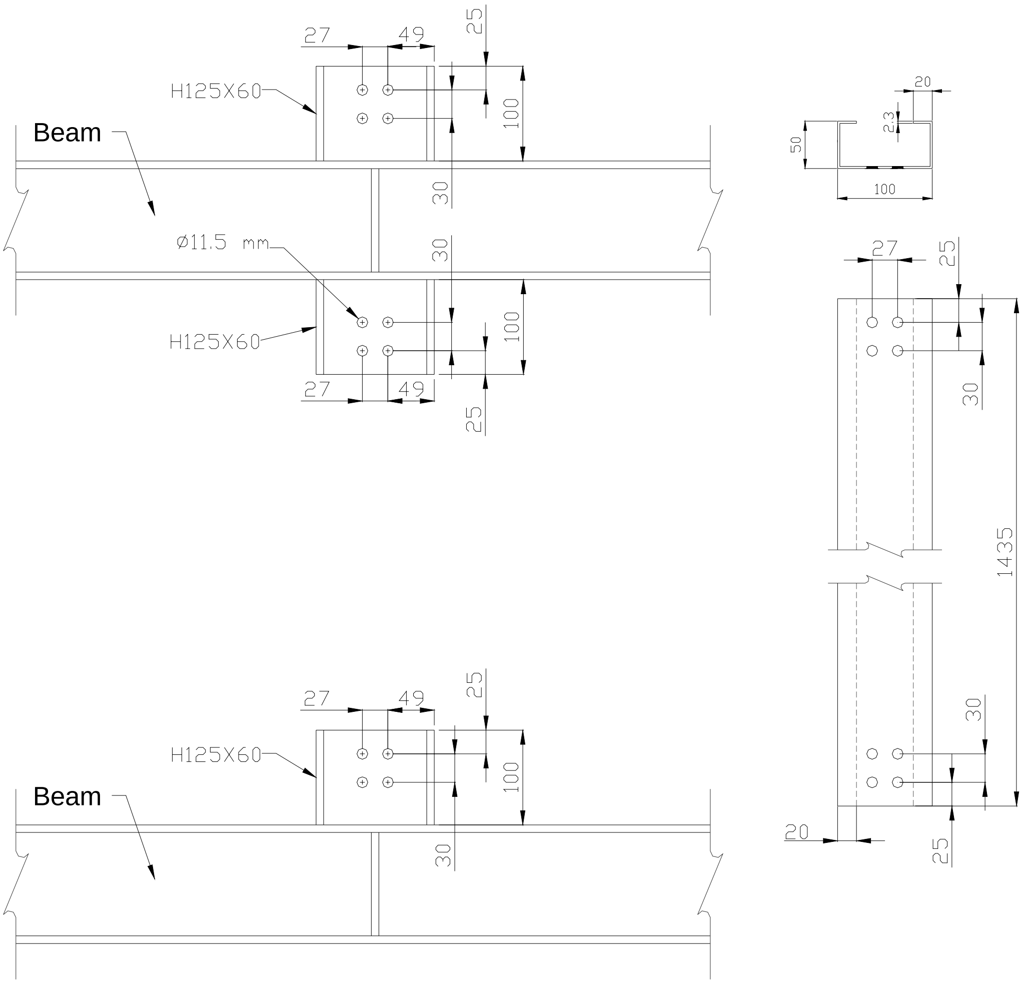


**Figure 4.19** Schematic diagrams of the SC and its connection

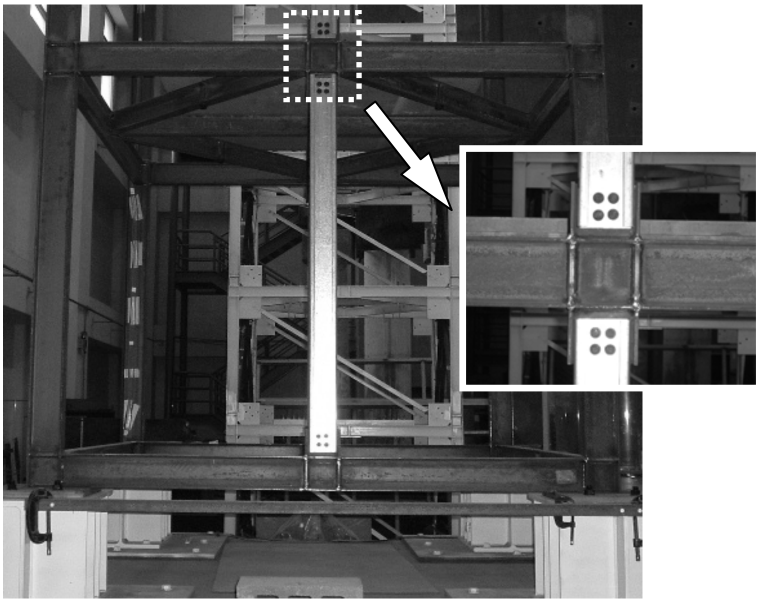

**Figure 4.20** Connections of the SC at the 1st story (left) and the 2nd floor (right)

**Figure 4.21** A photo of the intact structure

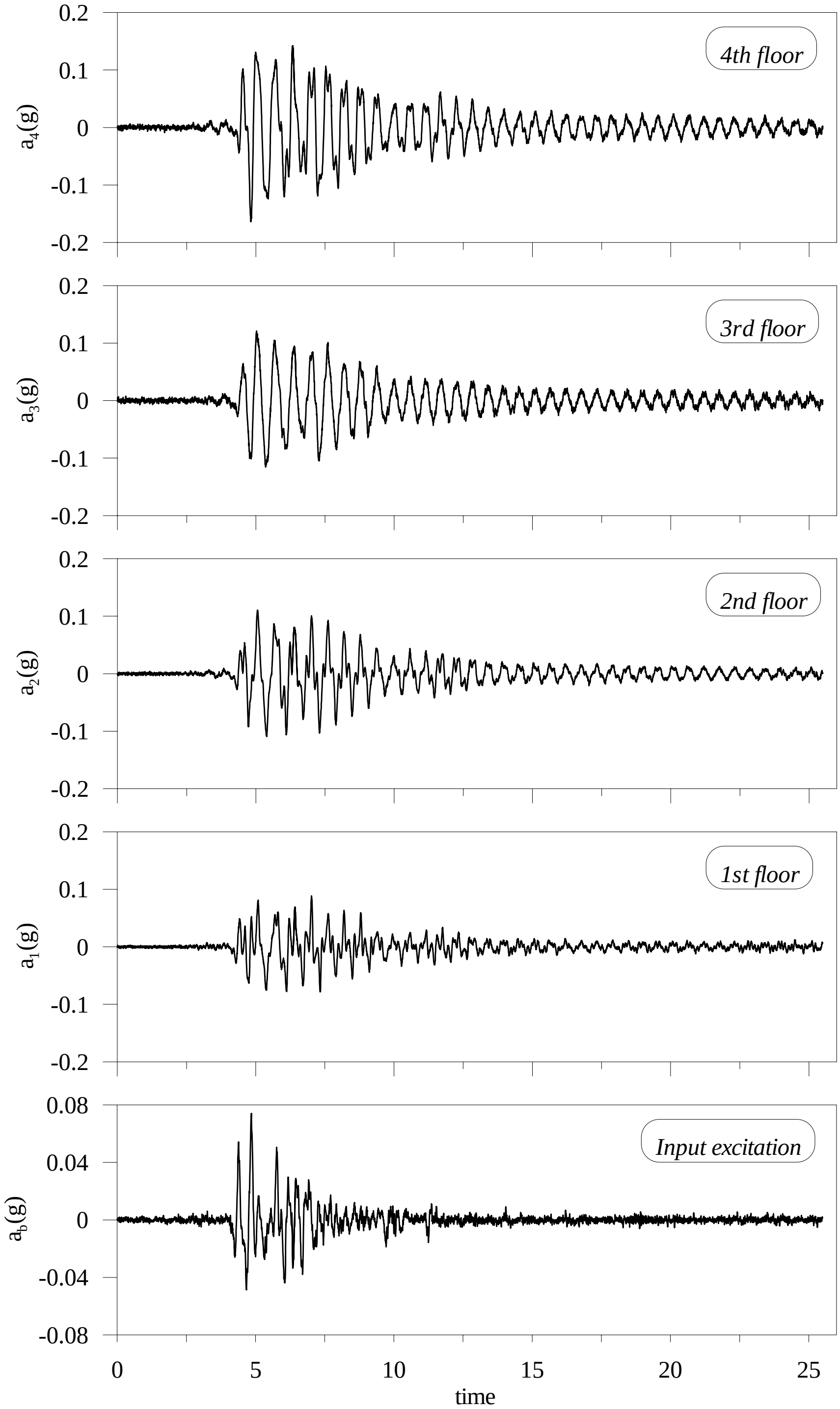


**Figure 5.1** Response histories of the AAA_acc measurement

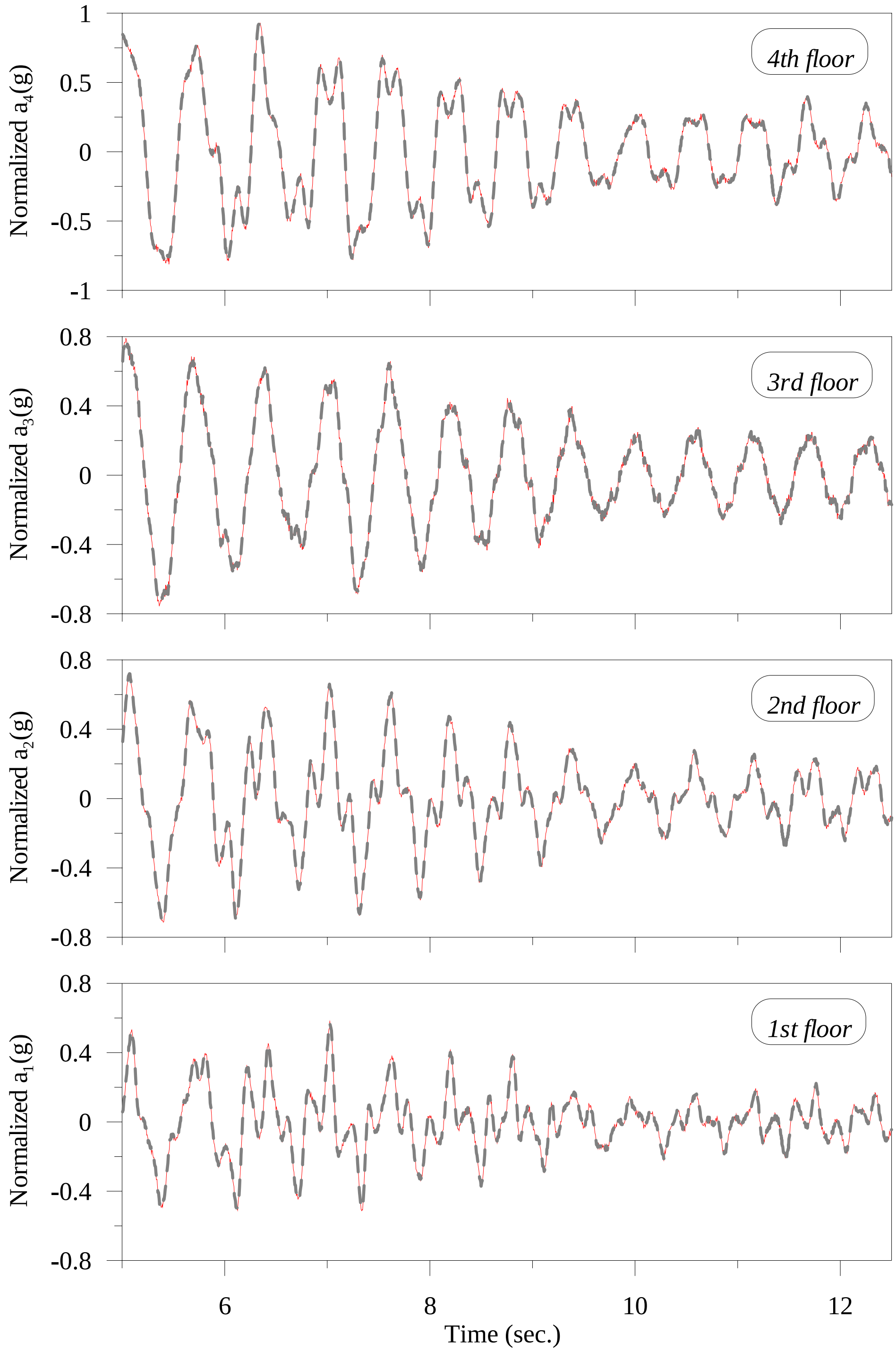


**Figure 5.2** Comparison between the measured (solid line) and computed (dash line) responses for the AAA_acc measurement

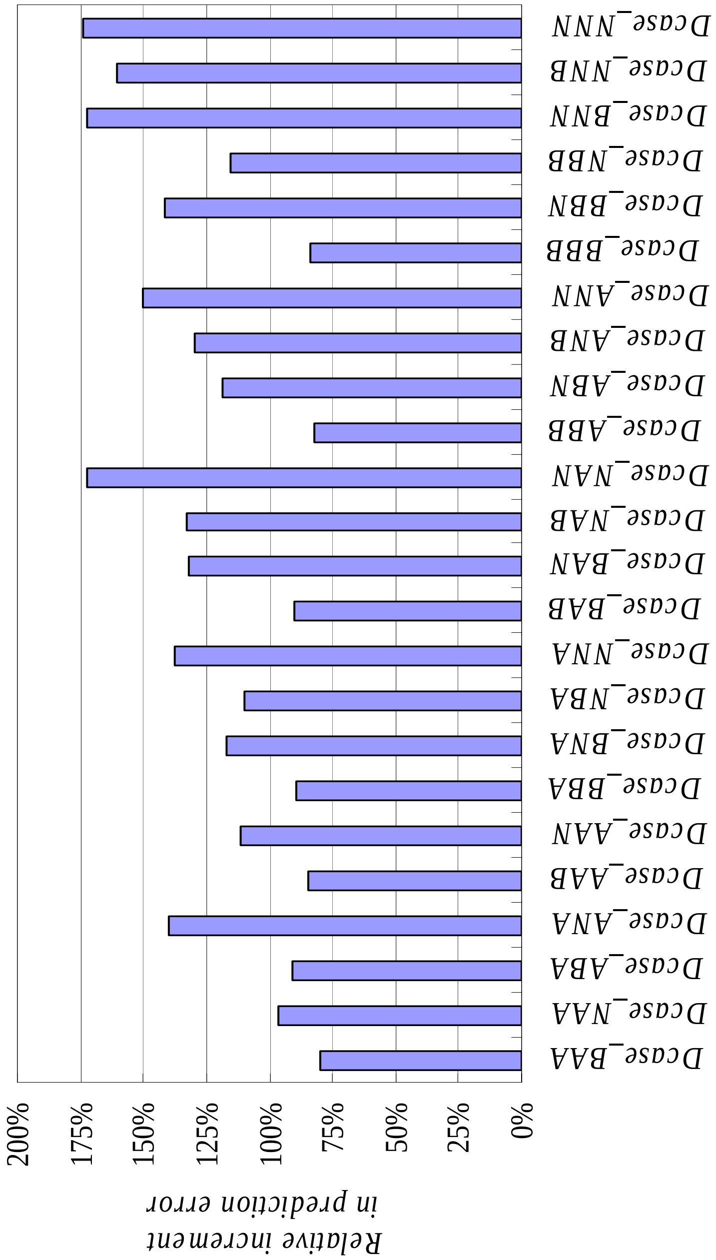


**Figure 5.3** Relative increments in prediction error in all damage cases based on acceleration measurements

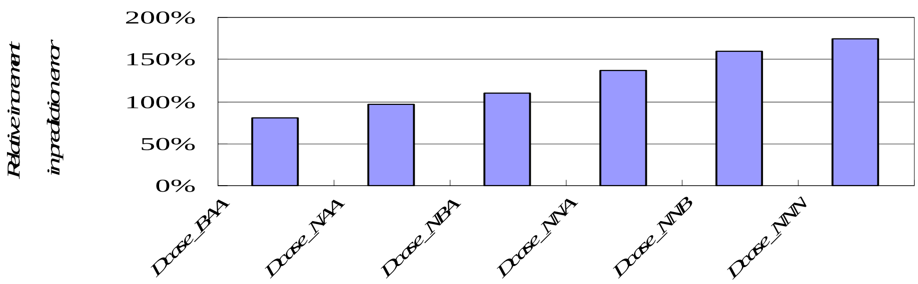


**Figure 5.4** Relative increments in prediction error in the structure of degradation based on acceleration measurements

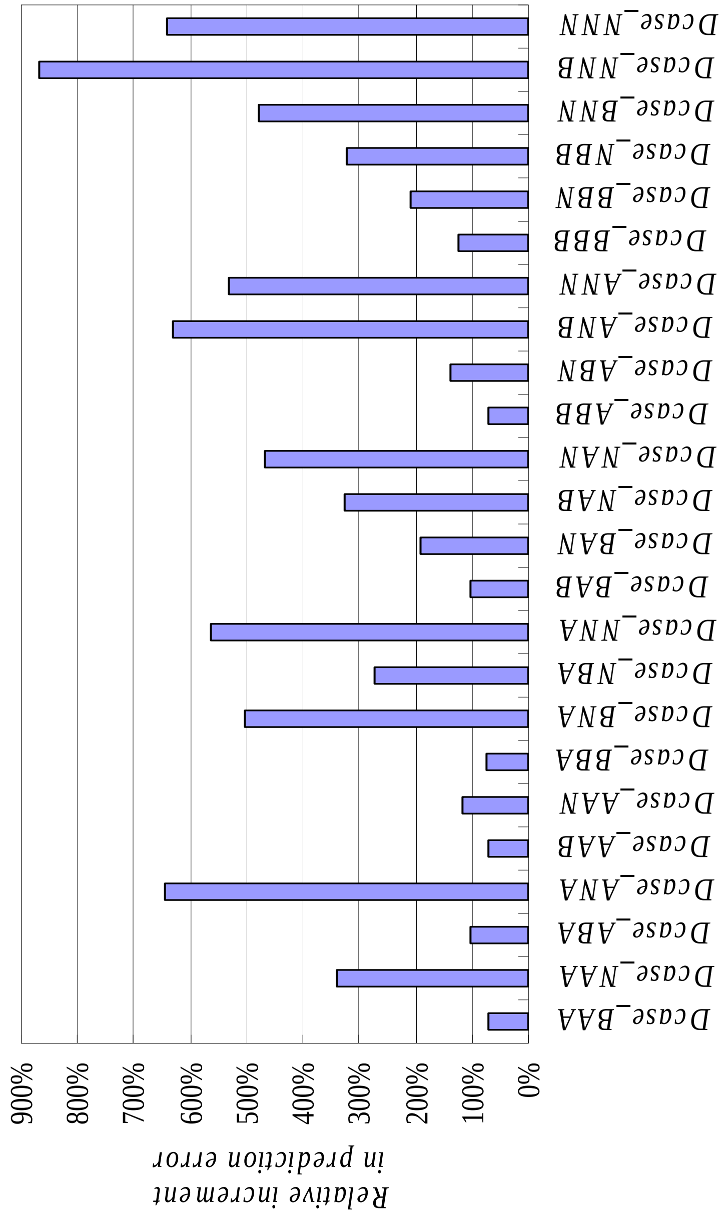


**Figure 5.5** Relative increments in prediction error in all damage cases based on strain measurements (from FBG sensors)

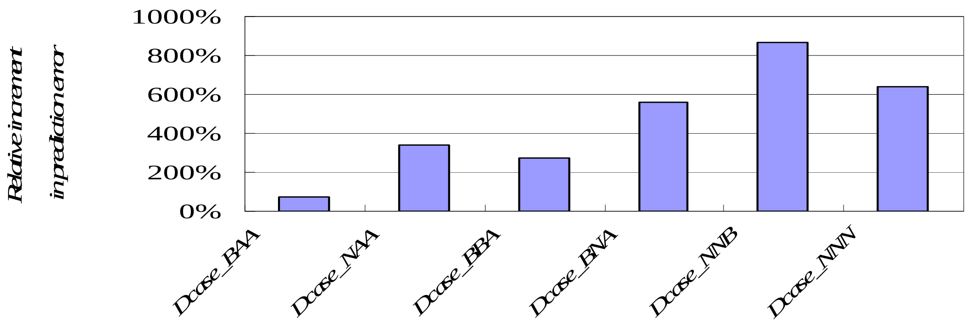


**Figure 5.6** Relative increments in prediction error in the structure of degradation based on strain measurements (from FBG sensors)